

**JOURNAL  
OF  
FOOD  
PROCESS  
ENGINEERING**

**D.R. HELDMAN  
and  
R.P. SINGH  
COEDITORS**

**FOOD & NUTRITION  
PRESS, INC.**

# JOURNAL OF FOOD PROCESS ENGINEERING

**Editor:** **D.R. HELDMAN**, Food Science/Engineering Unit, University of Missouri, Columbia, Missouri  
**R.P. SINGH**, Agricultural Engineering Department, University of California, Davis, California

**Editorial Board:**

**M.O. BALABAN**, Gainesville, Florida (1996)  
**S. BRUIN**, Vlaardingen, The Netherlands (1995)  
**M. CHERYAN**, Urbana, Illinois (1996)  
**J.P. CLARK**, Chicago, Illinois (1995)  
**A. CLELAND**, Palmerston North, New Zealand (1995)  
**K.H. HSU**, E. Hanover, New Jersey (1996)  
**J.L. KOKINI**, New Brunswick, New Jersey (1996)  
**E.R. KOLBE**, Corvallis, Oregon (1996)  
**J. KROCHTA**, Davis, California (1995)  
**L. LEVINE**, Plymouth, Minnesota (1996)  
**S. MULVANEY**, Ithaca, New York (1996)  
**M.A. RAO**, Geneva, New York (1995)  
**S.S.H. RIZVI**, Ithaca, New York (1995)  
**E. ROTSTEIN**, Minneapolis, Minnesota (1995)  
**T. RUMSEY**, Davis, California (1995)  
**S.K. SASTRY**, Columbus, Ohio (1995)  
**J.F. STEFFE**, East Lansing, Michigan (1995)  
**K.R. SWARTZEL**, Raleigh, North Carolina (1995)  
**A.A. TEIXEIRA**, Gainesville, Florida (1995)  
**G.R. THORPE**, Victoria, Australia (1995)  
**H. WEISSER**, Freising-Weihestephan, Germany (1995)

All articles for publication and inquiries regarding publication should be sent to DR. D.R. HELDMAN, COEDITOR, *Journal of Food Process Engineering*, Food Science/Engineering Unit, University of Missouri-Columbia, 235 Agricultural/Engineering Bldg., Columbia, MO 65211 USA; or DR. R.P. SINGH, COEDITOR, *Journal of Food Process Engineering*, University of California, Davis, Department of Agricultural Engineering, Davis, CA 95616 USA.

All subscriptions and inquiries regarding subscriptions should be sent to Food & Nutrition Press, Inc., 2 Corporate Drive, P.O. Box 374, Trumbull, CT 06611 USA.

One volume of four issues will be published annually. The price for Volume 18 is \$142.00, which includes postage to U.S., Canada, and Mexico. Subscriptions to other countries are \$162.00 per year via surface mail, and \$173.00 per year via airmail.

Subscriptions for individuals for their own personal use are \$112.00 for Volume 18, which includes postage to U.S., Canada and Mexico. Personal subscriptions to other countries are \$132.00 per year via surface mail, and \$143.00 per year via airmail. Subscriptions for individuals should be sent directly to the publisher and marked for personal use.

The *Journal of Food Process Engineering* (ISSN:0145-8816) is published quarterly (March, June, September and December) by Food & Nutrition Press, Inc.—Office of Publication is 2 Corporate Drive, P.O. Box 374, Trumbull, Connecticut 06611 USA.

Second class postage paid at Trumbull, CT 06602.

POSTMASTER: Send address changes to Food & Nutrition Press, Inc., 2 Corporate Drive, P.O. Box 374, Trumbull, Connecticut 06611 USA.

# RENEWAL INVOICE

# Journal of FOOD PROCESS ENGINEERING

Payment must accompany  
this Renewal Invoice

---

Your subscription is due for renewal.  
To avoid interruption in service  
or missing issues, please fill in  
and mail this form with your payment now.

---

Volume	Subscription Rates:	U.S., Canada & Mexico
19	___ 1 year	\$149.00
19 & 20	___ 2 years	\$288.00
19, 20 & 21	___ 3 years	\$432.00

Outside the U.S., Canada & Mexico, please  
add \$23.00 per year for surface shipment,  
or \$35.00 per year for air shipment.

---

Food & Nutrition Press, Inc.  
2 Corporate Drive  
P.O. Box 374  
Trumbull, Connecticut 06611 USA

Tel. (203) 261-8587  
FAX (203) 261-9724

# RENEWAL INVOICE

# Journal of FOOD PROCESS ENGINEERING

Payment must accompany  
this Renewal Invoice

---

Your subscription is due for renewal.  
To avoid interruption in service  
or missing issues, please fill in  
and mail this form with your payment now.

---

Enclosed is check for

Volume	Subscription Rates:	U.S., Canada & Mexico
19	1 year	\$149.00
19 & 20	2 years	\$288.00
19, 20 & 21	3 years	\$432.00

Outside the U.S., Canada & Mexico, please  
add \$23.00 per year for surface shipment,  
or \$34.00 per year for air shipment.

---

Food & Nutrition Press, Inc.  
6527 Main Street  
P.O. Box 374  
Trumbull, Connecticut 06611 USA

Tel. (203) 261-8587  
FAX (203) 261-9724

**JOURNAL OF FOOD PROCESS ENGINEERING**

# JOURNAL OF FOOD PROCESS ENGINEERING

*Editor:*

**D.R. HELDMAN**, Food Science/Engineering Unit, University of Missouri, Columbia, Missouri

**R.P. SINGH**, Agricultural Engineering Department, University of California, Davis, California

*Editorial Board:*

**M.O. BALABAN**, Department of Food Science and Human Nutrition, University of Florida, Gainesville, Florida

**S. BRUIN**, Unilever Research Laboratory, Vlaardingen, The Netherlands

**M. CHERYAN**, Department of Food Science, University of Illinois, Urbana, Illinois

**J.P. CLARK**, Epstein Process Engineering, Inc., Chicago, Illinois

**A. CLELAND**, Department of Biotechnology, Massey University, Palmerston North, New Zealand

**K.H. HSU**, RJR Nabisco, Inc., E. Hanover, New Jersey

**J.L. KOKINI**, Department of Food Science, Rutgers University, New Brunswick, New Jersey

**E.R. KOLBE**, Department of Bioresource Engineering, Oregon State University, Corvallis, Oregon

**J. KROCHTA**, Agricultural Engineering Department, University of California, Davis, California

**L. LEVINE**, Leon Levine & Associates, Plymouth, Minnesota

**S. MULVANEY**, Department of Food Science, Cornell University, Ithaca, New York

**M.A. RAO**, Department of Food Science and Technology, Institute for Food Science, New York State Agricultural Experiment Station, Geneva, New York

**S.S.H. RIZVI**, Department of Food Science, Cornell University, Ithaca, New York

**E. ROTSTEIN**, The Pillsbury Co., Minneapolis, Minnesota

**T. RUMSEY**, Agricultural Engineering Department, University of California, Davis, California

**S.K. SASTRY**, Agricultural Engineering Department, Ohio State University, Columbus, Ohio

**J.F. STEFFE**, Department of Agricultural Engineering, Michigan State University, East Lansing, Michigan

**K.R. SWARTZEL**, Department of Food Science, North Carolina State University, Raleigh, North Carolina

**A.A. TEIXEIRA**, Agricultural Engineering Department, University of Florida, Gainesville, Florida

**G.R. THORPE**, Department of Civil and Building Engineering, Victoria University of Technology, Melbourne, Victoria, Australia

**H. WEISSER**, University of Munich, Inst. of Brewery Plant and Food Packaging, Freising-Weihenstephan, Germany

# **Journal of FOOD PROCESS ENGINEERING**

**VOLUME 18  
NUMBER 3**

**Coeditors: D.R. HELDMAN  
R.P. SINGH**

**FOOD & NUTRITION PRESS, INC.  
TRUMBULL, CONNECTICUT 06611 USA**

© Copyright 1995 by  
Food & Nutrition Press, Inc.  
Trumbull, Connecticut 06611 USA

All rights reserved. No part of this publication may be reproduced, stored in a retrieval system or transmitted in any form or by any means: electronic, electrostatic, magnetic tape, mechanical, photocopying, recording or otherwise, without permission in writing from the publisher.

ISSN 0145-8876

Printed in the United States of America

## CONTENTS

Moisture Sorption and Volumetric Changes of Canola During Hydrothermal Processing <b>N.J. THAKOR, S. SOKHANSANJ, R.T. PATIL and S.D. DESHPANDE</b> . . . . .	233
Adsorption of Bile Acids on Cereal Type Food Fibers <b>C.-M. HUANG and N.H. DURAL</b> . . . . .	243
Mechanisms Involved in the Infusion of Starch Based Porous Food Materials by Oil Based Liquid Foods <b>Z. HIÇSASMAZ and J.T. CLAYTON</b> . . . . .	267
Evaluation of Die Swell and Volumetric Expansion in Corn Meal Extrudates <b>J.F. FALLER, H.E. HUFF and F. HSIEH</b> . . . . .	287
Simultaneous Heat and Mass Transfer During the Deep Fat Frying of Tortilla Chips <b>R. MOREIRA, J. PALAU and X. SUN</b> . . . . .	307
Mathematical Modeling of Particulate Two-Phase Flow in a Helical Pipe <b>Y. LIU and C.A. ZURITZ</b> . . . . .	321

# MOISTURE SORPTION AND VOLUMETRIC CHANGES OF CANOLA DURING HYDROTHERMAL PROCESSING

N.J. THAKOR

*Mahatma Phule Agricultural University, Rahuri, India*

SHAHAB SOKHANSANJ<sup>1</sup>, R.T. PATIL

*Department of Agricultural and Bioresource Engineering  
University of Saskatchewan, Saskatoon, SK S7N 0W0, Canada*

and

S.D. DESHPANDE

*Central Institute of Agricultural Engineering  
Nabi Bagh, Berasia Road, Bhopal 462 018, India*

Received for Publication April 27, 1995

## ABSTRACT

*The moisture content and volume change of canola seeds immersed in water or exposed to steam were measured. Three water temperatures of 22, 50 and 75C and one wet steam treatment (atmospheric pressure ~ 100C) were used in the experiments. The maximum moisture attained by the canola seed was 0.67 decimal (db) in soaking and 0.54 decimal (db) in steaming. The moisture sorption rates were higher at higher temperatures of soaking. The coefficient of expansion did not vary significantly among treatments and an average coefficient of 1.032 per unit change in moisture content was obtained.*

## INTRODUCTION

Canola seed contains approximately 40% oil and yields a meal containing about 38–43% protein (Shahidi 1990). The canola protein contains essential amino acids such as lysine, methionine, and cysteine (Schulz and Petersen 1981). However, the high content of crude fiber and tannin contributed mainly by its hull results in a low metabolizable energy content of the defatted canola meal. This is a limiting factor for the use of meal in feed formulations.

The present practice is to crush whole canola seed to remove oil by press followed by hexane extraction. Removal of the hull from the seed prior to crushing will improve the quality of crude oil and will yield meal with lower fiber and tannin content.

<sup>1</sup>Correspond with: Dr. Shahab Sokhansanj.

The hydrothermal treatment of canola results in effective removal of hull with very little loss in cotyledons (Thakor *et al.* 1992). Canola grain, like any other agricultural seed, undergoes several physical changes when subjected to hydrothermal treatments like steaming or soaking followed by drying. During moisture absorption, the weight and volume of the kernel increases and during drying, temperature and moisture gradients are superimposed within the kernel, resulting in differential shrinkages of different parts of the kernel. A temperature increase causes expansion and a moisture loss causes contraction.

Since moisture absorption takes place at different rates under different processing conditions, it is essential to characterize the whole sorption process. Sorption data has been fitted and interpreted by different kinds of mathematical models (Tang and Sokhansanj 1993a; Engels *et al.* 1987; Peleg 1988). Similar models were also applied to water absorption by Hendrickx *et al.* (1987). For characterizing expansion properties, both linear and volumetric expansion coefficients are used (Muthukumarappan *et al.* 1990; Tang and Sokhansanj 1993b). Relatively little information concerning thermal and hygroscopic expansion of canola is found in the literature. Most of the information available is for corn (Muthukumarappan and Gunasekaran 1990), rice (Muthukumarappan *et al.* 1990), lentils (Tang and Sokhansanj 1993b), and soybean (Misra and Young 1980). Variation in linear dimensions during drying of a wetted canola seed was reported by Thakor *et al.* (1992).

The purpose of this study was to characterize moisture absorption and volume change of canola grain in bulk when it is exposed to steam or immersed in water.

## MATERIALS AND METHODS

### Canola Samples

Grade No. 1 Westar canola seed (*Brassica napus* L.) from one lot was obtained from a commercial seed supplier in Saskatoon and was from the 1990 crop grown in Western Canada. The seed was cleaned using a 1.4 mm wire mesh sieve (No. 14) and placed in air-tight containers at 4C until the testing time. Moisture content<sup>2</sup> of the seed was brought to the level of 0.06 decimal (db) before each experiment. Samples with moisture contents lower than 0.06 decimal (db) were sprayed with a predetermined amount of distilled water in stages. Samples were mixed thoroughly from time to time. Samples higher than 0.06 moisture content were dried at 40–60C in a single layer in forced air oven. All these samples were stored in air-tight containers at 4C.

<sup>2</sup>Moisture content expressed in this paper are decimal dry basis unless specified.

### Moisture Determinations

Prior to each test, the moisture contents were determined for whole seed using air-oven method as specified in the ASAE Standard Procedure S352.2 (ASAE 1989) for Canola. The oven temperature was set at 130C and the samples were dried for 4 h. Moisture contents were determined in duplicate.

### Seed Composition

The physical composition of the seed used in the study was also determined. To determine the hull content of the seed, 20 g of sound kernels were soaked in distilled water for 24 h. Two subsamples of 1 g and 0.5 g in duplicate were taken for separation of hulls. A small cut on the seed surface was made by a sharp knife and pressure was applied by hand to push out the cotyledon. This facilitated the removal of cotyledon from the seed coat. The hulls were checked for any remaining cotyledon fraction. Pure hull and cotyledon samples were then dried in ambient air and weighed to express them as percentage of total mass. The mass of each component was taken with an electronic balance having an accuracy of 0.0001 g (Model GA 200D, Ohaus Corporation, Florham Park, NJ).

### Hygroscopic Changes

To determine the volume change, canola samples of about 10 g each in three replications were soaked with excess water (40 ml) in 60 ml test tubes. For the tests at 22C, the containers were placed at room temperature of 22C ( $\pm 1.0$ C). For the tests at 50C and 75C, containers were placed in a precision water bath set at required temperatures. Samples were soaked at different time intervals up to 24 h. At the end of each time interval, water was drained and the seeds were dried with paper towels to remove the surface water. The mass of the seeds was then measured on an electronic balance ( $\pm 0.01$  g) to determine the amount of absorbed water. The volume was measured before and after the end of the tests by the displacement of toluene in a graduated burette. The smallest graduation on the burette was 0.1 ml.

Volume changes and moisture absorbed during steaming were measured by exposing about 10 g sample in triplicate in the steaming unit. Samples were held in a strainer and exposed to the saturated steam at atmospheric pressure for different durations up to 2.5 h. Line steam temperature and pressure were 120C and 200 kPa, respectively. After steaming, samples were surface dried by paper towel. Mass and volume were recorded as described earlier. Moisture contents were determined at the end of each test.

## Data Analysis

To describe the general behavior of the moisture sorption process, the following three semi-empirical models were considered. Equations 1 and 2 were as used by Tang *et al.* (1993a,b) to describe water absorption of lentil seeds. Equation 3 was used by Peleg (1988) to describe a general water absorption relationship for food material.

$$\frac{M_f - M}{M_f - M_o} = \exp(-k_1 t) \quad (1)$$

$$\frac{M_f - M}{M_f - M_o} = \exp(-k_2 t^n) \quad (2)$$

$$M - M_o = \frac{t}{(k_3 + k_4 t)} \quad (3)$$

In Eq. 1, 2 and 3 the moisture contents used were on % dry basis. The  $k$  and  $n$  are the moisture sorption constants in Eq. 1 and 2. Equation 3 consists of two parameters  $k_3$  and  $k_4$ . Equations 1 and 2, were evaluated using the Nonlinear Least Squares (NLIN) procedures in the Statistical Analysis System (SAS) software (SAS 1985). The constants  $k_3$  and  $k_4$  in Eq. 3 were determined by GLM procedure on SAS with  $\frac{t}{M - M_o}$  as dependent variable and  $t$  as independent variable.

## RESULTS AND DISCUSSION

### Seed Composition

The initial moisture content of canola seeds used in the experiments, as determined by ASAE S352.2 method, was 0.06 decimal (db). The results of the experiment to determine physical composition of canola seed are given in Table 1. There was no significant difference in hull content of canola seed based on the variation in sample size. The hull content of the canola was found to be 14.4% of the seed mass. This was in agreement with the hull content reported in the literature for rapeseed and canola (Shahidi 1990).

### Moisture Sorption Characteristics

The seed moisture content with time during soaking or steaming is as shown in Fig. 1. The moisture content increased exponentially with the duration of soaking as well as steaming and approached an equilibrium value. The

absorption of moisture inside the kernel stopped when the kernel reached a moisture level of 0.65–0.67 decimal (db). At room temperature soaking attained saturation moisture content in almost 24 h, while 8 h were required for soaking at 50C; and 2 h for soaking at 75C. However, at temperatures above 75C, prolonged soaking for more than 2 h resulted in the leaching of solids, as was observed visually from changes in color and turbidity of the water. The exposure of canola seed to saturated steam at about 100C also showed a similar trend in increase in moisture content of the seed. The equilibrium moisture content attained in steaming was 0.54 decimal (db), lower than what was attained in soaking. This could be attributed to faster diffusion of water in the liquid phase than in the vapor phase.

TABLE 1.  
PHYSICAL COMPOSITION OF CANOLA SEED

Sample	Sample mass g	Cotyledons mass g	Hull mass g	Hull %
Large	1.1150 ± 0.0071*	0.7600 ± 0.0707	0.1650 ± 0.0026	14.8 ± 0.1
Small	0.6050 ± 0.0060	0.4350 ± 0.0071	0.0842 ± 0.0018	13.9 ± 0.4
Mean				14.4 ± 0.4

\* n = 2

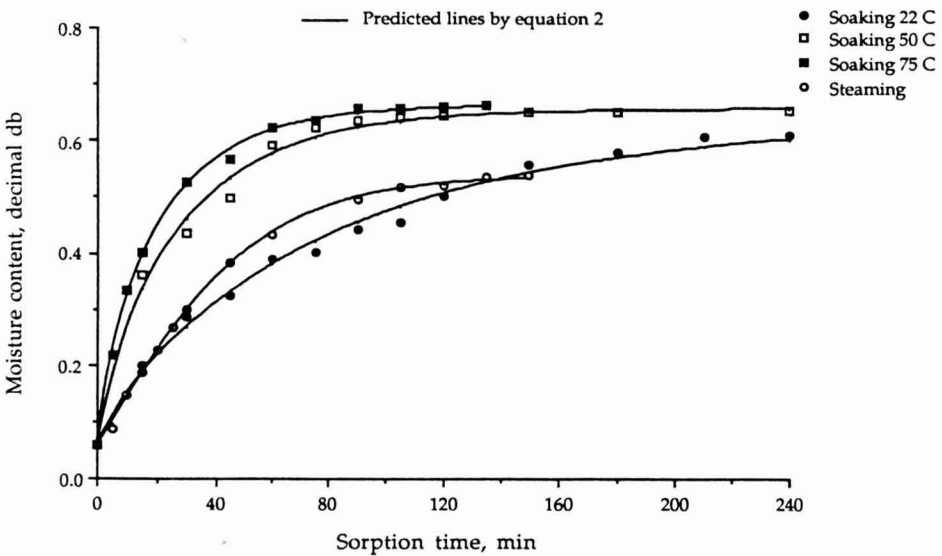


FIG. 1. RELATIONSHIP OF MOISTURE CONTENT AND SORPTION TIME FOR CANOLA

The parameters estimated for all three equations are listed in Table 2. The data were fitted better using the Page's model (Eq. 2) as indicated by low mean square error. The goodness of fit of this equation was as shown in Fig. 1 by the predicted lines. Similar observations were reported for absorption studies on lentils by Tang *et al.* (1990). The first and third equation (Peleg's model) did not fit data well, as evident from the higher MSE values. The MSE values were much higher for Peleg's equation compared to Eq. 1. The sorption constant  $k_2$  (in Eq. 2) varied with the soaking temperature. It increased 2.5 times with the increase of soaking temperature from 22C to 50C, whereas increase by 1.3 times was observed when soaking temperature was increased from 50 to 75C. The sorption coefficient due to steaming was lower than soaking even at 22C. It may be due to the fact that water absorption is faster due to liquid diffusion than vapor diffusion in fibrous hull, which was also reflected by a lower final moisture content in the case of steaming.

The relationship between rate constant  $k_2$  as calculated by best fitting model (Eq. 2) and absolute temperature for soaking was expressed by Arrhenius equation:

$$k_2 = k_0 \exp[-E_a/RT] = 267.57 \exp[-2424.2/T] \quad R^2 = 0.95 \quad (4)$$

The linear relationship was obtained when  $\ln(k_2)$  was plotted versus inverse of absolute temperature. Slope of the line represented  $E_a/R$ . Activation energy ( $E_a$ ) calculated was found to be  $20.16 \times 10^3$  kJ/kg mole.

TABLE 2.  
ESTIMATED PARAMETERS FOR SORPTION EQUATIONS FOR CANOLA AT  
DIFFERENT TEMPERATURES

Treatment	Eq. 1		Eq. 2			Eq. 3		
	k	MSE	n	k	MSE	k <sub>3</sub>	k <sub>4</sub>	MSE
Soaking								
22 C	0.0123	4.25	0.8443	0.0248	2.20	0.7065	0.0163	8.28
50 C	0.0359	3.75	0.8431	0.0635	2.96	0.1263	0.0166	21.33
75 C	0.0526	3.18	0.8365	0.0848	0.74	0.2121	0.0147	0.90
Steaming	0.0239	2.10	1.1747	0.0128	0.27	1.0362	0.0127	5.76

### Volumetric Changes in Canola

Initial volume of 10 g seed was about 9.2 ml at 0.059 moisture content and the final volume at 0.64 decimal (db) moisture content was 14.5 ml. The volume change was found to have a linear relationship with the increase in moisture content, as has been established for other agricultural products (Muthukumarappan *et al.* 1990; Tang and Sokhansanj 1993b).

The change in volume of 10 g seeds with respect to the time of soaking showed rapid increase in the volume of seeds with a soaking time of up to 120 min and then the volume remained almost constant for the rest of the soaking period of 1440 min.

The steaming was continued for 150 min. Similar to soaking, the volume of canola seeds was increased with steaming time up to about 120 min and after that there was no increase in volume until the end of 150-min steaming period.

Water absorption during soaking or steaming resulted in an increase in volume of seed. Figure 2 shows the linear relationship of volume and moisture content of seed. The coefficient of hygroscopic expansion was determined by relating volume change with per unit change in moisture by the following expression.

$$\frac{V - V_o}{V_o} = \beta_v(M - M_o) \quad (5)$$

The coefficients of cubical expansion obtained for soaking at 22, 50 and 75C temperatures and for steaming are given in Table 3. The coefficient of expansion for canola soaked at 75C is lower than for other treatments due to leaching losses at the prolonged soaking time. However, the difference in the values of  $\beta_v$  for all the conditions of soaking temperature and steaming were not significant ( $P < 0.01$ ). Therefore, Eq. 5 was fitted to the pooled data of soaking and steaming, which resulted in value of 1.032 ( $R^2 = 0.99$ ) for the coefficient of cubical expansion of canola seeds. Figure 2 shows the linear relationship of volume and moisture content of seed.

Thus the following relation was found to represent the change of volume of canola seeds:

$$\frac{V - V_o}{V_o} = 1.032(M - M_o) \quad (\text{RMSE}=0.036) \quad R^2=0.99 \quad (6)$$

The value of the hygroscopic coefficient of cubical expansion found in the case of canola is 50 times higher compared to corn (Muthukumarappan and Gunasekaran 1990). This may be due in the case of canola to the 14.5% of fibrous hull which expands more by absorbing water in its spongy intercellular spaces. The increase in moisture by 0.0 decimal (db) and increase in volume by

58% results during the sorption process, and reversal of these phenomena during a further drying process causes hydrothermal stresses in the hull which ultimately results in an efficient dehulling process.

TABLE 3  
HYGROSCOPIC COEFFICIENT OF CUBICAL EXPANSION OF CANOLA SEEDS AT DIFFERENT SOAKING TEMPERATURES OR STEAMING

Treatment	Coefficient of expansion, $\beta_v$ ( $M^{-1}$ )	RMSE	$R^2$
Soaking at			
22 C	1.052	0.0387	0.99
50 C	1.072	0.0333	0.99
75 C	0.975	0.0111	1.00
Steaming	1.026	0.0342	0.99

RMSE = Root Mean Squared Error  
M = Moisture content, decimal dry basis

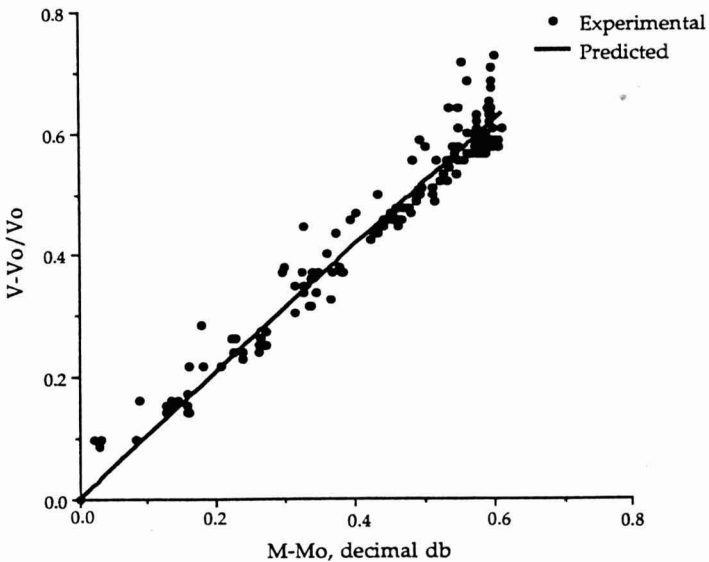


FIG. 2. RELATIONSHIP OF VOLUME AND MOISTURE CHANGE OF CANOLA DURING SOAKING OR STEAMING

## CONCLUSIONS

- (1) The moisture content has a strong effect on the expansion of canola seeds. Increasing the moisture content from 0.06 to 0.64 decimal (db) resulted in 58% seed volume expansion.
- (2) The coefficient of water absorption ( $k_2$ ) by soaking was 0.0248, 0.0635 and 0.0848 per min at 22, 50 and 75C. The coefficient  $k_2$  by steaming was 0.0128 per min. The coefficient  $n$  was 0.84 for soaking and 1.17 for the steaming operation.
- (3) The coefficient of cubical expansion  $\beta_v$  for canola seed was 1.032 per unit change in moisture on a dry basis.

## NOMENCLATURE

$M_f$	Final moisture content
$M$	Moisture content at time $t$
$M_o$	Initial moisture content
$k_1$	Sorption constants in Eq. 1
$k_{2,n}$	Sorption constants in Eq. 2
$k_3, k_4$	Sorption constants in Eq. 3
$k_o$	Preexponential or frequency factor
$E_a$	Apparent activation energy of the process, kJ/kg mole
$R$	Universal gas constant = 8.315 kJ/kmol.K
$T$	Absolute temperature in K
$V$	Volume of 10 g seeds at moisture content $M$ , $\text{cm}^3$
$V_o$	Volume of 10 g seeds at moisture content $M_o$ , $\text{cm}^3$
$\beta_v$	Coefficient of bulk volumetric expansion per unit change in moisture
$t$	Time of sorption, min

## REFERENCES

- ASAE. 1989. ASAE Standards. Am. Soc. of Agricultural Engineers, St. Joseph, MI.
- ENGELS, C., HENDRICKX, M. and TOBBACK, P. 1987. Axysymmetric TLM model for water vapor soaking of white rice. *J. Food Eng.* 6 (6), 445-454.
- HENDRICKX, M., ENGELS, C. and TOBBACK, P. 1987. Three dimensional TLM models for water diffusion in white rice. *J. Food Eng.* 6 (3), 187-197.

- MISRA, R.N. and YOUNG, J.H. 1980. Numerical solution of simultaneous moisture diffusion and shrinkage during soybean drying. *Trans. ASAE* 24, 1277-1282.
- MUTHUKUMARAPPAN, K. and GUNASEKARAN, S. 1990. Vapor diffusivity and hygroscopic expansion of corn kernels during adsorption. ASAE paper No. 906502, St. Joseph, MI.
- MUTHUKUMARAPPAN, K., JINDAL, V. K. and GUNASEKARAN, S. 1990. Volumetric changes of rice kernels during desorption and adsorption. ASAE paper No. 906549, Am. Soc. of Agricultural Engineers, St. Joseph, MI.
- PELEG, M. 1988. An empirical model for description of moisture sorption curves. *J. Food Sci.* 53 (4), 1216-1217, 1219.
- SAS. 1985. SAS User's Guide: Statistics, Statistical Analysis System Institute, Cary, NC.
- SCHULZ, E. and PETERSEN, U. 1981. Nutritive value of protein feeding stuffs from oilseed crops. In *Production and Utilization of Protein in Oilseed Crops*, (E.S. Bunting, ed.), Martinus Nijhoff Publishers, The Hague.
- SHAHIDI, F. 1990. *Canola and Rapeseed: Production, Chemistry, Nutrition and Processing Technology*, Van Nostrand Reinhold, New York.
- TANG, J. and SOKHANSANJ, S. 1993a. Moisture diffusivity in laid lentil seeds. *Trans. ASAE* 36(6), 1791-1798.
- TANG, J. and SOKHANSANJ, S. 1993b. Geometric changes in lentil seeds caused by drying. *J. Agric. Eng. Res.* 56, 313-326.
- TANG, J., SOKHANSANJ, S., SLINKARD, A.K. and SOSULSKI, F. 1990. Quality of artificially dried lentil. *J. Food Proc. Eng.* 13, 229-238.
- THAKOR, N.J. 1993. Dehulling of canola by hydrothermal treatments. Ph.D. thesis, University of Saskatchewan, Saskatoon, Canada.
- THAKOR, N.J., SOKHANSANJ, S. and YANNACOPOULOS, S. 1992. Instantaneous dimensional changes of a grain kernel during drying using dilatometry and thermogravimetry. ASAE Paper No. 92-6559 Am. Soc. of Agricultural Engineers, St. Joseph, MI.

# ADSORPTION OF BILE ACIDS ON CEREAL TYPE FOOD FIBERS

CHAO-MING HUANG

*Department of Chemical Engineering  
University of Missouri-Columbia  
Columbia, Missouri 65211*

and

NILUFER H. DURAL<sup>1</sup>

*Department of Chemical Engineering  
Cleveland State University  
Cleveland, Ohio 44115*

Received for Publication August 18, 1994

## ABSTRACT

*A study involving measurement and analysis of adsorption of common bile acids, namely cholic, deoxycholic, and lithocholic acids, on cereal type dietary fibers was conducted. The selected food fibers were oat fiber, rice fiber, barley fiber, corn bran, and wheat bran, which are all extensively used in processed foods. The adsorption data were measured at 37C and 25C, which correspond to approximate human body and room temperatures. Influence of particle size reduction, due to grinding, on a fiber's bile acid binding capacity was examined by using macro size (35–60 mesh) and micro size (100–300 mesh) fibers as adsorbents. The investigation also included the effects of medium pH and the chemical composition. The experimental data were correlated with the Langmuir and the Freundlich isotherms in order to utilize the data in future predictions and simulations.*

*It was found that the particle size reduction, accompanied by surface area increase, has a significant influence on the adsorption capacity of the fiber. Macro size fibers adsorbed the same bile acid with the following trend: oat > barley > rice > wheat > corn; while micro size fibers followed a somewhat different trend: rice > barley > oat > wheat > corn. This was due to the surface area change after grinding, and a positive correlation between the surface area and the adsorption capacity was observed in each case. The adsorption was favored by acid pH surroundings, and it was positively correlated with the hydrophobicity of the bile acid. In all cases, the bile acids*

<sup>1</sup>To whom correspondence should be directed: 1960 East 24th St., Stillwell Hall 455.

*were adsorbed on the same fiber with the following trend: lithocholic acid > deoxycholic acid > cholic acid. Fibers adsorbed more bile acid at 25C than they did at 37C. However, the increase in the uptake capacities were not very significant.*

## INTRODUCTION

The physiological claims for dietary fiber in maintaining health and preventing disease has become a subject of increased public attention. With the observed relationships between atherosclerotic heart disease, colon cancer and dietary fiber (Kirby *et al.* 1981; Burkitt *et al.* 1974), interest has been focused on the role played by dietary fiber in bile acid metabolism. Some dietary fiber containing foods and some isolated components of dietary fiber have the ability to adsorb bile acids and salts (Ebihara and Schneeman 1989; Weber and Chaudhary 1987; Mongeau and Brassard 1982; Story *et al.* 1982; Vahouny *et al.* 1980; Oakenfull and Fenwich 1978). This adsorption has been theorized to cause increased fecal bile excretion and in turn reduction in serum and tissue cholesterol (Story *et al.* 1979; Story 1980). Accordingly, increased bile acid excretion necessitates increased synthesis of bile acids from cholesterol (Story *et al.* 1979). In support of this theory, fecal bile acid and neutral sterol excretion has been shown to increase when various sources of fibers are fed to animals (Story *et al.* 1979; Story 1980; Kritchevsky and Story 1974; Shinnick *et al.* 1990; Illman 1985; Birkner and Kern 1974; Nishina *et al.* 1991; Nishina and Freeland 1990; Story and Kritchevsky 1976; Calvet and Yeates 1982; Nagyvary *et al.* 1980).

The chemical composition of a dietary fiber is known to influence its adsorption characteristics. The components of dietary fiber that are responsible for this influence have not yet been clearly identified, however, work of early investigators provided some clues. Isolated lignin has been shown to be active in adsorbing bile acids (Story and Kritchevsky 1976; Calvert and Yeates 1982). On the other hand, other isolated components of dietary fiber have also been shown to increase bile acid excretion (Nagyvary *et al.* 1980; Kelley *et al.* 1981). Birkner and Kern (1974) compared the adsorption of glycholic and chenodeoxycholic acids to nondigestible food residues. They concluded that the adsorption was hydrophobic and it was a monomolecular process. Story *et al.* (1982) supported the hydrophobic nature of the adsorption and reported that lignin was an important component in the interaction of dietary fiber and bile acids while holocellulose also played a significant role. All these results indicate the complexity of the interaction of dietary fiber and bile acid micelles and their subsequent effects on sterol balance.

While the focus of the preponderance of research has been on the relationship between the chemical composition of the fiber and its uptake

capacity, studies including the impact of physical properties of the fiber are generally lacking. Processing of foods can alter the physical characteristics of the plant fiber, and thus influence the degree of microbial degradation and the ability of the fiber to adsorb water and organic compounds (Mongeau and Brassard 1982; Cadden 1987; Eastwood and Robertson 1981; Rasper 1982). It is well established that the total surface area of a porous solid plays an important role in determining its adsorption capacity; thus, if the fiber porosity is affected by the processing treatment, such as grinding, this capacity may be greatly influenced. Mongeau and Brassard (1982) reported that insoluble dietary fiber from wheat bound less bile salts and held less water when its mean particle size is reduced, suggesting a negative alteration of the physicochemical characteristics of the fiber during grinding. Typically, reducing the particle size of an adsorbent material results in micropore opening, thus larger total surface area. Consequently, the adsorption uptake increases. However, if the particle size reduction leads to collapse of the fiber matrix and a consequent decrease in the total surface area available for adsorption, then a negative influence on the binding capacity may be observed. Thus, independent measurements of the total surface area of a food fiber before and after grinding is essential to evaluate the impact of the grinding on the fiber's adsorption capacity.

There is no doubt that dietary fiber is an important component of our diets and it is actively involved in bile acid and cholesterol metabolism. A systematic investigation of the bile acid adsorption behavior of food fibers can provide a great deal of useful information about the fibers' therapeutic use. Such knowledge enables the food processors to select the fiber types that increase the bile acid binding capacity in the gastrointestinal tract. Therefore, the present study was undertaken with the aim to examine the adsorption of bile acids on several cereal type food fibers, and to evaluate the impact of various factors involved, including particle size reduction, medium pH, temperature, and chemical composition.

## EXPERIMENTAL SECTION

### Materials

All fiber samples (adsorbents) used in the present study were supplied by the Canadian Harvest Co. in macro (35–60 mesh; i.e., number of openings per inch) and micro (100–300 mesh) sizes. In this way, the fiber compositions were identical with those of corresponding products sold commercially. The specifications of the fiber samples as received from Canadian Harvest are presented in Table 1. Bile acids were obtained from the Sigma Chemical Co. with purities 98% or higher by thin layer chromatography.

TABLE 1.  
SPECIFICATIONS OF THE FIBER SAMPLES EXAMINED (\*)

Fiber Source	Oat	Barley	Rice	Wheat	Corn
Uses in food industry (**)	1,2,5,6	1,3,6	1,2,5,6	1,2,3,4,6	1,2,3,6
Total dietary, fiber %	80	70	60	43	65
Crude fiber, %	40	27	30	10	15
Protein, %	1.5-2.5	4.0-6.0	2.0-3.5	16.0-19.0	4.0-6.0
Carbohydrates, %	0.0	8.0-12.0	10.0-12.0	16.0-17.0	18.0-22.0
Ash, %	4.0	7.0	19.0	6.0	0.5
Fat, %	0.5	1.0-2.0	0.5-1.0	4.0-6.0	1.0-2.0
Moisture, %	5-9	5-9	5-9	5-9	5-9
Calories, cal/g	0.34	0.70	0.60	1.80	1.13
Yeast, max/g	100	100	100	100	100
Mold, max/g	100	100	100	100	100

(\*) Analysis provided by the Canadian Harvest Co.

(\*\*) 1. Baked goods; 2. Cereals; 3. Supplements; 4. Pharmaceuticals; 5. Pasta; 6. Mixes.

## Methods

**Adsorption Measurements.** Experimental methods of study for adsorption from solutions are based on the determination and comparison of the concentration of a substance in a solution before and after this solution is brought into contact with the adsorbent. While adsorption equilibrium is being established, the solution is vigorously agitated to ensure uniformity. The equilibrium time is found from kinetic batch studies. After the equilibrium is established, the solution is usually centrifuged or filtered before the concentration is measured. Therefore, in the present study, adsorption of bile acids by dietary fibers were estimated from the change in bile acid concentration on exposure of the solution to the fiber as outlined below.

Prior to the experiments, the fiber samples were oven dried and kept in vacuum desiccators. Bile acids were dissolved in 0.1 M phosphate buffer ( $\text{NaH}_2\text{PO}_4\text{-Na}_2\text{HPO}_4$ ) at pH 6.9. The selection of buffer pH was based on the pH profile of intestinal juice of the small intestine, which varies from 4.0 to 8.3 and is commonly around 6.9 (Lenter 1981).

A 0.5 g of fiber sample and 20 ml of buffered bile acid solution were added to a 125 ml of stoppered Erlenmeyer flask. In a typical experiment, 12 solutions were prepared containing different concentrations of bile acids, ranging from 1 mM to 12 mM. This concentration range was determined based on the typical bile acid concentrations in the human proximal and terminal ileums where the bile acids are absorbed and returned to the liver in the portal vein

(Lenter 1981; Eastwood and Boyd 1967). Two additional flasks were included: one flask contained bile acid solution without fiber, for use as a standard; the other flask was prepared by mixing 0.5 g of fiber with 20 ml buffer solution, as the blank.

Each incubation was carried out at constant temperature (37C and 25C), until equilibrium was reached (approximately 4 h), in a reciprocating shaker bath fitted with a thermostat. The system was agitated at a rate which ensured that the fiber sample was mixed well with the solution during the experiment. At the end of the shaking period, the supernatant was cleared with filtration, and aliquots were taken for bile acid estimation. Experiments were carried out in duplicate; the final pH was checked after each adsorption experiment and found to be varying from 6.80 to 6.87.

In calculating the adsorption equilibrium uptake, it was assumed that the solution was uniformly distributed throughout the pores of the adsorbent and the supernatant, and that any decrease in the bile acid concentration of the supernatant was due to the adsorption of the bile acids by the fiber.

Prior to the equilibration experiments, the equilibrium time for each fiber-bile acid pair was determined from the sorption rate studies by repeating the procedure above, at several time intervals, until the saturation was observed.

**Bile Acid Estimations.** Bile acid concentrations were measured by using the colorimetric method described by Boyd *et al.* (1966), which involves spectrophotometric analysis by a modified Pettenkofer reaction. A 5 ml aliquot of the supernatant was mixed with 5 ml of 70% sulfuric acid. Two minutes later 1 ml of 25% aqueous furfural solution was added. A pink color appeared and took 5 min to develop to maximum intensity. The solution was poured into 1/2" 11 ml spectrophotometer cuvette of Milton Roy Spectronic 20 spectrophotometer. Readings were made at the absorbance maximum of 510 nm.

**Buffer and pH.** The effect of pH on the adsorption was studied by conducting the experiments at various pH levels. The minimum pH levels were 4.6 for cholic acid, 6.1 for deoxycholic acid, and 5.5 for lithocholic acid, because of the limited solubility at these levels. The maximum pH was selected to be 8.0, which represented the maximum pH level of intestinal juice of the small intestine (Lenter 1981). These tests were carried out with 20 ml of 1 mM bile acid solution on macro size fibers at 37C.

**Surface Area Determination.** Specific surface areas of the fibers were determined independently by using an automated BET sorptometer (Porous Materials, Inc.). The experimental measurements were based on the physical adsorption of nitrogen gas by the fiber samples at liquid nitrogen temperature (-195.8C). The amount of adsorbed gas corresponding to the monolayer

coverage (between equilibrium relative pressure values of 0.05–0.35) was estimated by the BET analysis (Brunauer 1938). Knowing the monolayer value, the total surface area per unit mass of fiber sample was calculated from the effective cross-sectional area of a nitrogen molecule ( $16.2 \text{ \AA}^2$ ).

## RESULTS AND DISCUSSION

### Adsorption Equilibrium Isotherms

Adsorption isotherms describing the binding tendencies of cholic acid, deoxycholic acid and lithocholic acid on wheat bran, corn bran, oat fiber, barley fiber and rice fiber were obtained at 37C and 25C, using macro size (35–60 mesh) and micro size (100–300 mesh) fiber samples. Equilibrium uptake values were determined using a wide initial concentration range, typically from 1 mM to 12 mM. This resulted in a final equilibrium concentration range from 0.016 mM to 6.872 mM, including the bile acid concentration range in the human proximal and terminal ileums (Lenter 1981). Therefore, the adsorption isotherms generated at 37C provide useful information for simulation of bile acid adsorption by dietary fibers in the gastrointestinal tract. The isotherms measured at 25C provide additional information that enables one to evaluate the heat of adsorption, which is an indication of the binding energy of the process.

For all dietary fiber-bile acid pairs examined, the isotherms were type I according to BET classification. They were convex in shape and showed a tendency to reach a plateau at high equilibrium concentrations, indicating that the system was approaching to the limiting monomolecular capacity of the fiber for the bile acid adsorption. The equilibrium isotherms at 37C describing the adsorption of cholic acid, deoxycholic acid and lithocholic acid on the dietary fibers investigated are presented in Fig. 1a through 2c.

The reproducibility of the experimental isotherms was examined selectively, by performing two adsorption experiments with the same fiber-bile acid pair. Several data points were reproduced within the limits of experimental error, which was no greater than 5%.

### Influence of Chemical Composition

**Major Constituents of Dietary Fiber.** The adsorption isotherms of a specific bile acid on the five food fibers were qualitatively similar, but the equilibrium uptakes corresponding to the same equilibrium concentration was different. As shown in Fig. 1, which describes the adsorption of cholic, deoxycholic and lithocholic acid on macro size fibers at 37C, different fibers adsorbed the same bile acid with the following trend: oat > barley > rice > wheat > corn. Analysis of the isotherms of the same pairs measured at 25C, as

presented in Fig. 3, also exhibited the same trend. The different uptake capacities of the fibers can be attributed to both the distribution of the major constituents and the physical structure of the fiber. The microsize fibers, on the other hand, adsorbed the bile acids with a somewhat different trend: rice > barley > oat > wheat > corn (Fig. 4-6). This was due to the surface area change after grinding, which will be discussed in a later section.

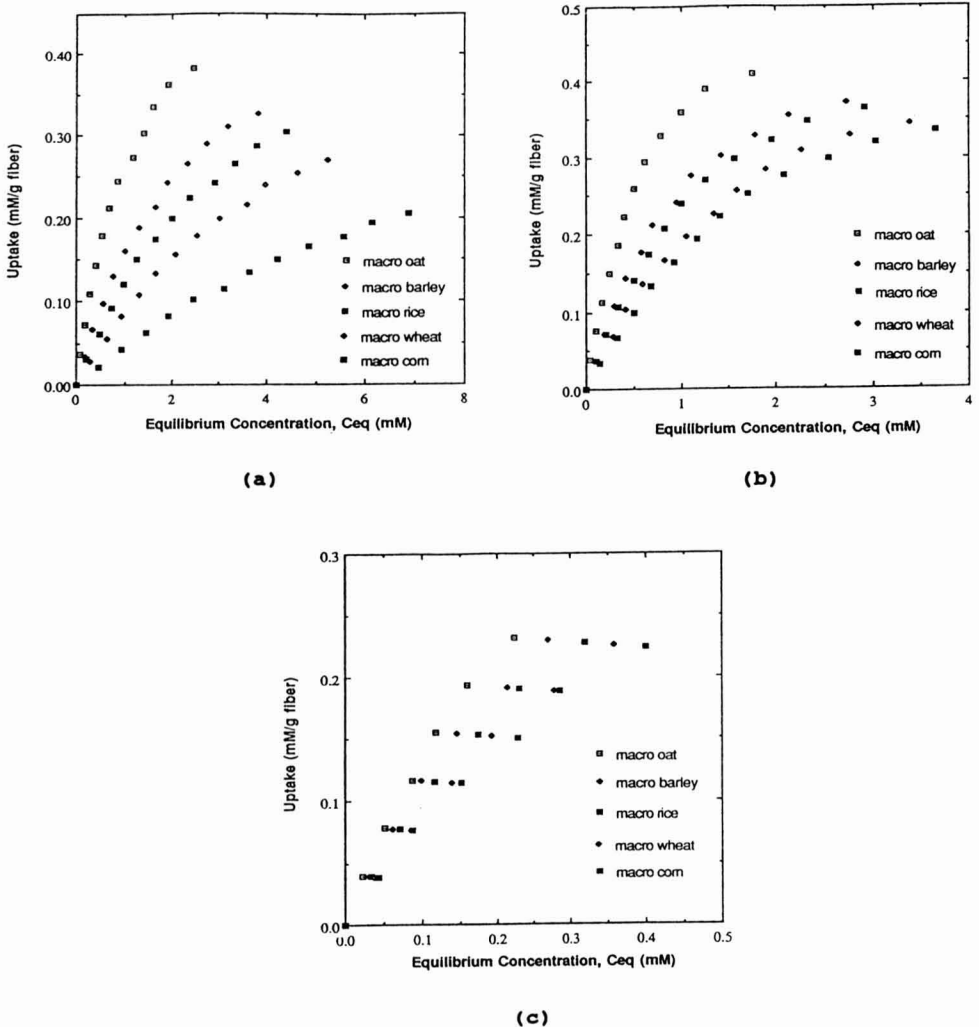


FIG. 1. ADSORPTION OF BILE ACIDS ON MACRO SIZE DIETARY FIBERS AT 37C (pH: 6.9)

(a) Cholic Acid; (b) Deoxycholic Acid; (c) Lithocholic Acid.

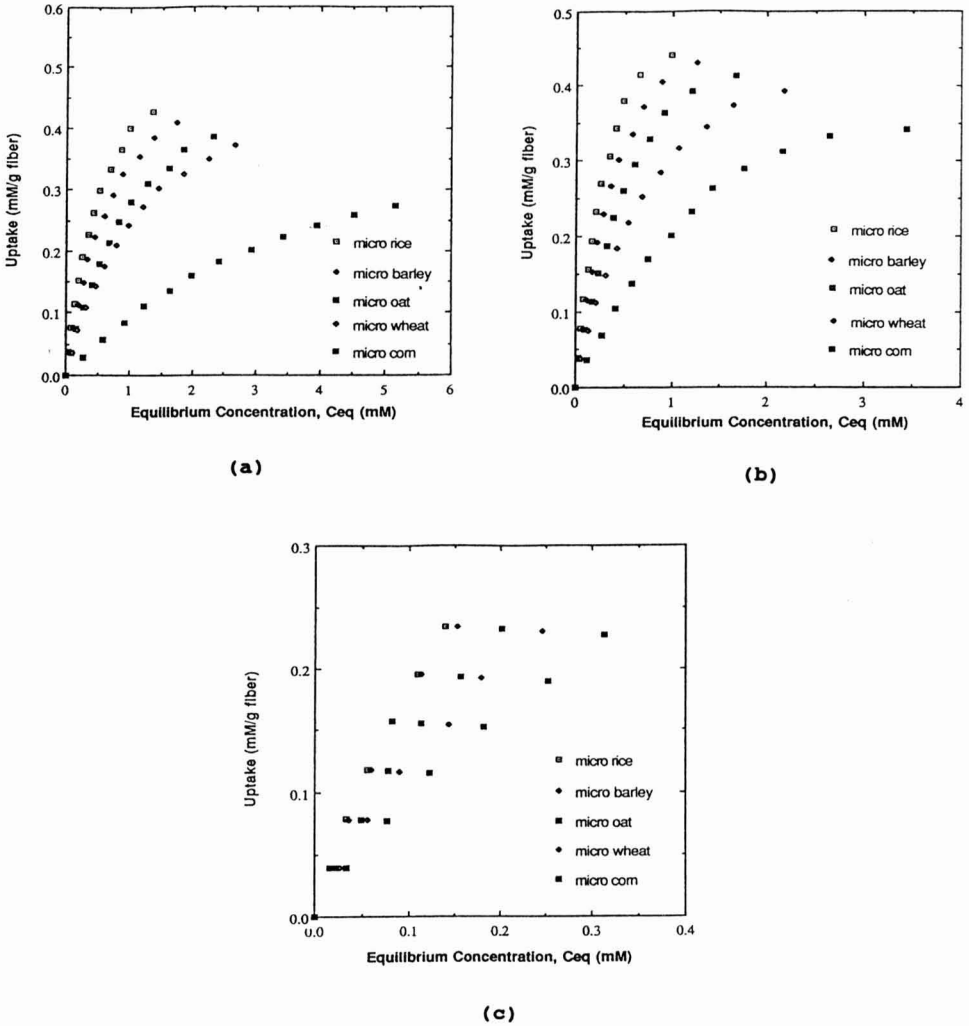
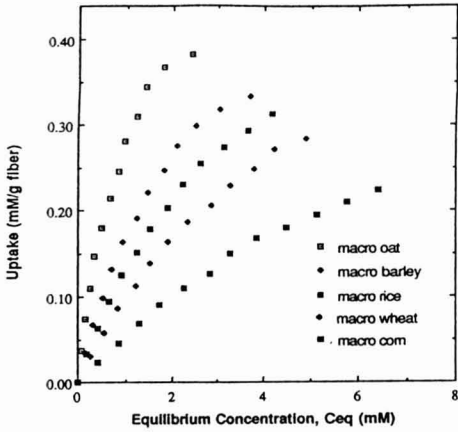
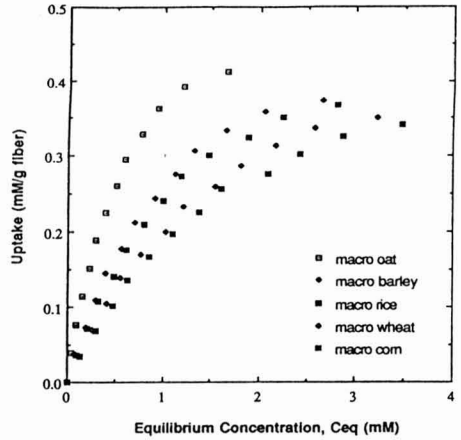


FIG. 2. ADSORPTION OF BILE ACIDS ON MICRO SIZE DIETARY FIBERS AT 37C (pH: 6.9)  
(a) Cholic Acid; (b) Deoxycholic Acid; (c) Lithocholic Acid.

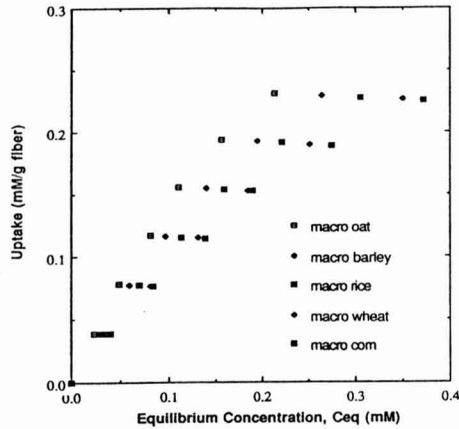
The total dietary fiber (TDF) and crude fiber (CF) percentages of each sample are reported in Table 1. The TDF values from the bread-and-cereal group correspond primarily to the hemicellulose, lignin and cellulose contents,



(a)



(b)



(c)

FIG. 3. ADSORPTION OF BILE ACIDS ON MACRO SIZE DIETARY FIBERS AT 25C (pH: 6.9)

(a) Cholic Acid; (b) Deoxycholic Acid; (c) Lithocholic Acid.

while for the fruit-and-vegetable groups, the pectic substances should also be included. The CF is the inert residue which remains after the sample is treated with a solvent, hot acid, and hot alkali, and it is composed basically of the lignin

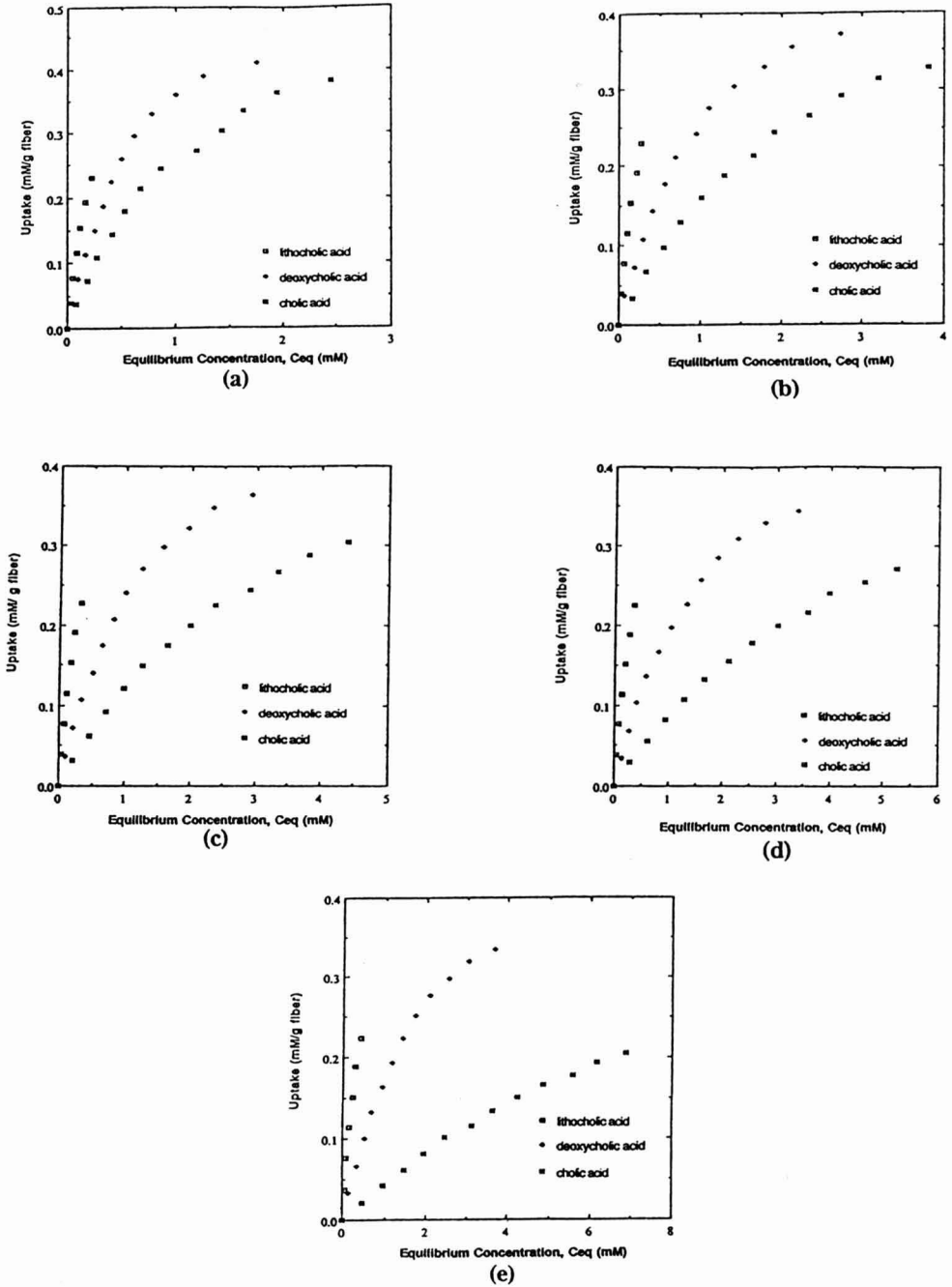


FIG. 4. COMPARISON OF CHOLIC ACID, DEOXYCHOLIC ACID AND LITHOCHOLIC ACID ADSORPTION ON MACRO SIZE FIBERS AT 37°C (Initial Concentration Range: 1–12 mM; pH: 6.9). (a) Oat; (b) Barley; (c) Rice; (d) Wheat; (e) Corn.

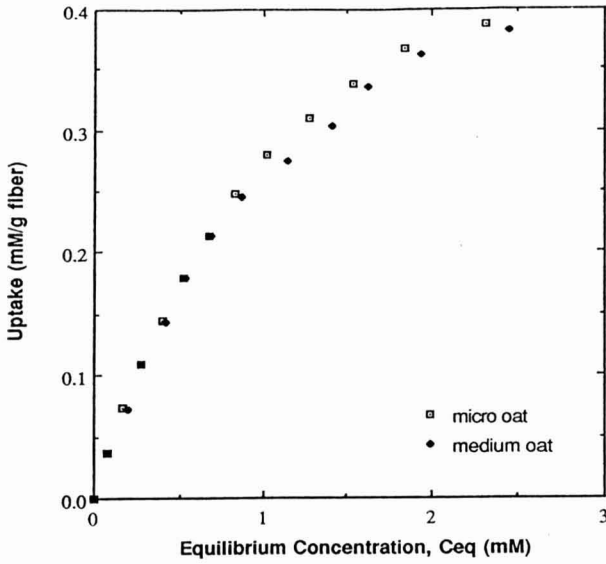


FIG. 5. INFLUENCE OF PARTICLE SIZE REDUCTION ON CHOLIC ACID ADSORPTION BY OAT FIBER AT 37C (pH: 6.9)

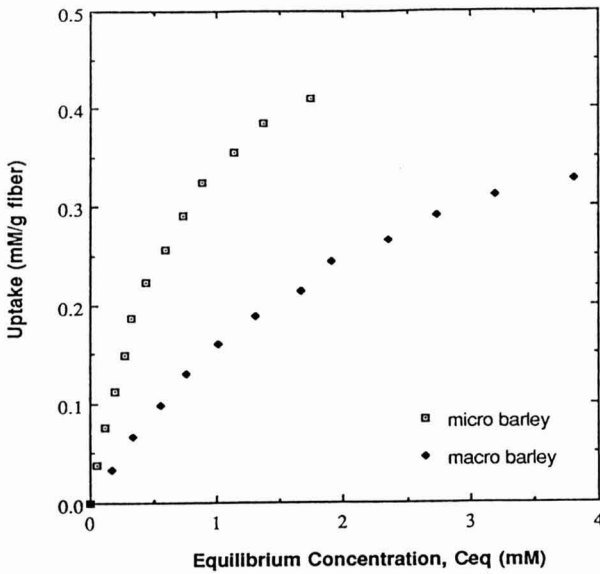


FIG. 6. INFLUENCE OF PARTICLE SIZE REDUCTION ON CHOLIC ACID ADSORPTION BY BARLEY FIBER AT 37C (pH: 6.9)

and most of the cellulose in the food being analyzed (Baker *et al.* 1979). Thus, the CF percentages given in Table 1 correspond primarily to the crude cellulose and crude lignin of the samples. The difference between the TDF and CF values is an estimate of hemicellulose content. The approximate ratio of crude fiber to total dietary fiber of corn, wheat, rice, barley and oat fibers are 0.23, 0.24, 0.50, 0.39, and 0.50, respectively. These estimates are comparable to the exact compositions obtained by Rasper (1979), who determined the composition of dietary fibers obtained from wheat, rice, barley, oat and corn brans and rye middlings, by the procedure of Southgate (Southgate 1969). According to the results of his analyses cellulose-lignin to total dietary fiber ratios of corn, wheat, rice, barley and oat fibers are 0.27, 0.32, 0.53, 0.46, and 0.47, respectively. With the exception of rice fiber, the trend of these ratios is the same as the trend of bile acid adsorption capacities of the macro size fibers. Thus, it may be suggested that the crude fiber content (cellulose + lignin) is positively correlated with the fiber's bile acid binding capacity. It is interesting to note that in a previous investigation (Dural and Hines 1993), an opposite trend was observed for the water sorption capacities of the fibers, confirming the hydrophobic nature of the bile acid sorption process.

Further examination of the analyses of Rasper (1979) and Table 1 shows that, with the exception of barley bran, the lignin content of the fibers has the same inclination with the decreasing order of bile acid adsorption. This result implies that lignin has the strongest bile acid binding capacity among the food fiber constituents, and is in agreement with the claims of some previous investigators (Story *et al.* 1982; Story and Kritchevsky 1976). Barley bran, although low in lignin content, has the highest cellulose content and the second highest adsorption capacity among the fibers used in this study. This result contradicts with some previous claims that cellulose may have little effect on binding bile acids (Vahouny *et al.* 1980; Story and Kritchevsky 1976). However, chemical composition is not the only factor that influences bile acid adsorption. Other factors such as the fiber matrix, porosity, surface heterogeneity and the adsorption field strength are also significant. Specific surface area measurements, which will be discussed in a later section, showed that barley bran has the second highest surface area among the fibers. Therefore, the high adsorption capacity observed in spite of the low lignin content may be attributed to the physical characteristics.

Hemicellulose content appeared to be negatively correlated with the bile acid binding tendencies of the fibers. However, based on the findings of a previous investigator (Birkner and Kern 1974), it may be suggested that although hemicellulose is responsible for a certain degree of adsorption, it is not very significant. Abundance of hemicellulose in the fiber results in low crude fiber contents, which in turn decreases its bile acid sorption capacity.

**Bile Acid.** Influence of the type of the bile acid on the fiber's sorption capacity was investigated. Sample results illustrating the adsorption of cholic, deoxycholic, and lithocholic acids on the same fiber (for macro size oat, barley, rice, wheat, and corn) at 37C are presented in Fig. 4a-e. As one can see from the figures, food fibers adsorbed appreciable quantities of lithocholic acid in comparison to deoxycholic acid and cholic acid adsorption. Results obtained at 25C and for micro size samples also showed the same behavior. In all cases, the following trend was observed: lithocholic acid > deoxycholic acid > cholic acid.

This trend is directly related to the extent of the forces involved in the binding process, which demonstrates that lithocholic acid interacts significantly with the binding sites on fibers. All three bile acids investigated contain a-hydroxyl group in the 3 position of the steroid nucleus. In addition to the 3-a-hydroxyl group, deoxycholic acid possesses a 12-a-hydroxyl group while cholic acid has 12-a-hydroxyl and 7-a-hydroxyl groups. The presence of additional hydroxyl group causes an increased degree of polarization of the steroid ring structure. Thus, cholic acid is more easily soluble in water than the others and lithocholic acid is the most hydrophobic. The results obtained in this study are consistent with the structure effect in that the most hydrophobic bile acid (lithocholic acid) is the most strongly held by the dietary fibers. It means that the more the number of hydroxyl groups on the steroid nucleus, the lower the affinity of the bile acid to the dietary fiber.

### **Influence of Particle Size Reduction**

Effect of particle size reduction on the fiber's bile acid adsorption capacity was investigated by performing experiments with macro (35-60 mesh) and micro (100-300 mesh) size fibers at 37C. Comparisons of cholic acid adsorption on different size fibers are presented in Fig. 5 through 9 as illustrating examples. Deoxycholic acid and lithocholic acid adsorption yielded qualitatively similar results which can be seen from Fig. 1 and 2.

Following the particle size reduction, an increase in the equilibrium uptake was observed for each bile acid-fiber pair, implying an increase in the surface area available for adsorption due to micropore opening. However, the changes in the sorption capacity of rice and barley fibers were much more pronounced than the ones in other fibers (Fig. 6 and 7), and in the case of oat fiber this change was minimal (Fig. 5). While macro fibers adsorbed bile acids with the trend oat > barley > rice > wheat > corn, micro fibers adsorbed in the following order: rice > barley > oat > wheat > corn.

In order to gain a better understanding of the trends above, the specific surface area of each fiber sample was determined independently by using a BET sorptometer surface analyzer with nitrogen gas at liquid nitrogen temperature as

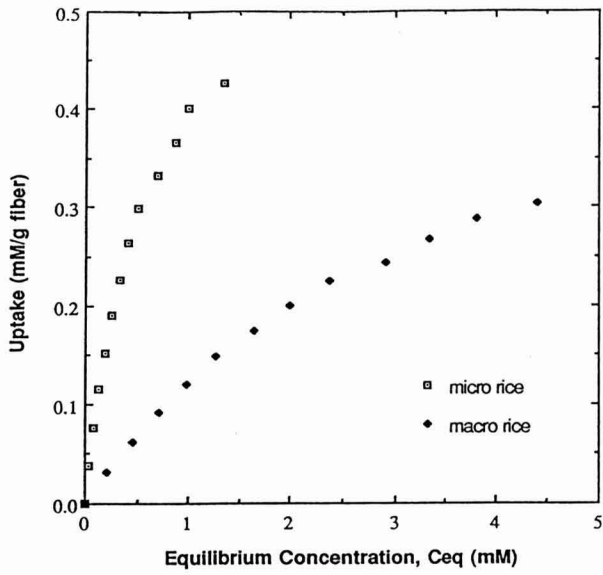


FIG. 7. INFLUENCE OF PARTICLE SIZE REDUCTION ON CHOLIC ACID ADSORPTION BY RICE FIBER AT 37C (pH: 6.9)

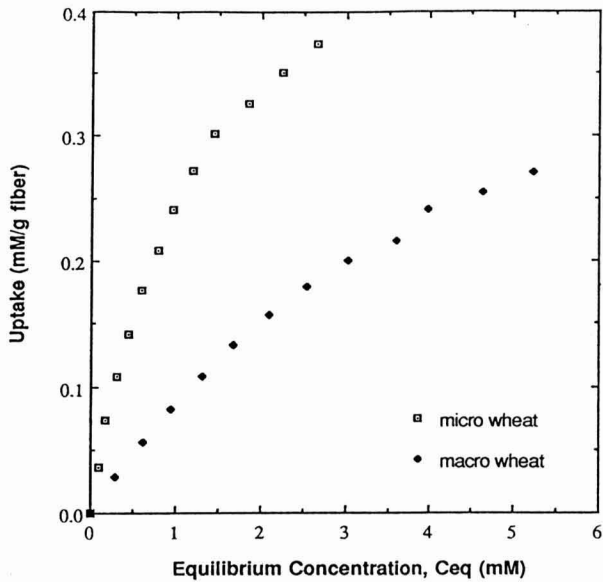


FIG. 8. INFLUENCE OF PARTICLE SIZE REDUCTION ON CHOLIC ACID ADSORPTION BY WHEAT FIBER AT 37C (pH: 6.9)

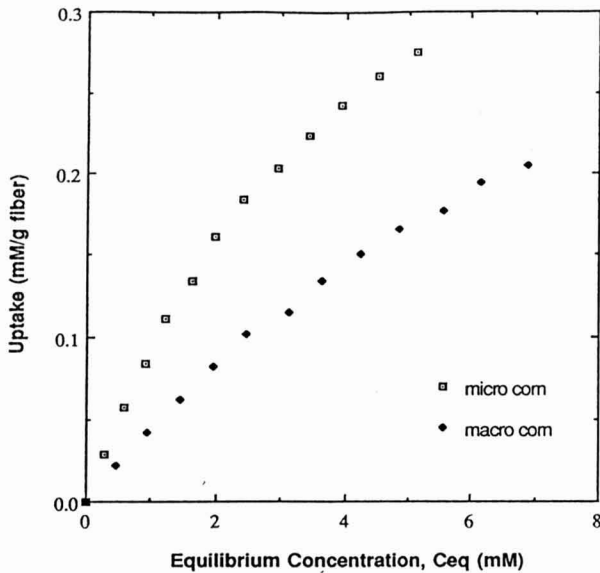


FIG. 9. INFLUENCE OF PARTICLE SIZE REDUCTION ON CHOLIC ACID ADSORPTION BY CORN FIBER AT 37C (pH: 6.9)

the adsorbent. Details of this procedure were given in the ‘Experimental Section’.

Results of the surface area analyses are presented in Table 2. As can be seen from these results, particle size reduction increased the surface area of all fibers; consequently, higher adsorption capacities were observed. However, increase in the rice fiber’s surface area was the highest, ranking at the top among other micro size fibers, and it was followed by barley fiber. Macro and micro size corn fibers had the smallest surface areas among the macro and micro size fibers, respectively. Thus, they adsorbed the least amounts in their respective groups (Fig. 1 and 2), although micro size corn fiber adsorbed more than the macro size one, due to its increased surface area (Fig. 9). In fact, the trends of the specific surface areas of micro and macro size fibers, shown in Table 2, are in complete agreement with the trends of their adsorption capacities. Therefore, the reason for the fibers adsorbing with a different trend after grinding is due to their resultant specific surface areas.

Further examination of Table 2 and Fig. 5–9 shows that the change in the sorption capacity is positively correlated to the change in the surface area. For instance, rice fiber exhibited the maximum surface area increase due to grinding (from 35.25 m<sup>2</sup>/g to 51.12 m<sup>2</sup>/g: 45% increase), while oat fiber did the

minimum one (from 46.50 m<sup>2</sup>/g to 46.79 m<sup>2</sup>/g: 0.6% increase). As a result, rice fiber had the largest uptake capacity increase (Fig. 7) while oat fiber had the smallest one (Fig. 5). Similar observations were made for all bile acid-fiber pairs.

TABLE 2.  
SPECIFIC SURFACE AREA AND DENSITY OF THE FIBER SAMPLES

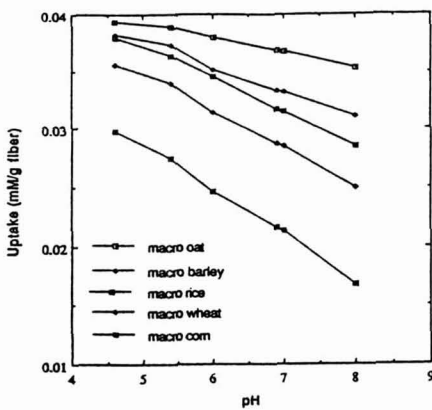
Fiber Type	Surface Area (m <sup>2</sup> /g)	Density (g/ml)
Macro Size Fibers		
Oat	46.50	0.34
Barley	37.90	0.31
Rice	35.25	0.34
Wheat	32.89	0.50
Corn	30.55	0.59
Micro Size Fibers:		
Rice	51.12	0.29
Barley	49.54	0.21
Oat	46.79	0.54
Wheat	42.91	0.39
Corn	33.39	0.52

The findings presented in this section clearly demonstrate that a fiber's specific surface area plays the major role in its bile acid sorption capacity, although its chemical composition has an impact on the strength of the binding forces. Thus, grinding or similar processing operations have an influence on the sorption behavior of food fibers. However, the nature and the degree of such influence depends on the degree of grinding as well as the specific fiber type; i.e., whether the surface area increases or the fiber matrix collapses. Studies involving total surface area determination and pore size distribution measurement before and after grinding or other processing treatments can be useful in predicting the changes in the adsorption capacity. This may lead to determination of the optimum particle size and/or other processing conditions for a fiber in terms of maximum bile acid sorption capacity. Also such approach may lead to a better understanding of the contradictory findings about the bile acid binding ability of wheat bran in relation to particle size (Mongeau and Brassard 1982; Kritchevsky and Story 1974; Eastwood *et al.* 1983; Gallaher and Franz 1990; Tarpila *et al.* 1978; Reddy *et al.* 1980).

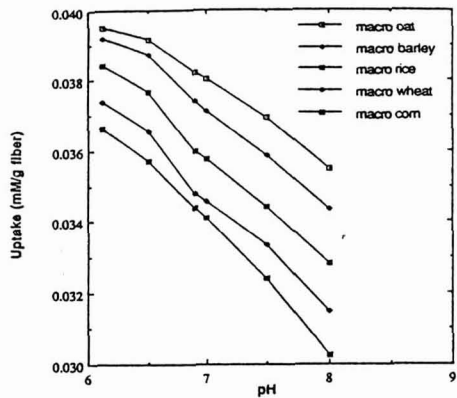
During the surface area measurements, solid density of the fibers were automatically determined through the BET sorptometer. These values are also reported in Table 2. However, no specific correlation between the fiber's density and its bile acid sorption capacity was observed.

**pH Effect**

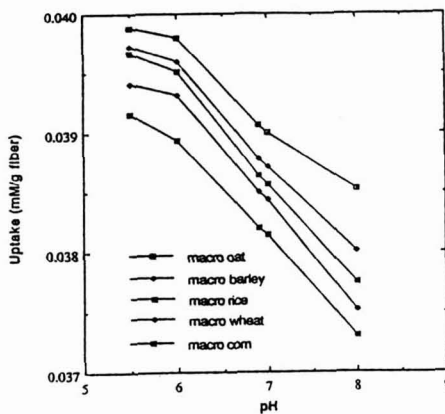
Food fibers interact with the bile acids in the human small intestine where the pH levels varies from 4.0 to 8.3 (Reddy *et al.* 1980). In Fig. 10, influence of the medium pH on bile acid adsorption behavior of various dietary fibers is illustrated for 1 mM initial concentration. Accordingly, equilibrium uptake is negatively correlated to pH. All of the fibers studied have their maximum adsorption capacities at acid pH where bile acids are of limited solubility. At alkaline pH, all bile acids are so easily soluble that the adsorptions are minimal. These results support the observations of previous investigators (Birkner and Kern 1974) that food residues bond significant amounts of bile salts and acids at low pH.



(a)



(b)



(c)

FIG. 10. pH EFFECT ON ADSORPTION OF BILE ACIDS ON DIETARY FIBERS AT 37C  
 (a) Cholic Acid; (b) Deoxycholic Acid; (c) Lithocholic Acid.

### Temperature Effect

Influence of temperature was investigated by conducting experiments at 37C and 25C. This provided data to determine the energy required for the adsorption process and to evaluate the heat sensitivity of the system. Since physical adsorption is an exothermic process, decreasing the temperature results in an upward shift of the sorption isotherm. This effect is illustrated for cholic acid-macro size rice fiber in Fig. 11. Other pairs yielded similar results, as can be observed by comparing Fig. 1 and 3. However, the isotherm shift due to the temperature change was not very significant, ranging from 1% to 5.2%. It was concluded that the systems studied herein were not highly temperature sensitive.

Heat of adsorption is a differential quantity that is directly related to the energy interaction between the adsorption mechanisms involved. Knowing the amount of bile acid adsorbed at different temperatures, the isosteric heat of adsorption for each pair was calculated in the usual manner from the Clasius Clapeyron relationship. A detailed description of the calculational procedure for liquid phase adsorption is given by Farrier *et al.* (1979).

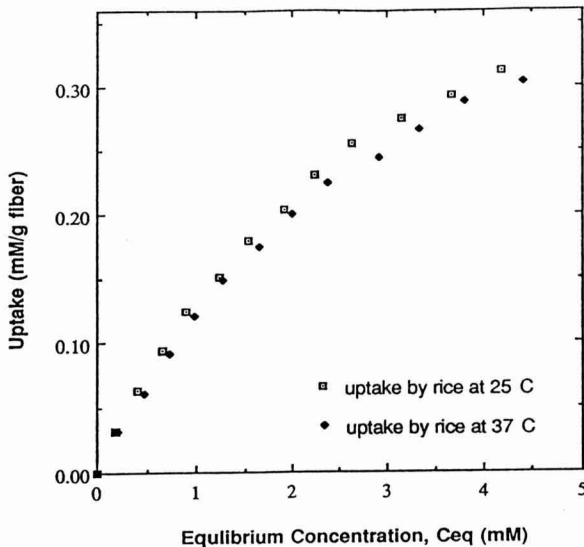


FIG. 11. TEMPERATURE EFFECT ON ADSORPTION OF CHOLIC ACID BY MACRO SIZE RICE FIBER (pH: 6.9)

Figure 12 shows the average magnitudes of isosteric heat of adsorption of the bile acid-fiber pairs examined. Relatively low heat of adsorption values (0.92–3.31 kcal/mole) are the indication of low binding energy involved for the adsorption. For each fiber, the values of heat of adsorption were in the following order: cholic acid > deoxycholic acid > lithocholic acid. This may be due to the magnitude of the strength of affinity; that is, the more interaction that exists between bile acid and water molecules, the more the heat will be released when the bile acid is adsorbed by the fiber. For instance, cholic acid has the strongest affinity to water molecules among the other bile acids, since it has three hydroxyl groups on its steroid ring; thus, its heat of adsorption is the largest on the fibers. However, for the same reason, less cholic acid was adsorbed, as discussed previously.

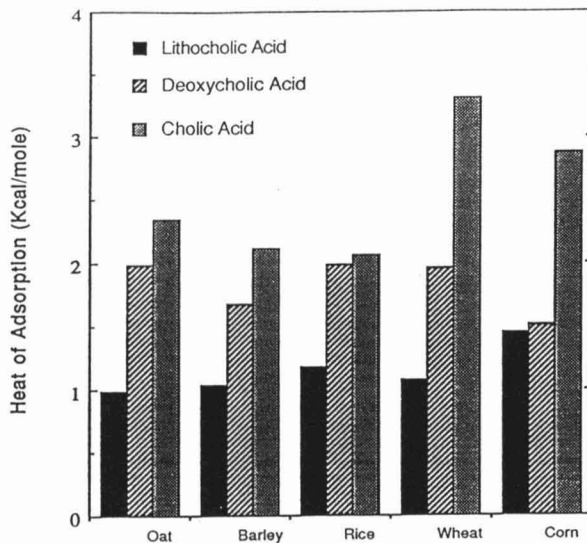


FIG. 12. AVERAGE MAGNITUDES OF ISOSTERIC HEAT OF ADSORPTION OF THE FIBER-BILE ACID PAIRS EXAMINED

### Adsorption Data Correlation

The experimental data were correlated by the Freundlich (1926) and the Langmuir (1938) isotherm models for future simulations. Probably the most widely used model for liquid phase adsorption, particularly in the low to intermediate concentration range, is the Freundlich equation. It is expressed as

$$q = K(C_{eq})^{1/n} \quad (1)$$

where  $q$  is the uptake of adsorbate per unit weight of adsorbent,  $C_{eq}$  is the equilibrium adsorbate concentration,  $K$  is a constant for the adsorbate-adsorbent system, and  $n$  is another constant that is restricted to values greater than unity. By taking mathematical transform of Eq. (1), a plot of  $\ln q$  versus  $\ln C_{eq}$  yields a straight line. Using the least squares regression, the value of  $n$  and  $K$  can be calculated from the slope and the intercept, respectively.

Langmuir model can be classified as applying to localized adsorption of monolayer coverage. It is based on the assumptions that the adsorbed species are held onto definite points of attachment on the surface, and the differential energy of adsorption is independent of surface coverage. The resulting equation for the Langmuir isotherm is

$$q = \frac{k_1 k_2 C_{eq}}{1 + k_1 C_{eq}} \quad (2)$$

where  $q$  and  $C_{eq}$  are the same as defined in the Freundlich equation,  $k_1$  is the maximum amount of adsorbate for complete monolayer coverage per unit weight of adsorbent, and  $k_2$  is the Langmuir constant, which is related to the magnitude of the forces involved in the binding process. According to Eq. (2), a plot of  $C_{eq}/q$  vs.  $C_{eq}$  gives a straight line. Thus, the constants  $k_1$  and  $k_2$  can be obtained from the least squares regression analysis.

For each bile acid-fiber pair, the data were correlated using the Freundlich and the Langmuir models, and the absolute average percentage deviations of the predicted isotherms from the experimental ones were calculated. The best fit model parameters were obtained by using linear regression analysis of the experimental data as explained above. Error percentages were calculated from the following expression:

$$\text{Abs. \% Deviation} = 100 \times \frac{(\text{experimental uptake} - \text{theoretical uptake})}{\text{experimental uptake}} \quad (3)$$

A comparison of the theoretical isotherms predicted by the Freundlich and the Langmuir isotherm equations with the experimental data is illustrated for deoxycholic acid adsorption on rice fiber in Fig. 13, as a typical example. The Freundlich model predicted the experimental data well in the low concentration

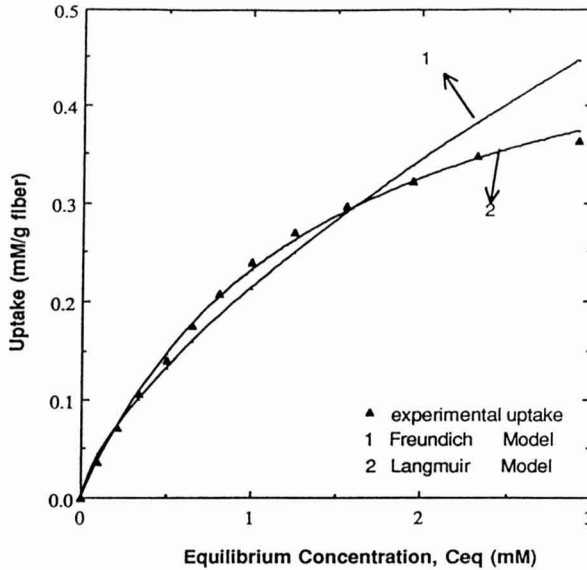


FIG. 13. COMPARISON OF MODEL PREDICTIONS Deoxycholic acid on macro size rice fiber at 37C.

range ( $C_{eq} < 0.8$  mM); however, the predictions were poor as the equilibrium concentration increased, resulting in a 6.3% average deviation for the entire set. This can be attributed to the semi-empirical nature of the Freundlich isotherm, which failed to represent the limiting monolayer capacity at high equilibrium concentrations.

The Langmuir equation gave much better overall predictions than did the Freundlich model, with an average deviation of 2.1%. For each pair, the best fit Langmuir parameters and the percent deviations are presented in Table 3. Since the Freundlich equation did not fit the data well, Freundlich parameters were not included in the table. The experimental isotherms of bile acid-fiber pairs are convex in shape and show a tendency to reach a plateau at high equilibrium concentrations (Fig. 1-3). This means that the system is approaching the saturation capacity. Since the Langmuir isotherm is based on the assumption that the adsorption is limited to a single layer, it is not surprising that it represented the experimental data adequately. Furthermore, a positive correlation between the Langmuir constant  $k_1$ , which relates to the saturation capacity, and the fiber's specific surface area was observed (Tables 2 and 3). This was consistent with the positive correlation found between the experimental sorption capacity and the specific surface area.

TABLE 3.  
LANGMUIR MODEL PREDICTIONS FOR BILE ACID ADSORPTION  
ON DIETARY FIBERS

Fiber Type	T,C	Cholic Acid			Deoxycholic Acid			Lithocholic Acid		
		k <sub>1</sub>	k <sub>2</sub>	Error,%	k <sub>1</sub>	k <sub>2</sub>	Error,%	k <sub>1</sub>	k <sub>2</sub>	Error,%
Macro Wheat	37	0.19	1.09	1.32	0.55	1.09	2.36	1.97	1.09	1.52
	25	0.22	1.09	1.60	0.60	1.09	1.88	2.08	1.09	1.53
Micro Wheat	37	0.83	1.08	2.00	1.28	1.08	2.98	2.94	1.09	1.87
Macro Oat	37	0.84	1.15	2.72	1.57	1.15	3.31	3.03	1.16	2.19
	25	0.99	1.12	3.25	1.68	1.15	2.87	3.20	1.15	1.31
Micro Oat	37	0.87	1.17	1.54	1.35	1.16	3.50	3.16	1.19	1.03
Macro Corn	37	0.01	1.06	1.21	0.47	1.09	2.45	1.83	1.07	2.69
	25	0.11	1.07	1.73	0.52	1.08	8.32	1.97	1.08	1.30
Micro Corn	37	0.21	1.06	1.14	0.62	1.07	3.65	2.27	1.07	2.21
Macro Rice	37	0.29	1.09	1.45	0.73	1.09	2.12	2.28	1.09	1.23
	25	0.32	1.09	1.10	0.78	1.09	1.58	2.39	1.09	0.92
Micro Rice	37	1.83	1.21	1.72	3.05	1.21	3.40	4.16	1.26	1.16
Macro Barley	37	0.40	1.10	1.66	0.84	1.10	2.68	2.62	1.10	2.59
	25	0.45	1.10	1.97	0.88	1.10	1.98	2.75	1.10	1.18
Micro Barley	37	1.31	1.19	1.89	2.21	1.20	3.16	4.05	1.23	0.93

## CONCLUSIONS

Adsorption of cholic acid, deoxycholic acid, and lithocholic acid on oat, rice, wheat, corn, and barley fibers were measured at 37C and 25C, using macro size (35–60 mesh) and micro size (100–300 mesh) samples. For all pairs examined the isotherms were of Type I, implying a limiting saturation capacity of the fiber for the bile acid binding.

It was concluded that, particle size reduction, accompanied with surface area change, has the most profound effect on a fiber's adsorption behavior. Uptake capacities of the macro size fibers for the same bile acid were in the following order: oat > barley > rice > wheat > corn. On the other hand, micro size fibers adsorbed with a different trend: rice > barley > oat > wheat > corn. These trends were in complete agreement with the trends of the specific surface areas of the fibers.

The results suggested that the distribution of the major constituents of the dietary fiber influences the fiber's bile acid sorption capacity. This capacity positively correlates with the crude fiber (cellulose-lignin) content in the fiber source.

The adsorption was positively correlated with the hydrophobicity of the bile acid, and it was favored by acid pH surroundings. In all cases, the bile acids

were adsorbed by the same fiber in the following order: lithocholic acid > deoxycholic acid > cholic acid.

Fibers adsorbed more bile acid at 25C than they did at 37C. However, the increase in the uptake capacities were somewhat insignificant. The magnitudes of the isosteric heat of adsorption values, ranging from 0.92 kcal/mole to 3.31 kcal/mole, suggested a relatively low binding energy involved for the adsorption.

The experimental data were correlated by using the Freundlich and the BET isotherm models. Both models provided accurate correlations for low concentration range ( $C_{eq} < 0.8$  mM), while the Langmuir equation gave much better predictions than did the Freundlich model for the entire concentration range.

## REFERENCES

- BAKER, D., NORRIS, K.H. and LI, B.W. 1979. In *Dietary Fibers: Chemistry and Nutrition*, (G.E. Inglett and S.I. Falkehag, eds.) p. 67, Academic Press, New York.
- BIRKNER, H.J. and KERN, F. 1974. *Gastroenterology* 67, 237.
- BOYD, G.S., EASTWOOD, M.A. and MACLEAN, N. 1966. *J. Lipid Res.* 7, 83.
- BRUNAUER, S., EMMETT, P.H. and TELLER, E. 1938. *J. Am. Chem. Soc.* 60, 309.
- BURKITT, D.P., WALKER, A.R.P. and PAINTER, N.S. 1974. *J. Am. Med. Assoc.* 229, 1068.
- CADDEN, A. M. 1987. *J. Food Sci.* 52, 1595.
- CALVERT, G.D. and YEATES, R.T. 1982. *Br. J. Nutr.* 47, 54.
- DURAL, N.H. and HINES, A.L. 1993. *J. Food Eng.* 20, 17.
- EASTWOOD, M.A. and BOYD, G.S. 1967. *Biochim. Biophys. Acta* 137, 393.
- EASTWOOD, M.A., KIRKPATRICK, J.R., MITCHELL, W.D., BONE, A. and HAMILTON, T. 1983. *Br. Med. J.* 4, 392.
- EASTWOOD, M.A. and ROBERTSON, J.A. 1981. *Br. J. Nutr.* 46, 247.
- EBIHARA, K. and SCHINEEMAN, B.O. 1989. *J. Nutr.* 119, 1100.
- FARRIER, D.S., HINES, A.L. and WANG, S.W. 1979. *J. Colloid Interface Sci.* 69, 233.
- FREUNDLICH, H. 1926. *Colloid and Capillary Catalysis*, Methuen and Co., London.
- GALLAHER, D.D. and FRANZ, P.M. 1990. *J. Nutr.* 120, 1320.
- GALLO, L.L. 1980. *Lipids* 15, 1012.
- ILLMAN, R.J. 1985. *Nutr. Res.* 5, 839.
- KELLEY, M.J., THOMAS, J.N. and STORY, J.A. 1981. *Fed. Proc.* 40, 845.

- KIRBY, R.W. *et al.* 1981. *Am. J. Clin. Nutr.* *34*, 824.
- KRITCHEVSKY, D. and STORY, J.A. 1974. *J. Nutr.* *104*, 458.
- LANGMUIR, I. 1938. *J. Am. Chem. Soc.* *40*, 1361.
- LENTER, C. 1981. In *Geigy Scientific Tables*, p. 143, Ciba-Geigy Co., New Jersey.
- MONGEAU, R. and BRASSARD, R. 1982. *Cereal Chem.* *59*, 413.
- NAGYVARY, J.J., FALK, J.D. and NAUSS, J.L. 1980. *Fed. Proc.* *39*, 784.
- NISHINA, P.M. and FREELAND, R.A. 1990. *J. Nutr.* *120*, 800.
- NISHINA, P.M., SCHNEEMAN, B.O. and FREELAND, R.A. 1991. *J. Nutr.* *121*, 431.
- OAKENFULL, D.G. and FENWICK, D.E. 1978. *Br. J. Nutr.* *40*, 299.
- RASPER, V.F. 1982. *Food Carbohydrates*, Van Nostrand Reinhold/AVI, New York.
- RASPER, V.F. 1979. In *Dietary Fibers: Chemistry and Nutrition*, (G.E. Inglett and S.I. Falkehag, eds.) pp. 93–115, Academic Press, New York.
- REDDY, B.S., WATANABE, K. and SHIENFIL, A. 1980. *J. Nutr.* *110*, 1247.
- SHINNICK, F.L., INK, S.L. and MARLETT, J.A. 1990. *J. Nutr.* *120*, 561.
- SOUTHGATE, D.A.T. 1969. *J. Sci. Food Agric.* *20*, 331.
- STORY, J.A. 1980. In *Medical Aspects of Dietary Fiber*, p. 137, Plenum Press, New York.
- STORY, J.A. and KRITCHEVSKY, D. 1976. *J. Nutr.* *106*, 1292.
- STORY, J.A., KRITCHEVSKY, D. and EASTWOOD, M.A. 1979. In *Dietary Fibers: Chemistry and Nutrition*, (G.E. Inglett and S.I. Falkehag, eds.) pp. 49–56, Academic Press, New York.
- STORY, J.A., WHITE, A. and WEST, L.G.J. 1982. *Food Sci.* *47*, 1276.
- TARPILA, S., MIETTINEN, T.A. and METSARANTA, L. 1978. *Gut* *19*, 137.
- VAHOUNY, G.V., TOMBES, R., CASSIDY, M.M., KRITCHEVSKY, D. and WEBER, F.E. and CHAUDHARY, V.K. 1987. *Cereal Foods World* *32*, 548.

# MECHANISMS INVOLVED IN THE INFUSION OF STARCH BASED POROUS FOOD MATERIALS BY OIL BASED LIQUID FOODS

Z. HIÇSASMAZ<sup>1</sup>

*Middle East Technical University  
Food Engineering Department  
Ankara 06531, Turkey*

and

J.T. CLAYTON

*University of Massachusetts  
Food Engineering Department  
Amherst, MA 01003*

Accepted for Publication August 15, 1994

## ABSTRACT

*Mechanisms involved in "infusion", defined as filling in the pores of starch based solid foods with high calorie liquid foods to obtain calorically dense food products, were investigated. Parameters under investigation were the effect of: Pore structure of the solid matrix on infusion uniformity, wettability of the solid matrix on the rate of liquid uptake, viscosity (apparent viscosity for non-Newtonian liquids) and surface tension of the infusing liquid on the rate of liquid uptake and the pressure gradient to be imposed. Infusion uniformity could not be achieved with chocolate syrup, no matter whether the porous solid matrix was highly expanded (Bread, porosity = 0.9) or relatively compact (Cookies, porosity = 0.6), due to the filtration of particulate solids. Infusion was found to be a fast, efficient process which takes place between a moderate vacuum and barometric pressure. For Newtonian oils, wettability was found to be the major mechanism of infusion.*

<sup>1</sup>Contact Person: Asst. Prof. Dr. Zeynep Hiçsasmaz, Work Address: Middle East Technical University Food Engineering Department, Ankara 06531 TURKEY; Phone #: (90) 4 2237100 Ext. 2766; FAX: (90) 4 286 86 29; Home Address: Ataç Sok. 55/13 Yeniflehir Ankara 06420 TURKEY; Phone #: (90) 4 4310933.

## INTRODUCTION

Starch based food materials are puffed, extruded or baked grain products with a pore volume of 60–90%. Filling in the available pore space with a high calorie liquid food material thus, yields a higher calorie food product in a relatively low bulk volume, and the process is called "infusion". Currently, the infusion process is used to produce a type of calorically dense ration component. Partially wetting oils and oil based liquid foods are used as the infusing liquids. The main aim of this study was to investigate the mechanisms involved in infusion and the relative effects of these mechanisms in obtaining a uniformly infused product. Infusion uniformity is especially important when the infusing liquid contains particulate solids. Filtration of these particulate material may occur within the porous matrix causing local nonuniformities in the final product where only the lipid phase is infused (Barrett and Ross 1990; Barrett *et al.* 1990).

Infusion is a capillary penetration process in which the infusing liquid rises in the capillaries of the starch based porous food material until it fills up the available pore space. The pressure gradient required for capillary penetration is dictated both by the characteristics of the infusing liquid and the pore size of the starch based solid matrix (Hiçsasmaz 1990; Hiçsasmaz and Clayton 1992) as given by the Laplace-Young equation;

$$P_c = \frac{4\sigma\cos\theta}{D} \quad (1)$$

where  $P_c$  is the capillary pressure imposed (Pa),  $s$  is the surface tension of the infusing liquid (N / m),  $\theta$  is the contact angle between the infusing liquid and the starch based solid (degrees) and  $D$  is the diameter (m) of the capillary segments filled by the infusing liquid corresponding to a particular capillary pressure imposed.

High calorie liquid foods usually contain suspended particulate material such as cocoa particles in chocolate syrup. Thus, in order to be able to obtain uniformly infused final products, pore sizes of the starch based solids should always be considerably larger than the particle size of the particulate solids in the infusing liquid. Also, the pore structure is important in selecting an effective solid matrix with the desired interconnectedness of the pore structure. Moreover, for partially wetting oil based liquids, wettability mechanism is a major factor which affects the uniformity of infused starch based products (Hiçsasmaz 1990; Hiçsasmaz and Clayton 1992, 1993).

Infusion uniformity has been found to be strongly correlated with the pore size of the solid matrix and the particle size of the particulate solids in the

infusing liquid while uncorrelated with the concentration of the particulate solids (Barrett and Ross 1990; Barrett *et al.* 1990). However, effect of the flow behavior of the infusing liquid on the rate of capillary penetration during the infusion process, also the effect of wettability of the starch based solid by the infusing liquid have not been investigated.

For partially wetting Newtonian liquids, the wettability mechanism of starch based solids has been found to correlate with the contact angle. However, for non-Newtonian liquids, wettability does not only depend on the contact angle, but also on the yield stress. Moreover, the rate of wetting between starch based solids and infusing liquids with densities close to each other has been found to be very slow. Wettability tests proved that the lipid phase in the infusing liquids containing particulate solids has an affinity towards the starch based solid matrices. Also, wettability in terms of the liquid absorption capacity has been found to depend on the relative proximate compositions of the infusing liquid and the solid matrix (Hiçsasmaz 1990; Hiçsasmaz and Clayton 1993).

Capillary penetration and immiscible displacement of Newtonian fluids have extensively been studied in the literature (Huh and Scriven 1970; van Brakel and Heertjes 1976; Levine *et al.* 1977; Dussan 1977; Dullien *et al.* 1977; Dullien 1979) basing on the Washburn equation;

$$\dot{Q} = \left[ \frac{N}{128\mu L} \right] \left[ \frac{4\sigma\cos\theta}{D} \right] \pi D^4 \quad (2)$$

where;

- $\theta$  : contact angle between the fluid and the solid capillary wall (degrees)
- $L$  : average length of capillaries with diameter  $D$  (m)
- $N$  : number of capillaries with diameter  $D$
- $\dot{Q}$  : rate of capillary penetration ( $\text{m}^3 / \text{s}$ )
- $\sigma$  : surface tension of the fluid (N / m)
- $\mu$  : viscosity of the fluid (kg / m-s)
- $D$  : capillary diameter (m)

Washburn equation which combines the Laplace-Young equation with the Hagen-Poiseuille equation represents a pseudo-steady-state approach in which the rate of capillary rise is constant.

Washburn equation, however, is true for Newtonian fluids only, and does not include the effect of the absorption capacity of the solid towards the penetrating liquid which has a major role in the infusion process. Starch based solid matrices exhibit wettability in the form of oil absorption capacity towards Newtonian edible oils (Hiçsasmaz 1990; Hiçsasmaz and Clayton 1993). Also,

most of the oil based liquid food materials exhibit non-Newtonian flow behavior with yield stress due to the presence of stabilizers, thickeners, emulsifiers and particulate solids. Therefore, in order to assess the effect of non-Newtonian fluid behavior on the infusion process, it was necessary to study the separate influences of viscosity, surface tension and wettability by using Newtonian oils. Also, in order to investigate the effect of the pore structure, starch based foods on the two extremes of porosity (0.6 and 0.9) were used.

## MATERIALS AND METHODS

### Materials

Hain safflower oil and Dow-Corning methyl silicone oils were selected as the Newtonian oils for infusion studies. Dow-Corning methyl silicone oils which had a surface tension of  $20 \times 10^{-3}$  N / m, and viscosities of  $47 \times 10^{-3}$  kg / m-s (SILICONE OIL I) and  $490 \times 10^{-3}$  kg / m-s (SILICONE OIL II) were selected to assess the effect of viscosity. SILICONE OIL I which had the same viscosity with the Hain safflower oil (surface tension =  $32 \times 10^{-3}$  N / m) was used to assess the effect of surface tension on the infusion process. Chocolate syrup was selected as the non-Newtonian liquid to be used in infusion studies. Chocolate syrup is a Casson type fluid stable to phase separation (Barbosa Canovas and Peleg 1983).

In order to assess the effect of pore structure on the capillary pressure needed to be imposed for infusion, a highly expanded starch based product, Wonder White Sandwich Bread (ITT Continental Baking Co.) with a porosity of 0.9 and a relatively compact starch based product, Chessmen Butter Cookies (Pepperidge Farms) with a porosity of 0.6 were used in the infusion experiments. Wonder White Sandwich Bread and Chessmen Butter Cookies exhibit different wettabilities towards the selected infusing liquids (Hiçsasmaz 1990; Hiçsasmaz and Clayton 1993), thus allowing the effect of wettability to be investigated, as well.

### Preparation and Characterization of Materials

**Characterization of Infusing Liquids.** Viscosities of Hain safflower oil and Dow-Corning methyl silicone oils, also the flow curve of the non-Newtonian chocolate syrup were determined by the 'HAAKE RV3 Rotovisco' using the DMK 500 measuring head and the MVI viscosity sensor.

Chocolate syrup obeys Casson's equation given as (Barbosa Canovas and Peleg 1983);

$$\sqrt{\tau} = K_1 + K_2 \sqrt{\dot{\gamma}} \quad (3)$$

where;

$K_1, K_2$  : regression constants  
 $\tau$  : shear stress (N / m<sup>2</sup>)  
 $\dot{\gamma}$  : shear rate (s<sup>-1</sup>)

The yield stress,  $\sigma_0$ , is given by;

$$\tau_0 = K_1^2 \quad (4)$$

and the viscosity coefficient,  $m$ , is;

$$m = K_2^2 \quad (5)$$

As a result of regression analysis by SPSS nonlinear regression program,  $\sigma_0$  and  $m$  were found as  $3.6 \times 10^{-1}$  N / m<sup>2</sup> and  $4.6 \times 10^{-2}$  N-s / m<sup>2</sup>, respectively. Apparent viscosity,  $\eta_{app}$  for a non-Newtonian fluid is given as;

$$\tau - \tau_0 = \eta_{APP} \dot{\gamma} \quad (6)$$

where  $\eta_{app}$  is a function of shear rate. For a Casson type fluid;

$$\eta_{app} = 2 \sqrt{\frac{\tau_0 m}{\dot{\gamma}}} + m \quad (7)$$

indicating that chocolate syrup is a shear-thinning fluid (Fig. 1).

Surface tensions of the infusing liquids were determined by the 'ROSANO' ring tensiometer (BIOLAR Co.). Wettability and contact angle measurements between Newtonian oils and the starch based solid food materials were carried out by the sedimentation volume technique, while the contact angles of chocolate syrup with the starch based solids were determined from the sessile drop geometry (Hiçsasmaz 1990; Hiçsasmaz and Clayton 1993). Measured viscosities, surface tensions, contact angles and wettability data for Newtonian and non-Newtonian liquids used in infusion studies are given in Table 1.

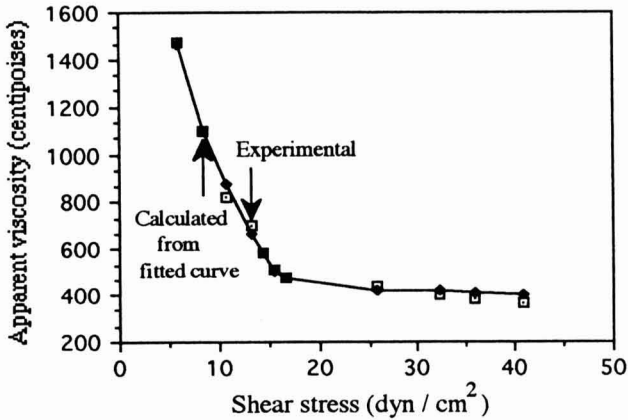


FIG. 1. APPARENT VISCOSITY VS. SHEAR STRESS DATA FOR CHOCOLATE SYRUP (Temperature = 20C)

**Preparation of Starch Based Solids.** For infusion experiments under static pressure heads,  $0.04 \times 0.06 \times 0.01 \text{ m}^3$  samples of bread and  $0.05 \times 0.06 \times 0.006 \text{ m}^3$  samples of cookies were used, while  $2.5 \times 10^{-6} \text{ m}^3$  samples were used for the vacuum infusion experiments. Samples were dried at 65C for 72 h before infusion experiments and their porosities were measured in order to be able to measure the percentage of the total pore volume infused.

\* **Characterization of Starch Based Solids.** As a preliminary approach to infusion studies, pore structures of the selected starch based solids were investigated in terms of macroscopic and microscopic pore structure parameters. Bulk density, true density and porosity were the macroscopic pore structure parameters, while the percentage closed pore volume, the smallest pore size and the pore size distribution were the microscopic pore structure parameters investigated (Hiçsasmaz, 1990; Hiçsasmaz and Clayton 1992). Measured pore structure parameters for cookies and bread are given in Table 2.

## Infusion Experiments

**Vacuum Infusion Experiments.** A series of vacuum infusion experiments were carried out to find out whether the infusion process is governed by the rate of capillary penetration. A vacuum infuser was designed (Fig. 2) by making use of the operating principles of mercury porosimetry. The cell housing of the vacuum infuser was made of reinforced Plexiglass ( $2.5 \times 10^{-2} \text{ m}$  ID,  $6.4 \times 10^{-3} \text{ m}$  wall thickness, 0.3 m length). The  $4 \times 10^{-3} \text{ m}$  stem diameter sample cell of the mercury porosimeter corresponding to a stem volume of  $2 \times 10^{-6} \text{ m}^3$  was used as

TABLE I.  
PHYSICAL PROPERTIES OF SELECTED INFUSING LIQUIDS  
(Temperature = 20C)

Flow Behavior	Newtonian		NonNewtonian		Surface		Vol.		Contact		
	Viscosity ( $\text{kg}/\text{m}\cdot\text{s})\times 10^3$	Viscosity Coefficient ( $\text{N}\cdot\text{s}/\text{m}^2)\times 10^2$	Yield Stress ( $\text{N}/\text{m}^2)\times 10^1$	Density ( $\text{kg}/\text{m}^3)\times 10^{-3}$	Tension ( $\text{N}/\text{m})\times 10^3$	Liq. Abs. ( $\text{m}^3/\text{kg})\times 10^3$	Angle (degrees)	Cookies	Bread	Cookies	Bread
Silicone											
oil I Newtonian	47	-	-	0.93	20	0.56	1.10	48	41		
Silicone											
oil II Newtonian	490	-	-	0.98	20	0.58	1.12	47	40		
Safflower											
oil Newtonian	47	-	-	0.84	32	0.52	1.06	51	44		
Chocolate											
syrup NonNewtonian	-	4.6	4	1.40	52	-	-	65	126		

TABLE 2.  
PORE STRUCTURE PARAMETERS OF SELECTED STARCH BASED POROUS SOLIDS

Porosity Range	Percentage		Capillary Hysteresis		Smallest Pore		Largest Pore		Mean Pore	
	Closed Pore Volume Range	(%)	Range	(%)	Diameter (m)×10 <sup>6</sup>	Diameter (m)×10 <sup>6</sup>	Diameter (m)×10 <sup>6</sup>	Diameter (m)×10 <sup>6</sup>	Diameter Range	Diameter Range (m)×10 <sup>6</sup>
Cookies 0.57 - 0.60	10 - 15		80 - 85		6		200		75 - 105	
Bread 0.90 - 0.91	0.7 - 1.2		90 - 95		6		645		110 - 135	

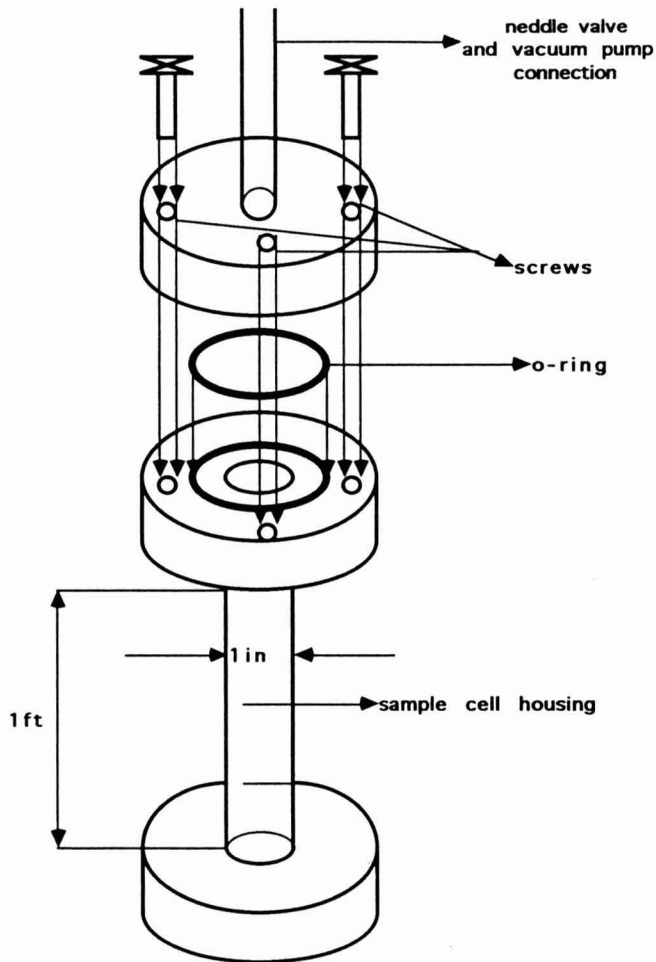


FIG.2. INFUSER CELL HOUSING

the vacuum infuser sample cell. The plexiglass chamber was connected to a roughing vacuum pump. A Parker needle valve ( $3.2 \times 10^{-3}$  m diameter) was inserted between the sample cell housing and the vacuum pump to regulate the air flow rate into the sample cell. The strategy in Fig. 3 was followed by filling the cell housing with the infusing liquid up to 0.2 m when in vertical position. Then, the sample cell which contained the starch based solid with known porosity was inserted into the cell housing. Evacuation was carried out (Fig. 3a), then the sample cell filling stage was accomplished (Fig. 3b). By the time the

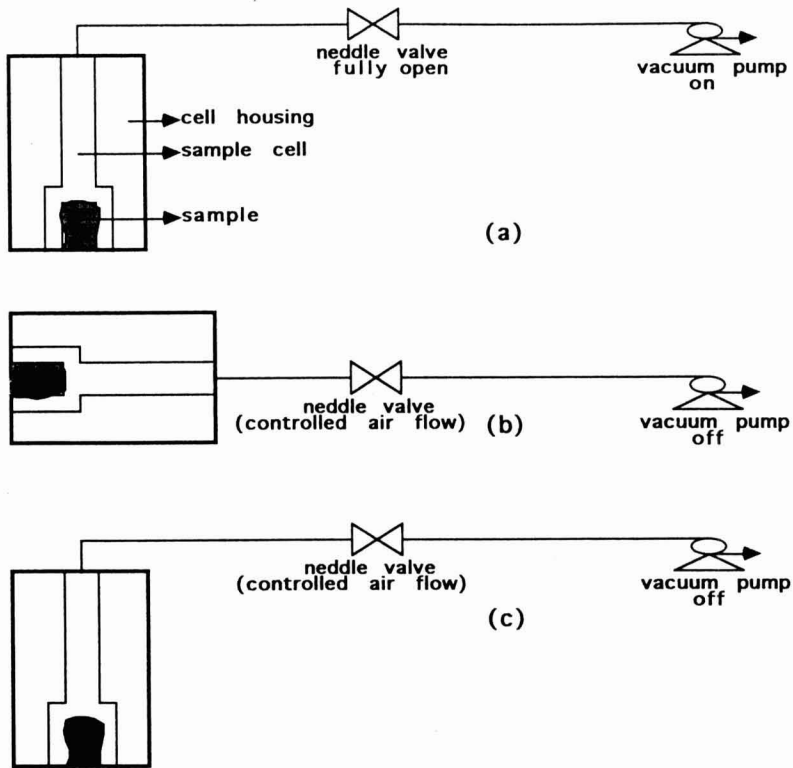


FIG. 3. SCHEMATIC REPRESENTATION OF VACUUM INFUSION EXPERIMENTS  
 (a) Evacuation of the sample cell, (b) Sample cell filling, (c) Infusion.

sample cell was filled, the pressure had increased to 21,000 Pa vacuum. The sample cell filling stage took about five minutes. The results of vacuum infusion experiments were evaluated in terms of liquid uptake where the infused sample was removed from the sample chamber, then the excess infusing liquid on the exterior of the sample was carefully removed by tissue paper and the liquid uptake was calculated from the difference between the initial and final weights as;

$$\text{Pore volume of sample} = \text{Bulk volume of sample} \times \text{Porosity of sample} \quad (8)$$

$$\text{Volume of liquid infused} = \frac{\text{Final sample weight} - \text{Initial sample weight}}{\text{Density of liquid}} \quad (9)$$

$$\text{Liquid uptake} = \frac{\text{Volume liquid infused}}{\text{Sample pore volume}} \quad (10)$$

**Infusion Experiments under Static Pressure.** A series of infusion experiments under static liquid pressure heads without evacuation was designed so as to assess the effect of wetting by the lipid phase during infusion. Low pressure driving forces imposed by static pressure heads allowed the investigation of the effect of wettability in terms of oil absorption capacity and capillary penetration parameters (surface tension and viscosity) separately. Infusion experiments under static oil pressure heads were carried out in a  $5 \times 10^{-4}$  m<sup>3</sup> beaker with Newtonian oils. Static pressures of 0.02, 0.05 and 0.10 m oil were applied. The porous solid sample was dipped into the oil and was kept at the bottom of the beaker by a strainer. Each sample was kept in the oil for a different period of time. After the required wetting time was accomplished, the surface oil was carefully removed by tissue paper and the liquid uptake was calculated from the difference between the initial and final weights by using Eq. (8)-(10).

As set up by the preliminary experiments, data were taken lengthening the time of infusion of each sample by ten seconds for bread and by fifteen seconds for cookies using a different sample for each experiment until no change in the liquid uptake occurred. The first data point was taken at five seconds. The liquid uptake at each data point was assigned the arithmetic mean of three replicates.

## RESULTS AND DISCUSSION

Viscosity (apparent viscosity for non-Newtonian fluids), surface tension and wettability are the basic properties of the infusing liquids which affect infusion as a capillary penetration process. Surface tension of the liquid and the contact angle between the liquid and the solid material determine the pressure gradient needed to start capillary penetration, while viscosity governs the rate of penetration. Partially wetting infusing liquids also have an affinity towards the solid matrix which causes the solid material to have an absorption capacity towards the infusing liquid, thus playing an important role in the infusion process. Moreover, the flow behavior of non-Newtonian liquids affect the process conditions, while the yield stress for non-Newtonian liquids affect the wettability as well.

process conditions, while the yield stress for non-Newtonian liquids affect the wettability as well.

The first step of infusion studies, involved derivation of the Washburn analog for chocolate syrup to find out whether the yield stress affects the pressure required for capillary penetration in comparison with the capillary pressure needed for the penetration of a Newtonian fluid. For a Newtonian fluid, the rate of capillary penetration given by Washburn equation (Eq. (2)) is directly proportional to the capillary pressure indicated by the Laplace-Young equation and indirectly proportional with the viscosity of the fluid. However, when the Washburn analog for a Casson type fluid is derived by area-averaging along with the no slip boundary condition;

$$\dot{Q} = \left[ \frac{N}{128\text{mL}} \right] \left[ \frac{4\sigma\cos\theta}{D} \right] \left[ 1 - \frac{16}{7}\xi^2 + \frac{4}{3}\xi - \frac{1}{21}\xi^4 \right] \pi D^4 \quad (11)$$

is obtained for N number of capillaries which have a certain diameter D indicated by the pore size distribution of the solid material where;

$$\xi = \tau_0 \frac{L}{\sigma\cos\theta} \quad (12)$$

and;

- $\theta$  : contact angle between the fluid and the solid capillary wall (degrees)
- L : average length of capillaries with diameter D (m)
- m : viscosity coefficient of the fluid (N-s / m<sup>2</sup>)
- N : number of capillaries with diameter D, dimensionless
- Q : rate of capillary penetration (m<sup>3</sup> / s)
- $\sigma$  : surface tension of the fluid (N / m)
- $\tau_0$  : yield stress of the fluid (N / m<sup>2</sup>)
- D : capillary diameter (m)

Equation (12) indicates that, as long as  $0 < \xi < 1$ , the rate of capillary penetration for a Casson type fluid through a particular porous medium is lower when compared to a Newtonian fluid (Eq. (2)) with the same surface tension and contact angle whose viscosity is identical with the viscosity coefficient, m, of the Casson fluid. However, if  $\xi \geq 1$ , capillary penetration cannot proceed even if the imposed pressure gradient is enough to overcome surface effects, since it is not adequate to overcome the fluid yield stress. When;

$$\xi = 1; \tau_0 = \frac{\sigma \cos \theta}{L} \quad (13)$$

which yields  $L \sim 6 \times 10^{-2}$  m for cookies and  $L \sim 8 \times 10^{-2}$  m for bread. These values of  $L$  correspond nearly to the largest dimension of bread slices and cookies. Both bread and cookies are formed of a tortuous network of highly interconnected capillary segments with diameters varying between  $6 \times 10^{-6}$  -  $200 \times 10^{-6}$  m for cookies and  $6 \times 10^{-6}$  -  $645 \times 10^{-6}$  m for bread (Table 2) as detected by mercury porosimetry and SEM photomicrographs (Hiçsasmaz 1990; Hiçsasmaz and Clayton 1992). Thus, no capillary segment with a specific diameter  $D$  is expected to continue throughout the sample bearing in mind that  $L$  is the average length of the capillary segments with diameter  $D$ . Therefore, for chocolate syrup, the yield stress does not pose problems with respect to the pressure gradient required for infusion. This indicates that supplying the capillary penetration pressure (Eq. (1)) required to infuse the capillary segments with the smallest diameter ( $6 \times 10^{-6}$  m for both cookies and bread) is enough to fulfill the infusion requirements (Table 3).

TABLE 3.  
CRITICAL CAPILLARY PRESSURES NEEDED FOR THE INFUSION PROCESS

	Capillary Pressure for Sample Cell Filling (Pa)	Capillary Pressure for Infusion of the Smallest Pore Diameter (Pa)	
		Cookies	Bread
Silicone oil I	20	9,000	10,000
Silicone oil II	20	9,000	10,000
Safflower oil	32	13,500	15,500
Chocolate syrup	52	14,700	20,400

Vacuum infusion experiments showed that the infusion process is almost accomplished during the sample cell filling stage which took about five minutes. Thus, infusion is an efficient process which takes place between moderate vacuum and the barometric pressure and is not penetration rate controlled. For Newtonian oils, the liquid uptake (Eq. (10)) was found to be greater than one which indicates that the volume of liquid infused is greater than the available pore volume. The only explanation for this behavior is the wettability of the starch based materials by the infusing liquids. For chocolate syrup, on the other hand, the liquid uptake was about 0.95 - 0.97 which indicates that the effect of wettability for non-Newtonian liquids at such short periods of time is negligibly small.

In the infusion of chocolate syrup, infusion uniformity could not be achieved due to the filtration of particulate solids. The most important factor which causes filtration is: no matter highly expanded (bread) or relatively compact (cookies), the selected starch based solids contain pores in the order of  $6 \times 10^{-6}$  m in diameter while the particle size of the cocoa particles to be infused are in the order of  $10^{-5}$  m. Since these small pore segments are randomly distributed within the porous matrix, cocoa particles which reach such pores are immediately filtered out blocking the pores, thus causing nonuniform infusion. Also, long term wettability experiments with chocolate syrup had proved that the starch based solids have an affinity towards the lipid phase in the chocolate syrup (Hiçsasmaz 1990; Hiçsasmaz and Clayton 1992; Hiçsasmaz and Clayton, 1993). During vacuum infusion, affinity of the liquid towards the starch based solid capillary walls may cause the particulate solids to concentrate and agglomerate around the wall area, thus blocking the capillary channels.

Experiments carried out at static oil pressure heads to assess the effect of the oil absorption capacity showed that maximum liquid uptake was about 0.75 for bread and 0.55 for cookies with the effect of wettability inclusive. The smallest pore diameters penetrated due to the imposed static pressure heads were calculated using the Laplace-Young equation (Table 4). As indicated by mercury porosimetry 95% of the pore volume for bread and 60% of the pore volume for cookies are in the diameter range of  $60 \times 10^{-6}$  -  $560 \times 10^{-6}$  m (Hiçsasmaz 1990; Hiçsasmaz and Clayton 1992). Air entrapment due to no evacuation during infusion under static pressure heads seems to be likely, considering that the effect of wettability is also included in the results on the final liquid uptake. The difference between the liquid uptake of cookies and bread can be attributed to the fact that the oil absorption capacity of bread is almost twice that for cookies (Table 1).

TABLE 4.  
PORE DIAMETERS INFUSED UNDER VARIOUS STATIC PRESSURE HEADS

	Static Pressure (m oil)	Pore Diameter (m) $\times 10^6$	
		Cookies	Bread
Silicone oil I	0.10	60	65
Silicone oil II	0.10	55	65
Safflower oil	0.10	100	110
	0.05	195	225
	0.02	490	560

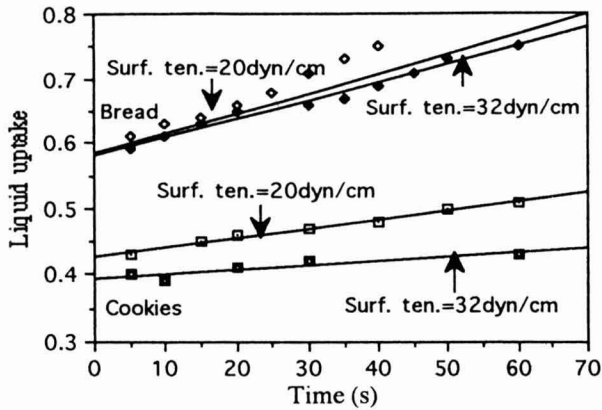


FIG. 4. EFFECT OF SURFACE TENSION ON LIQUID UPTAKE WITH SAFFLOWER OIL AND SILICONE OIL I UNDER 0.1 m STATIC PRESSURE HEAD

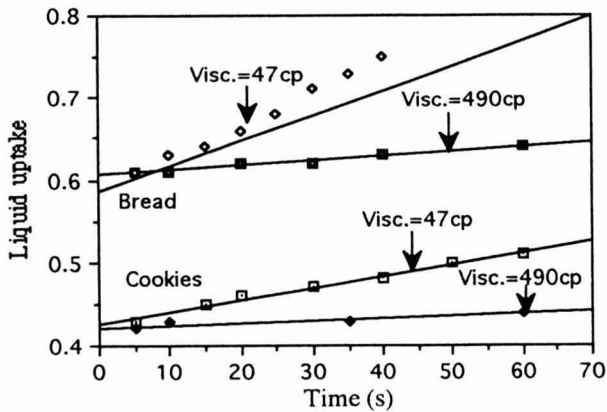


FIG. 5. EFFECT OF VISCOSITY ON LIQUID UPTAKE WITH SILICONE OIL I AND SILICONE OIL II UNDER 0.1 m STATIC PRESSURE

Linear regression applied to liquid uptake vs. time data (Fig. 4 and 5) yielded correlation coefficients between 0.95 - 0.98, which indicates that the rate of liquid uptake is fairly constant and can be estimated from the slopes of the fitted straight lines. On the other hand, the liquid uptake is expected to be zero at the start of the process, however, the regression results indicated an intercept. This could not be verified experimentally, since the first possible sensitive data

at the start of the process, however, the regression results indicated an intercept. This could not be verified experimentally, since the first possible sensitive data point could be taken at five seconds, and what happens during the first five seconds in reality is unknown. Thus, this intercept which refers to the unknown five seconds was referred to as 'instantaneous "extrapolated" wettability'. The rate of liquid uptake was fairly low compared to the effect of the 'instantaneous "extrapolated" wettability' (Tables 5 and 6) which comprises about 70% of infusion into the porous matrices. Thus, 'instantaneous "extrapolated" wettability' was further investigated in terms of the oil absorption capacity (Table 1) of bread and cookies as;

$$\text{Volume of oil absorbed} = \text{Sample weight} \times \text{Oil absorption capacity} \quad (14)$$

$$\text{Volume infused due to wettability} = \text{Extrapolated "instantaneous" wettability} \times \text{Sample pore volume} \quad (15)$$

$$\text{Percentage extrapolated "instantaneous" wettability due to oil absorption} = \frac{\text{Volume of oil absorbed}}{\text{Volume oil infused due to extrapolated "instantaneous" wettability}} \quad (16)$$

obtained showed that 100% of the 'extrapolated "instantaneous" wettability' was due to oil absorption for cookies, while only 20-35% of it was due to oil absorption for bread. This indicates that some of the surface pores on bread samples are so large that they are filled "instantaneously", while the pores on the cookie skin are not large enough which was also supported by SEM photomicrographs (Hiçsasmaz 1990; Hiçsasmaz and Clayton 1992). It was observed that the effect of oil absorption is more profound for bread samples which contain a high percentage of closed pore volume. This indicates that oil penetrates into the closed pores due to diffusion through the solid matrix.

The mean rate of infusion was compared based on the liquid uptake in forty seconds (Tables 5 and 6) which was the period of time required for the fastest experiment (with bread and silicone oil I) to reach completion. When the data for safflower oil and silicone oil I were compared under a static pressure of 0.10 m oil (Fig. 4, Tables 5 and 6), it was found that a decrease in surface tension resulted in an increase in the mean rate of liquid uptake both for bread and cookies. At the first sight, this behavior looks contrary to what is expected from the Washburn equation (Eq. (2)). However, implicitly, it is evident that as the surface tension decreases at a given value of capillary pressure, pores smaller

TABLE 5.  
RESULTS OF STATIC PRESSURE EXPERIMENTS FOR CHESSMEN BUTTER COOKIES  
(Peppertidge Farms)(Temperature = 20C)

	Static Pressure Head (m oil)	Density ( $\text{kg/m}^3 \times 10^{-3}$ )	Surface Tension ( $\text{N/m} \times 10^{-3}$ )	Viscosity ( $\text{kg/m-s} \times 10^3$ )	Extrapolated "Instantaneous" Wettability ( $\text{m}^3 \text{ oil/m}^3 \text{ pore vol}$ )	Liquid Uptake after 40s	Mean Rate of Liquid Uptake ( $\text{Liquid uptake} \times 10^{-4}/\text{s}$ )
	0.10	0.84	32	47	0.40	0.42	6.6
Safflower oil	0.05	0.84	32	47	0.40	0.40	6.0
	0.02	0.84	32	47	0.38	0.42	10.0
Silicone oil I	0.10	0.93	20	47	0.42	0.48	10.0
Silicone oil II	0.10	0.98	20	490	0.42	0.43	1.0

TABLE 6.  
RESULTS OF STATIC PRESSURE EXPERIMENTS FOR WONDER WHITE SANDWICH BREAD  
(Temperature = 20C)

	Static Pressure Head (m oil)	Density (kg/m <sup>3</sup> )×10 <sup>3</sup>	Surface Tension (N/m)×10 <sup>3</sup>	Viscosity (kg/m·s)×10 <sup>3</sup>	Extrapolated "Instantaneous" Wettability (m <sup>3</sup> oil/m <sup>3</sup> pore vol)	Liquid Uptake after 40s	Mean Rate of Liquid Uptake (liquid uptake×10 <sup>-4</sup> /s)
	0.10	0.84	32	47	0.58	0.69	30
Safflower oil	0.05	0.84	32	47	0.58	0.66	20
	0.02	0.84	32	47	0.58	0.66	20
Silicone oil I	0.10	0.93	20	47	0.58	0.75	40
Silicone oil II	0.10	0.98	20	490	0.61	0.63	1

in diameter can be penetrated, thus the number of pores or the pore volume infused at a given time period increases. When the data for silicone oils I and II were compared, the rate of liquid uptake decreased as indicated by the Washburn equation (Fig. 5, Tables 5 and 6). Raising the static pressure head from 0.02 to 0.10 m safflower oil increased the rate of liquid uptake for both bread and cookies (Tables 5 and 6) which indicates that both materials contain a major amount of pores in the diameter range of  $100610^{-6}$  -  $560610^{-6}$  m (Table 4). On the other hand, raising the static pressure head from 0.02 to 0.05 m safflower oil head did not have any profound effect on the rate of liquid uptake of bread samples, while a little effect was observed in the case of cookies (Tables 5 and 6). This supports the fact that bread samples contain large surface pores in the order of  $500 \times 10^{-6}$  m which are out of the mercury porosimetry range accompanied with quite a few amount of pores in the  $100 \times 10^{-6}$  -  $200 \times 10^{-6}$  m range which is just the starting range for mercury porosimetry.

## CONCLUSIONS

Infusion is a fast, efficient process which takes place between a moderate vacuum and barometric pressure both for Newtonian oils and the non-Newtonian chocolate syrup. For Newtonian oils, wettability of the solid matrix by the oil phase is the main mechanism of infusion.

However, the major problem with the infusion process is that; infusion uniformity cannot be obtained for non-Newtonian oil based liquids which contain particulate solids due to the filtration of these particulate material, since pores smaller than the particle size of these particulate solids exist within the pore structure. Since filtration is a physical phenomenon, the only way to prevent this is to produce starch based entities with controlled pore size distributions representing large enough pore sizes which would prevent solid deposition.

Although the wettability mechanism is very slow for non-Newtonian oil based liquids containing particulate solids, starch based solids have an affinity towards the lipid phase in such liquids. Thus the particulate solids drawn towards the pore walls together with the lipid phase tend to agglomerate during deposition blocking the pores. Therefore, techniques which would decrease the affinity of the particulate solids in the suspension towards the starch based solids to be infused should be investigated. One of such techniques could be the addition of food-grade cohesives towards the particulates in the food suspension into the initial recipe of the starch based porous material to be infused.

**REFERENCES**

- BARBOSA CANOVAS, B.V. and PELEG, M. 1983. Flow Parameters of Selected Semi-Liquid Food Products. *J. Text. Stud.* *14*, 213–233.
- BARRETT, A.H. and ROSS, W.R. 1990. Correlation of Extrudate Infusibility with Bulk Properties Using Image Analysis. *J. Food Sci.* *55*, 1378–1382.
- BARRETT, A.H. and ROSS, W.R. 1990. Simulation of the Vacuum Infusion Process Using Idealized Components: Effects of Pore Size and Suspension Concentration. *J. Food Sci.* *55*, 989–993 and 999.
- DULLIEN, F.A.L. 1979. *Porous Media Fluid Transport and Pore Structure*. pp. 76–230, 251–324. Academic Press, New York.
- DULLIEN, F.A.L., EL-SAYED, M.S. and BATRA, V.K. 1977. Rate of Capillary Rise in Porous Media with Nonuniform Pores. *J. Colloid & Interface Sci.* *60*, 491–502.
- DUSSAN, E.B. 1977. Immiscible Displacement in a Capillary Tube: The Moving Contact Line. *A.I.Ch.E.J.* *23*, 131–133.
- HIÇSASMAZ, Z. 1990. Study of Mechanisms Underlying the Infusion of Starch Based Food Materials by Oil Based Liquid Foods. Ph.D. Dissertation, Univ. of Mass., Food Eng. Dept.
- HIÇSASMAZ, Z. and CLAYTON, J.T. 1992. Characterization of the Pore Structure of Starch Based Food Materials. *Food Structure.* *11*, 115–132.
- HIÇSASMAZ, Z. and CLAYTON, J.T. 1993. Applicability and Comparison of various Techniques for Measurement of Wettability and Contact Angles between Oil Based - Starch Based Food Materials. *J. Food Eng.* *18*, 127–143.
- HUH, C. and SCRIVEN, L.E. 1970. Hydrodynamic Model of Steady Movement of a Solid / Liquid / Fluid Contact Line. *J. Colloid & Interface Sci.* *35*, 85–99.
- LEVINE, S., REED, P. and SHUTTS, G. 1977. Some Aspects of Wetting / Dewetting of a Porous Medium. *Powder Technol.* *17*, 163–181.
- VAN BRAKEL, J. and HEERTJES, P.M. 1977. Capillary Rise in Porous Media. Part I: A Problem. *Powder Technol.* *16*, 75–81.

# EVALUATION OF DIE SWELL AND VOLUMETRIC EXPANSION IN CORN MEAL EXTRUDATES<sup>1</sup>

J.F. FALLER, H.E. HUFF and F. HSIEH<sup>2</sup>

*Departments of Agricultural Engineering  
and Food Science and Human Nutrition  
University of Missouri, Columbia  
Columbia, MO 65211*

Accepted for Publication September 24, 1994

## ABSTRACT

*A method to determine die swell in the presence of volumetric expansion due to moisture vaporization in extruded food products is proposed. The method is applied to twin screw extrusion of corn meal in a study to investigate the effects of extruder die parameter (exit capillary length and entrance cone angle), screw speed, and specific feeding load on die swell and volumetric expansion. The die swell results are compared with known effects for nonexpanded polymers.*

*Die swell tended to decrease with increasing exit length, but had only a weak response to entrance angle. Increasing specific feeding load (SFL) increased die swell, where as increasing screw speed produced increases or decreases in die swell, depending on the SFL. Die swells ranged from approximately 1.2 to 1.7, accounted for approximately 10 to 22% of the total radial expansion, and for approximately 18 to 38% of the extrudate cross sectional area.*

*Volumetric expansion increased with increasing die exit length, but was insensitive to entrance angle with a slight concave upward response. Increasing screw speed produced large increases in volumetric expansion, while increasing SFL produced only slight increases.*

*Observations about die swell compare favorably with previous studies of nonexpanded polymers, suggesting that the proposed analysis method may be useful for food viscoelasticity evaluation studies.*

<sup>1</sup>Contribution from the Missouri Agricultural Experiment Station, Journal Series No. 12,059.

<sup>2</sup>To whom all correspondence should be addressed.

## INTRODUCTION

Die swell in high molecular weight polymer and polymer solution extrusion, a long observed phenomenon, is related to fluid viscoelastic properties. Die swells for Newtonian fluids have been reported to range from 0.89 at large Reynolds number laminar flow to 1.13 at small Reynolds number laminar flow (Bird *et al.* 1987). For viscoelastic fluids, die swells above 1.13 and up to 4 have been observed (Bird *et al.* 1987).

The ease of die swell measurement in extruded products has made it attractive for evaluating viscoelastic properties of nonexpanded polymers; in addition, die swell has been the subject of many numerical studies using fundamental rheological properties to make predictions (Graessley *et al.* 1970; Han 1976; Mitsoulis *et al.* 1985; Tanner 1988; and Goublomme *et al.* 1992). Although general agreement on theoretical relationships is lacking, die swell is still widely considered to be a measure of viscoelasticity. Therefore, an evaluation of die swell in expanded food products is desirable.

## BACKGROUND

Fluid viscoelasticity is exhibited in many ways. Important phenomena for describing the effects mathematically are the presence of normal stress differences arising from shear flow and a memory (or recoil) effect upon cessation of flow. The normal stress differences define characteristic fluid properties, the primary and secondary normal stress coefficients ( $\Psi_1$  and  $\Psi_2$ ), in a constitutive relationship relating normal stresses to shear rate (Bird *et al.* 1987). Recoil effects are observed in both simple shearing flow and in elongational flow. Lodge (1964) shows experimental results for recoil due to shear for flow in a capillary using photographic methods. Han (1976) presents experimental data for the dependence of die swell on both the length-to-diameter ratio of a capillary and the entrance reservoir-to-capillary diameter ratio, supporting the observation that elongational flow recoil effects are present. Recoil phenomena for fluids are described by Maxwell type constitutive relationships using either tensile or shear moduli of elasticity (Steffe 1992).

Normal stress and memory effects in food extrusion are shown in the study performed by Ofoli *et al.* (1993). The die swell (radial expansion) of a nonexpanded extrudate was analyzed with respect to two of the elastic fluid phenomena discussed above, namely the entrance recoil effect (arising from elongational flow at the die entrance) and the secondary normal stress difference effect at the capillary exit. Recoil due to entrance elongational stresses was assumed to be inversely proportional to the fluid residence time within the die,

and the normal stress difference at the die exit was considered to be a function of the shear rate within the die, with an Arrhenius temperature correction for viscous properties applied. When swelling due to entrance effects alone was considered the model produced a correlation coefficient of around 0.5, but when both entrance effects and normal stresses due to shear rate were considered the model correlation coefficient was improved to above 0.9.

Ofoli *et al.* (1993) shows die swell is an important phenomena in food extrusion. However, many extruded products undergo volumetric expansion due to moisture vaporization, and die swell cannot be directly measured. Launay and Lisch (1983) and Alvarez-Martinez *et al.* (1988) studied radial (or sectional) expansion of expanded extrudates and concluded that the radial expansion is partially due to elastic properties. Launay and Lisch (1983) attributed the degree of longitudinal expansion to melt viscosity properties and radial expansion to melt elastic properties. Alvarez-Martinez *et al.* (1988) found sectional (or radial) expansion to be highly correlated to the shear strains within the die, which apparently resulted from normal stress differences. They also found a negative correlation between radial and longitudinal expansion, and thus concluded that radial expansion occurs at the expense of longitudinal expansion, which seems intuitive from a conservation of mass argument. Alvarez-Martinez *et al.* (1988), in agreement with Launay and Lisch (1983), also found longitudinal expansion to be favored by a lower melt viscosity. Neither study, however, quantified the degree to which elasticity affected radial expansion.

Kokini *et al.* (1992) investigated total extrudate expansion (volumetric) by analyzing the relationship of extrudate specific volume with respect to the ratio of swelling driving force to swelling resistance. The ratio was calculated as the difference between the local steam pressure within the extrudate and atmospheric pressure, all divided by the fluid viscosity ( $\Delta P_s/\eta$ ). In this simplified analysis, elastic effects were neglected and good correlation between the specific volume and  $\Delta P_s/\eta$  was found for both Amioca<sup>TM</sup> (waxy corn starch) and Hylon 7<sup>TM</sup> (70% amylose corn starch) extrudates when the moisture content was low (20% or less). This study suggests that elastic radial expansion and total volumetric expansion can be analyzed separately. Also, the analysis failed to accurately predict expansion above 20% moisture content, suggesting that more is involved than a simple analysis of expansion driving force divided by expansion resistance, possibly due to extrudate collapse as the increased moisture decreased the glass transition temperature (Slade and Levine 1991) or set point.

In the present study, a theoretical analysis based on a model which separates the radial expansion into die swell and volumetric expansion components is proposed. The model is then applied to an expanded corn meal product extruded under various conditions and using dies of varying geometry. The objective of the study is two-fold: to evaluate its effectiveness in predicting die swells in relation to previous studies for nonexpanded polymers, and to assess die

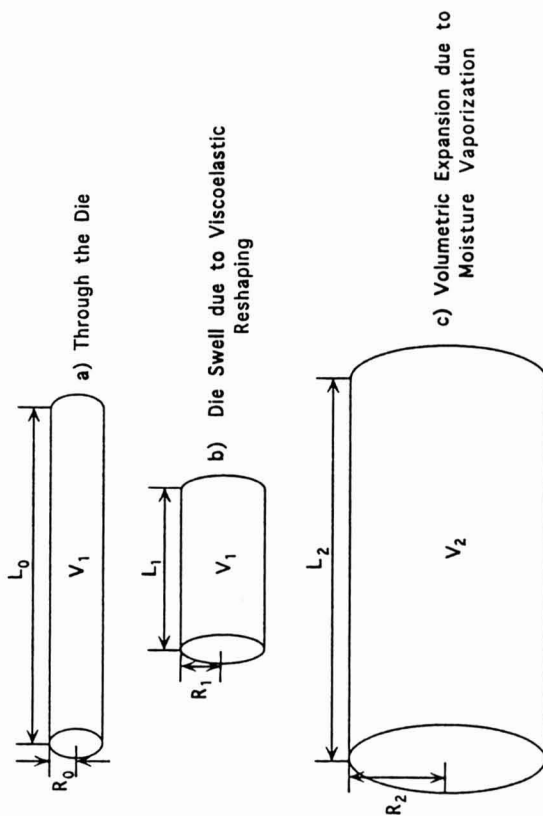


FIG. 1. EXTRUDATE RESHAPING AND VOLUMETRIC EXPANSION DUE TO VISCOELASTICITY AND MOISTURE VAPORIZATION

geometry and extruder condition influence on die swell and volumetric expansion.

## THEORETICAL ANALYSIS

The number of processing variables affecting the final shape of an expanded, extruded product are many and are complicated. As discussed above, however, the final product is the result of die swell due to melt viscoelasticity and volume expansion due to moisture vaporization. These effects, assumed to be separable for analysis purposes, are shown in Fig. 1. Note that the intent of this figure is not to suggest that die swell occurs before volumetric expansion, as both will occur simultaneously. Note also that reversing the order of die swell and volumetric expansion does not influence the following analysis.

First, the model assumes reshaping due to die swell [Fig. 1(a) to 1(b)] of a fluid element emerging from the die does not result in any volumetric expansion (mass is conserved), and therefore a relationship between radial expansion and longitudinal contraction can be derived using simple geometric considerations:

$$V_1 = \pi R_0^2 L_0 = \pi R_1^2 L_1 \quad (1)$$

By rearranging Eq. (1) as:

$$R_1/R_0 = (L_0/L_1)^{1/2} \quad (2)$$

it is seen that die swell due to viscoelasticity is equal to the square root of the longitudinal contraction. This result is qualitatively in accordance with the observations of Launay and Lisch (1983) and Alvarez-Martinez *et al.* (1988) that radial expansion is inversely related to longitudinal expansion.

Next, the model assumes the solid fluid element, after viscoelastic reshaping, is expanded in volume due to porosity formation [Fig. 1(b) to 1(c)]. In this process, the final size is the result of total volumetric expansion due to moisture vaporization plus volumetric contraction due to evaporative cooling and moisture vapor loss. The resulting volume is achieved when the extrudate reaches a critical temperature and moisture content based on the extrudate glass transition temperature (Slade and Levine 1991). In this step, the longitudinal and radial expansions and contractions are assumed to be equal in magnitude and direction, so that the final expanded product maintains the length-to-diameter ratio of the pre-expanded fluid element:

$$R_1/L_1 = R_2/L_2 \quad (3)$$

This assumption is reasonable since volumetric expansion should primarily be controlled by fluid viscous effects, which are generally considered to be isotropic. Note also that total volumetric expansion is:

$$V_2/V_1 = R_2^2 L_2 / R_0^2 L_0 \quad (4)$$

and this can be determined from the final extrudate dimensions ( $R_2$  and  $L_2$ ) and the extrudate dimensions before viscoelastic reshaping ( $R_0$  and  $L_0$ ).  $R_0$  is the known die radius, and  $L_0$  can be calculated from the measured weight of extrudate, the dough melt density, and the die radius according to:

$$L_0 = PPW / \pi R_0^2 \rho_D \quad (5)$$

Now to determine the die swell due to viscoelastic effects, the ratio  $R_1/R_0$  must be expressed in terms of the initial fluid element dimensions,  $R_0$  and  $L_0$ , and the final product dimensions,  $R_2$  and  $L_2$ . Combining Eq. (2) and (3) and rearranging to achieve the proper ratio results in:

$$R_1/R_0 = [(R_2/R_0)/L_2/L_0]^{1/3} \quad (6)$$

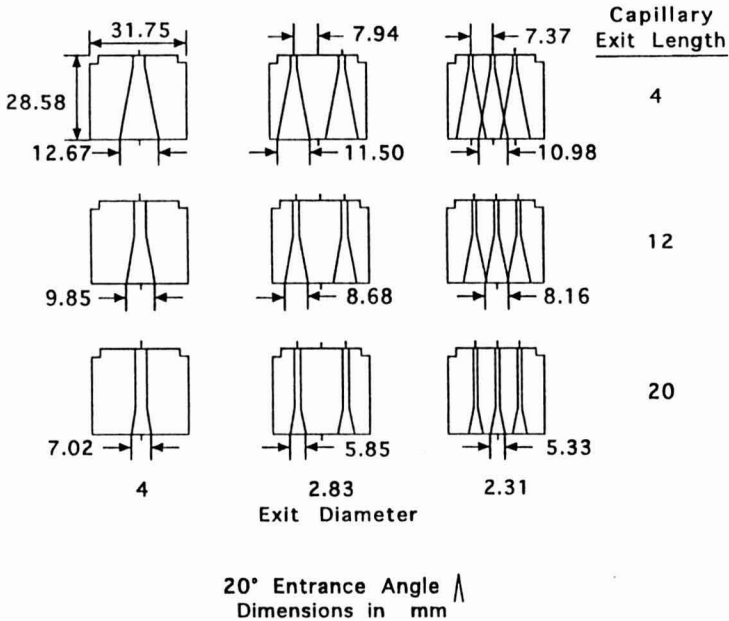
Analysis of this result shows that the die swell due to viscoelastic effects equals the cube root of the ratio of overall radial expansion to overall longitudinal expansion.

## EXPERIMENTAL METHODS

The experiment was a  $3 \times 3 \times 3 \times 3$  full factorial design with respect to screw speed, specific feeding load (SFL = feed rate/screw speed), die entrance cone angle, and die exit capillary length and contained two replications. The treatment levels are shown in Table 1, and the die designs are shown in Fig. 2. The experiment was executed as a split plot design (Cochran and Cox 1957). Each plot consisted of one extrusion run with one die and the die for each run was selected at random. The extrusion conditions were executed in a nonrandom order since complete randomization was incompatible with the extruder operation, however, this will only affect the interpretation of the statistical

TABLE 1.  
EXPERIMENTAL TREATMENT LEVELS

Screw Speed (rpm)	Specific Feeding Load (kg/h/rpm)	Conic Entrance Angle (°)	Capillary Exit Length (mm)
200	0.136	20	4
300	0.182	32.5	12
400	0.227	45	20



a) Variable exit length and diameter

FIG. 2. EXTRUDER DIE DESIGNS

analysis results and will have no influence on the theoretical model. Extrusion was accomplished using a Baker-Perkins 50/25 corotating and intermeshing twin-screw extruder (APV Baker, Grand Rapids, MI). Corn Meal (CCM250, Lauhoff Grain Company, Danville, IL) was starve-fed at 19% wet basis moisture content. Extrudate was cut as it emerged from the die using a center mounted cutter with four blades. Samples were collected after steady state operation was achieved and were subsequently dried for approximately 5 min at

66C in a fluidized bed drier. The dough melt temperature at the die was measured at the die entrance by a J-type thermocouple (Omega Engineering, Stamford, CT) in direct contact with the melt.

Final extrudate dimensions were determined by measuring the lengths and widths of 50 pieces with a digital vernier caliper and averaging. The per piece weight (PPW) was determined by averaging the weight of 50 pieces; three determinations were made for each treatment and the results were averaged. A dough melt density,  $\rho_D$  of 1200 kg/m<sup>3</sup> was used in the calculation of  $L_0$ , which has been reported by Alvarez-Martinez *et al.* (1988) and Padmanabhan and Bhattacharya (1989).

The results were analyzed using PROC REG in the Statistical Analysis System and response curves were created from reduced second order models determined using the BACKWARD selection criteria (SAS 1990).

## RESULTS AND DISCUSSION

The goal of this experiment was to analyze the results of the proposed theoretical analysis for die swell and volumetric expansion in relation to the literature; that is, to explain results in terms of fundamental material properties (elastic and viscous effects) and die geometry effects. The fundamental material properties are functions of the system thermodynamic state variables, namely the product temperature and chemical condition at the die. The die geometry effects are related to the magnitude of the shear rate within the die, the die entrance effects, and the product residence time in the die. The die geometry effects are expected to directly influence only the die swell, but may also indirectly influence the system state variables, which complicates the analysis.

Table 2 contains the regression model coefficients for the reduced second order models used to prepare the response surfaces. Note that the statistical models were determined using variable levels adjusted by subtracting the mean treatment levels to control multicollinearity (Neter *et al.* 1989). Therefore, the mean treatment levels must be subtracted from the absolute levels when using these models.

Figures 3, 4, and 5 show the response surfaces for die swell, volumetric expansion, and temperature, respectively. The response surface plots showing die design effects are for the central point extruder condition of 0.182 kg/h/rpm SFL and 300 rpm screw speed. The plots showing extruder condition effects are for the central point die with an entrance cone angle of 32.5° and an exit capillary length of 12 mm. Only response surfaces for the central point extruder condition and the central point die are shown, and while interactions between die parameters and extruder conditions were significant in some models (Table 2), the interactions were not large enough to reverse trends.

TABLE 2.  
 STATISTICAL MODELS FOR DIE SWELL, VOLUMETRIC EXPANSION,  
 AND TEMPERATURE. PARENTHESES CONTAIN COEFFICIENT P-VALUES<sup>1</sup>  
 AND "\*" INDICATES NOT SIGNIFICANT AT THE 0.1 LEVEL

Coefficient <sup>2</sup>	Die Swell	Volumetric Expansion	Temperature (C)
Intercept	1.45	17.2	138
DEL	$-6.61 \times 10^{-3}$	0.213	0.507
DEA	$6.48 \times 10^{-4}$ (b)	0.0296(a)	*
RPM	*	0.0225	0.0140
SFL	2.49	23.8	-37.4
DEL×DEL	$1.77 \times 10^{-4}$ (b)	$-9.50 \times 10^{-3}$ (a)	-0.0282
DEL×DEA	$-1.77 \times 10^{-4}$ (b)	*	0.0188
DEL×RPM	$1.36 \times 10^{-5}$ (a)	*	$-8.35 \times 10^{-4}$ (c)
DEL×SFL	*	*	*
DEA×DEA	$-1.33 \times 10^{-4}$	$6.40 \times 10^{-3}$	0.0123
DEA×RPM	*	*	$7.29 \times 10^{-4}$ (b)
(b)DEA×SFL	*	*	1.29(a)
RPM×RPM	$-2.27 \times 10^{-6}$	$-6.70 \times 10^{-5}$ (a)	$-2.42 \times 10^{-4}$
RPM×SFL	0.0108	0.0850(c)	-0.490
SFL×SFL	*	*	*
Model R <sup>2</sup>	0.938	0.812	0.749

<sup>1</sup>No parentheses indicates significance level < 0.001; (a) < 0.01; (b) < 0.05; (c) < 0.1.

<sup>2</sup>DEL-Die exit length; DEA-Die entrance angle; RPM-Screw speed; SFL-Specific feeding load. Variables must be adjusted by subtracting the experimental design parameter median values (see text).

### Effects of Extrusion Conditions

Figure 3(a) for die swell shows an increasing die swell with increasing SFL at constant screw speed. This is as would be expected for a stable thermoplastic polymer under controlled temperature conditions (Han 1976) since increasing

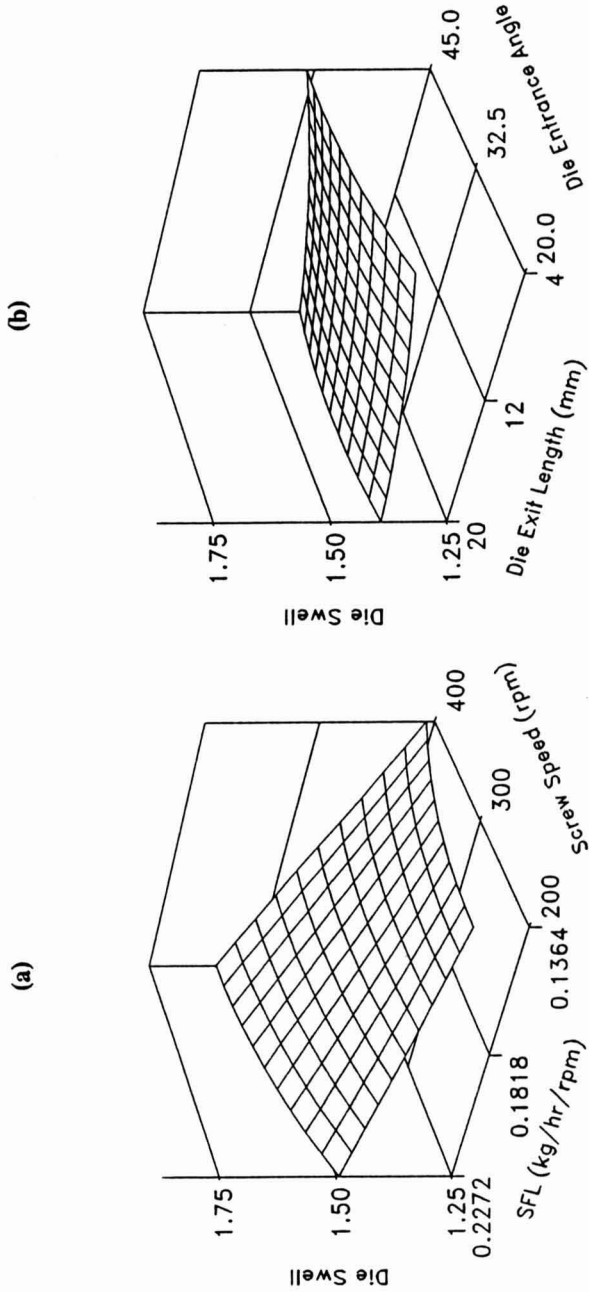


FIG. 3. DIE SWELL RESPONSE TO (a) EXTRUDER CONDITIONS AND (b) DIE PARAMETERS

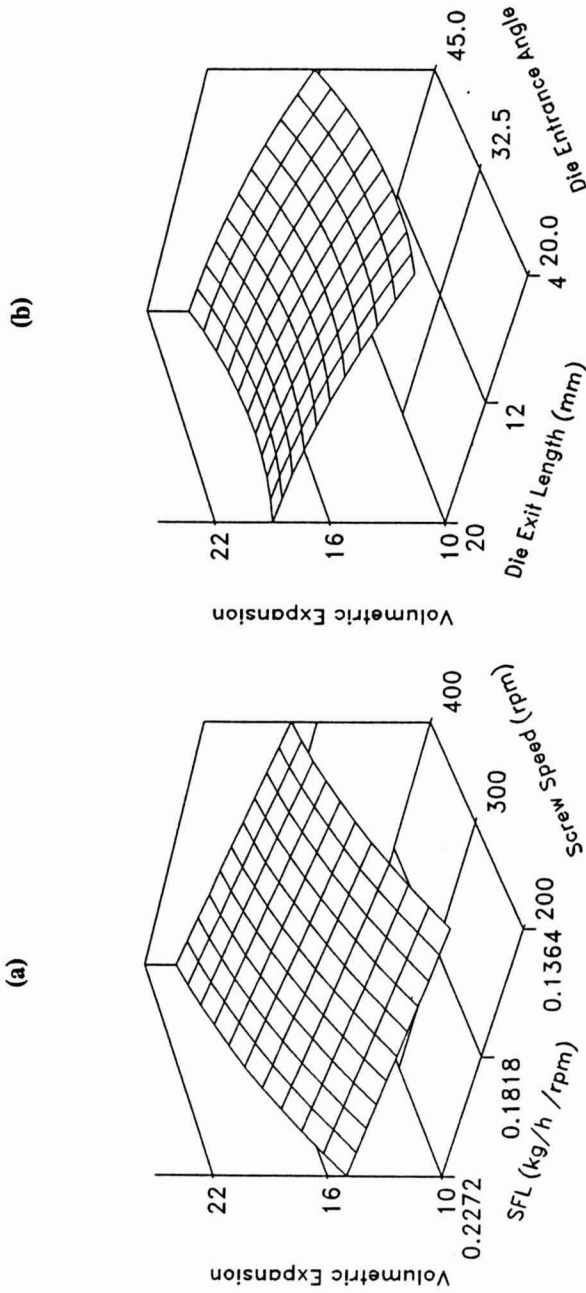


FIG. 4. VOLUMETRIC EXPANSION RESPONSE TO (a) EXTRUDER CONDITIONS AND (b) DIE PARAMETERS

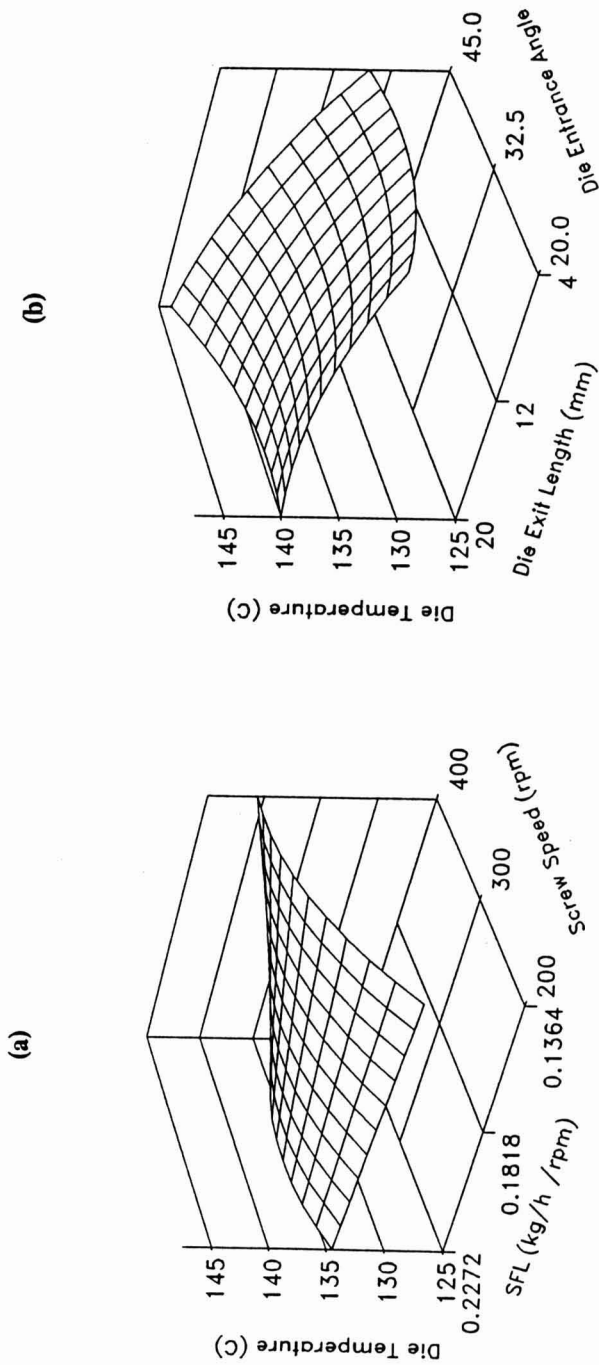


FIG. 5. TEMPERATURE RESPONSE TO (a) EXTRUDER CONDITIONS AND (b) DIE PARAMETERS

SFL increases the feed rate and, therefore, increases the shear rate within the extruder die as well as the elongation rate at the die entrance. Both effects tend to increase the normal stress difference at the die exit. The die swell response to screw speed shows an interaction, with an increasing trend at low SFL and a decrease at high SFL. The slightly decreasing trend in die swell with increasing screw speed at constant SFL is contrary to that expected for stable polymer extrusion. Because the experimental extruder variable is SFL, increasing the screw speed also increases the feed rate (for example, the feed rate increases from 36.4 to 72.7 kg/h as screw speed increases from 200 to 400 rpm for the 0.182 kg/h/rpm SFL), and therefore increases the shear rate within the die. If the state variables were held constant, an increased feed rate would produce an increased die swell; therefore, the contrary trend strongly indicates that either the temperature or the chemical state changes with screw speed.

The temperature response [Fig. 5(a)] is concave downward with respect to screw speed and also has an interaction with SFL. The temperature interaction may have caused the trend reversal in die swell with screw speed as SFL changes, but does not appear to have a great influence on the die swell response to SFL. Also, the temperature alone can not account for the lack of die swell increase with increasing screw speed as described above, and therefore the screw speed response appears to be explained by a change in chemical state. This is reasonable since the screw speed in twin-screw extrusion of corn meal has been shown to produce changes in starch polymer molecular weight and molecular weight distribution by Wen *et al.* (1990).

Figure 4(a) for volumetric expansion shows only a slight increase with SFL at constant screw speed, but a large increase with increasing screw speed at constant SFL. When doubled the screw speed produced nearly a two-fold increase in volumetric expansion. Because the product flow rate should not have direct effects on volumetric expansion, the trends in volumetric expansion must be related to the state variables. The temperature [Fig. 5(a)] is directly responsible for the expansion driving force, i.e. the moisture vapor pressure, but also will affect the extrudate viscosity or resistance to expansion (Kokini 1992). The lack of correlation between temperature and volumetric expansion with respect to extruder condition suggests that the extruder condition influence the chemical state. The chemical state influences the melt viscosity, or resistance to expansion (Kokini 1992); the glass transition of the dough melt, which will determine at what point the extrudate sets (Slade and Levine 1991); and the moisture solubility within the dough, which may affect the driving force for expansion (Han 1981). A comparison between the volumetric expansion to screw speed and SFL shows the screw speed to be the more influential parameter, and therefore suggests screw speed to have greater influence on the chemical state. This supports the die swell results.

## Effects of Die Parameters

Figure 3(b) for die swell shows a decreasing trend with increasing exit capillary length and a concave upward but insensitive response to entrance cone angle. The trend for exit length indicates a decaying elongational entrance flow elastic recoil, which is found in thermoplastic extrusion (Han 1976). The insensitivity of die swell to entrance angle is somewhat surprising since entrance angle effects on die swell have been reported (Han 1976). Flow in the entrance region is composed of both shear flow and elongational flow, and the degree to which each type of flow occurs is extremely complicated (Padmanabhan and Bhattacharya 1993). As the entrance angle changes, so will the relationship between elongational and shear flow.

However, the temperature response to die parameters [Fig. 5(b)] shows trends opposite to the die swell. Die swell has been found to decrease with increasing temperature due to a decreased elastic decay time constant and decreased primary normal stress coefficient (Bird *et al.* 1987; Han 1976). Therefore, the temperature may be a major factor in the die swell response to die parameters. Note that conclusions concerning the influence of die parameters on chemical state are lacking. An increased die restriction has been found to increase residence time within a twin-screw extruder (Altomare and Ghossi 1986), but how this influences chemical structure responsible for elastic and viscous responses is not known.

The volumetric expansion tends to increase with increasing exit capillary length and has a slight concave upward response to entrance cone angle [Fig. 4(b)]. The die temperature response surface has a similar shape [Fig. 5(b)], suggesting that the temperature is highly influential in the volumetric expansion (as well as the die swell) response to die parameters. The direct correlation between die temperature and volumetric expansion is reasonable since higher temperatures produce lower viscosity (less resistance to expansion) and a greater driving force for expansion.

## CONCLUSIONS AND RECOMMENDATIONS

The proposed analysis method for extrudate expansion and shape appears to produce results which are largely explainable in terms of die geometry effects (die design and product flow rate) and the state variables (temperature and chemical condition of the food product). The die swell and volumetric expansion responses to die parameters appear to be dominated by temperature; the responses to screw speed suggest structural changes in the food polymers; and the responses to SFL appear to be driven by shear rate (for die swell) and to some degree by chemical state (for volumetric expansion). Die swells calculated

from this method are quantitatively similar to those found for nonexpanded food and thermoplastic polymers, ranging from approximately 1.2 to 1.7 (see Appendix). The die swell phenomenon in this study represents from 10 to 22% of the total radial expansion of the corn meal product and accounted for from 18 to 38% of the extrudate cross sectional area.

Further work in validating the model is needed. Verification by applying the method to starch and protein extrusion with added minor ingredients such as sugar, salt, fiber, and lipids, which are known to have large influences on the product (Hsieh *et al.* 1990; Badding-Smithey 1993; Lin 1994), will be useful. Application of the model to extrusion of different starch types for comparison purposes would also provide support for the model. In addition, the die swell and volumetric expansion should be related to the chemical state of the food product, as defined by the molecular weight, molecular weight distribution, degree of cross-linking, glass transition temperature, etc.

Finally, the proposed analysis method can be used to predict die swell and volumetric expansion as long as the extrudate meets the underlying analysis assumptions. Exceptions to the assumptions, such as extrudate curling, a large degree of surface bubble collapse, or moisture vaporization inside the die, will skew the results, and must be taken into consideration when interpreting the data. For well behaved extrudates, the analysis method should be useful for evaluating extruded food viscoelasticity. The true value in the model lies in quantifying the degree to which elasticity influences the product shape. Some examples of areas in which the model could be applied are for evaluating the influence of extrusion variables on viscoelasticity, relating molecular parameters to viscoelasticity, and relating viscoelasticity to product sensory properties.

## NOMENCLATURE

$\eta$	Viscosity of fluid extrudate, Pa·s
$\Psi_1$	Primary normal stress coefficient, P·as <sup>2</sup>
$\Psi_2$	Secondary normal stress coefficient, Pa·s <sup>2</sup>
$\rho_D$	Density of extruded, nonexpanded corn meal, 1200 kg/m <sup>3</sup>
$L_0$	Length of extrudate before die swell and volumetric expansion, m
$L_1$	Length of extrudate after die swell and before volumetric expansion, m
$L_2$	Final expanded extrudate length, m
PPW	Measured per piece weight of extrudate, kg
$\Delta P_s$	Pressure differential between extrudate steam pressure and atmospheric pressure, Pa/m <sup>2</sup>
$R_0$	Radius of extruder die, m
$R_1$	Radius of extrudate after die swell and before volumetric expansion, m
$R_2$	Final expanded extrudate radius, m

SFL	Specific feeding load, feed rate/screw speed, kg/h/rpm
$V_1$	Volume of nonexpanded extrudate, $m^3$
$V_2$	Volume of expanded extrudate, $m^3$
%DSRAD	Percentage of the extrudate radius resulting from die swell
%VERAD	Percentage of the extrudate radius resulting from volumetric expansion
%DSCSA	Percentage of the extrudate cross sectional area resulting from die swell

## APPENDIX

This appendix is provided to illustrate the calculation of the percentage of extrudate radial expansion and cross sectional area attributed to die swell. Table A1 shows extrudate length, width, and per piece weight raw data for two extruder conditions, the low and high SFLs at an extruder screw speed of 400 rpm, for all dies and both replications. These two conditions contained the smallest and largest die swell values obtained in this experiment. Table A1 also contains the die swell and volumetric expansion values determined according to Eq. (1) through (6) above. These data represent a portion of the data set used in developing the statistical models which were subsequently used in preparing the response surfaces in Fig. 3 and 4.

The final three columns in Table A1 show the degree to which die swell and volumetric expansion influence the final product radius and cross sectional area. The percentage of the total extrudate radius resulting from die swell and volumetric expansion were determined according to:

$$\%DSRAD = 100[0.002(\text{DieSwell}-1)/(R_2 - 0.002)] \cdot 100 \quad (\text{A1})$$

$$\%VERAD = 100[1 - \%DSRAD/100 - (0.002/R_2)] \quad (\text{A2})$$

Where the initial radius is 0.002 m. Note that the die exit radius is taken out of the %DSRAD and %VERAD values.

The percentage of the extrudate cross sectional area attributed to die swell is calculated by comparing with an extrudate with a die swell of unity. This is obtained by subtracting the radius attributed to die swell from the total extrudate radius according to:

$$\%DSCSA = 100[(R_2^2 - (R_2(1 - \%DSRAD/100))^2)/(R_2^2)] \quad (\text{A3})$$

TABLE A1.  
 RAW LENGTH, WIDTH, AND PER PIECE WEIGHT DATA AND MODEL ANALYSIS RESULTS FOR THE LOW AND HIGH SFL CONDITIONS AT 400 RPM SCREW SPEED, ALL DIES AND BOTH REPLICATIONS. " ." INDICATES MISSING DATA

SFL (kg/hr/ rpm)	Screw Speed (rpm)	Entrance Cone Angle (°)	Exit Capillary Length (mm)	Extrudate Length (mm)	Extrudate Width (mm)	Per Piece Weight (g)	Die Swell	Volume- tric Expansion	% Radius from Die Swell	% Radius from Vol- umetric Expansion	% Cross Sectional Area from Die Swell
0.136	400	20.0	4	.	.	.	1.33	.	13.9	56.3	25.9
0.136	400	20.0	4	33.4	13.4	0.352	.	16.1	.	.	.
0.136	400	20.0	12	44.7	13.0	0.370	1.21	19.1	9.44	59.7	18.0
0.136	400	20.0	12	42.0	12.2	0.356	1.20	16.6	9.58	57.7	18.2
0.136	400	20.0	20	40.8	13.3	0.351	1.24	19.3	10.2	59.6	19.4
0.136	400	20.0	20	43.8	13.4	0.362	1.22	20.5	9.54	60.6	18.2
0.136	400	32.5	4	31.1	13.4	0.351	1.36	15.1	15.3	55.0	28.2
0.136	400	32.5	4	35.2	12.8	0.352	1.28	15.3	12.9	55.7	24.2
0.136	400	32.5	12	41.5	13.2	0.369	1.25	18.6	10.8	59.0	20.4
0.136	400	32.5	12	40.1	13.1	0.370	1.26	17.5	11.5	58.0	21.6
0.136	400	32.5	20	39.8	13.2	0.362	1.26	18.0	11.2	58.4	21.2
0.136	400	32.5	20	43.3	12.6	0.364	1.21	17.9	9.58	58.8	18.2
0.136	400	45.0	4	35.7	13.0	0.372	1.31	15.3	13.8	55.5	25.6
0.136	400	45.0	4	34.7	13.2	0.363	1.32	15.8	13.8	55.9	25.7
0.136	400	45.0	12	41.2	13.0	0.361	1.24	18.2	10.5	58.8	20.0
0.136	400	45.0	12	37.3	13.6	0.360	1.30	17.9	12.4	58.2	23.2
0.136	400	45.0	20	42.2	13.2	0.346	1.22	20.1	9.40	60.4	17.9
0.136	400	45.0	20	45.2	13.3	0.354	1.20	21.3	8.59	61.4	16.4
0.227	400	20.0	4	.	.	.	.	.	.	.	.
0.227	400	20.0	4	39.2	16.9	0.610	1.64	17.4	19.6	56.7	35.4
0.227	400	20.0	12	48.2	17.3	0.629	1.55	21.5	16.6	60.2	30.5
0.227	400	20.0	12	48.0	17.0	0.598	1.52	21.9	16.0	60.5	29.4
0.227	400	20.0	20	46.5	18.1	0.608	1.58	23.7	16.4	61.6	30.1
0.227	400	20.0	20	47.9	18.0	0.613	1.56	23.8	16.1	61.6	29.6

TABLE A1. (Continued)

SFL (kg/hr/ rpm)	Screw Speed (rpm)	Entrance Cone Angle (°)	Exit Capillary Length (mm)	Extrudate Length (mm)	Extrudate Width (mm)	Per Piece Weight (g)	Die Swell	Volume- tric Expansion	% Radius from Die Swell	% Radius from Vol- umetric Expansion	% Cross Sectional Area from Die Swell
0.227	400	32.5	4	39.1	17.0	0.677	1.70	15.7	21.4	55.0	38.3
0.227	400	32.5	4	39.2	17.5	0.606	1.65	18.6	19.3	57.8	34.8
0.227	400	32.5	12	43.4	17.2	0.618	1.60	19.7	18.0	58.8	32.8
0.227	400	32.5	12	48.3	16.5	0.624	1.52	19.9	16.7	59.0	30.7
0.227	400	32.5	20	49.3	16.9	0.821	1.67	16.1	20.8	55.5	37.3
0.227	400	32.5	20	46.3	17.2	0.629	1.57	20.5	17.3	59.4	31.6
0.227	400	45.0	4	40.7	18.0	0.605	1.64	20.5	18.4	59.4	33.4
0.227	400	45.0	4	40.6	18.1	0.601	1.64	20.9	18.3	59.6	33.2
0.227	400	45.0	12	43.6	18.1	0.615	1.62	21.8	17.5	60.3	32.0
0.227	400	45.0	12	44.0	18.2	0.607	1.61	22.7	17.1	60.9	31.4
0.227	400	45.0	20	49.2	17.6	0.596	1.52	24.1	15.4	61.9	28.4
0.227	400	45.0	20	50.9	17.2	0.594	1.49	23.9	14.9	61.8	27.6

## REFERENCES

- ALTOMARE, R.E. and GHOSHI, P. 1986. An analysis of residence time distribution patterns in a twin screw cooking extruder. *Biotech. Prog.* 2, 157-163.
- ALVAREZ-MARTINEZ, L., KONDIRY, K.P. and HARPER, J.M. 1988. A general model for expansion of extruded products. *J. Food Sci.* 53, 609-615.
- BADDING-SMITHEY, S. 1993. Effects of Screw Speed and Additives on Extrusion of Corn Meal. Ph.D. Dissertation. University of Missouri-Columbia, Columbia, MO.
- BIRD, R.B., ARMSTRONG, R.C. and HASSAGER, O. 1987. *Dynamics of Polymeric Liquids*, 2nd Ed., John Wiley & Sons, New York.
- COCHRAN, W.G. and COX, G.M. 1957. *Experimental Designs*, 2nd Ed., John Wiley & Sons, New York.
- GOUBLOMME, A., DRAILY, B. and CROCHET, M.J. 1992. Numerical prediction of extrudate swell of a high-density polyethylene. *J. Non-Newtonian Fluid Mech.* 44, 171-195.
- GRAESSLEY, W.W., GLASSCOCK, S.D. and CRAWLEY, R.L. 1970. Die swell in molten polymers. *Trans. Soc. Rheol.* 14, 519-544.
- HAN, C.D. 1976. *Rheology in Polymer Processing*. Academic Press, New York.
- HAN, C.D. 1981. *Multiphase Flow in Polymer Processing*. Academic Press, New York.
- HSIEH, F. PENG, I. and HUFF, H.E. 1990. Effects of salt, sugar, and screw speed on processing and product variables of corn meal extruded with a twin-screw extruder. *J. Food Sci.* 55, 224-227.
- KOKINI, J.L., CHANG, C.N. and LAI, L.S. 1992. The role of rheological properties on extrudate expansion. In *Food Extrusion Science and Technology*, (Kokini, Chi-Tang Ho, and Karwe, eds.) pp. 631-652, Marcel Dekker, New York.
- LAUNAY, B. and LISCH, J.M. 1983. Twin-screw extrusion cooking of starches: flow behaviour of starch pastes, expansion and mechanical properties of extrudates. *J. Food Eng.* 2, 259-280.
- LIN, S. 1994. Utilization of Beef Tallow in the Production of extruded Dry Pet Food. Ph.D. Dissertation. University of Missouri-Columbia, Columbia, MO.
- LODGE, A.S. 1964. *Elastic Liquids*. Academic Press, New York.
- MITSOULIS, E., VLACHOPOULOS, J. and MIRZA, F.A. 1985. A numerical study of the effect of normal stresses and elongational viscosity on entry vortex growth and extrudate swell. *Polym. Eng. Sci.* 25, 677-689.
- NETER, J., WASSERMAN, W. and KUTNER, M.H. 1989. *Applied Linear Regression Models*, 2nd Ed., Richard D. Irwin, Boston, MA.

- OFOLI, R.Y., MORGAN, R.G. and STEFFE, J.F. 1993. Characterization of the swelling of starch doughs during extrusion. *J. Food Eng.* 18, 297-312.
- PADMANABHAN, M. and BHATTACHARYA, M. 1989. Analysis of pressure drop in extruder dies. *J. Food Sci.* 54, 709-713.
- PADMANABHAN, M. and BHATTACHARYA, M. 1993. Planar extensional viscosity of corn meal dough. *J. Food Eng.* 18, 389-411.
- SAS. 1990. *Statistical Analysis System*, Version 6.07. SAS Institute, Inc., Cary, NC.
- SLADE, L. and LEVINE, H. 1991. Beyond water activity: recent advances based on an alternative approach to the assessment of food quality and safety. *Crit. Rev. Food Sci. Nutr.* 30, 115-360.
- STEFFE, J.F. 1992. *Rheological Methods in Food Process Engineering*. Freeman Press, East Lansing, MI.
- TANNER, R.I. 1988. Recoverable Elastic Strain and Swelling Ratio. In *Rheological Measurement*, (A.A. Collyer and D.W. Clegg, eds.) Elsevier, New York.
- WEN, L., RODIS, P. and WASSERMAN, B.P. 1990. Starch fragmentation and protein insolubilization during twin-screw extrusion of corn meal. *Cereal Chem.* 67, 268-275.

# SIMULTANEOUS HEAT AND MASS TRANSFER DURING THE DEEP FAT FRYING OF TORTILLA CHIPS

ROSANA MOREIRA<sup>1</sup>, JAIME PALAU and XIUZHI SUN

*Department of Agricultural Engineering  
Texas A&M University  
College Station, TX 77843-2117*

Accepted for Publication September 30, 1994

## ABSTRACT

*The heating and water loss of a single tortilla chip during deep fat frying was investigated experimentally and the data were analyzed by writing two heat and mass transfer balances. The equations were solved using explicit finite difference technique. Oil uptake as a function of frying time was described by a first order exponential equation. The empirical and theoretical heat and mass transfer agreed well.*

*The effect of oil temperature on the moisture loss and oil uptake as a function of frying time was analyzed. Moisture loss rate increased as temperature increased. The effects of temperature on oil uptake were not significant during the first 15 s of frying, however, the final oil content was higher for the tortilla chip fried at 190C than at 150C for 60 s.*

## INTRODUCTION

Deep fat frying is a process that involves simultaneous heat and mass transfer. Heat is transferred from the oil to the food, water is evaporated from the product and oil is absorbed by the product. Factors that affect heat and mass transfer are the thermal and physical properties of the food and the oil, the geometry of the food, the temperature of the oil, and the conditions that will lead to the degradation of the oil during the process.

Pravisanı and Calvelo (1991) studying the heat and mass transfer mechanisms in potato strips proposed the existence of a moving boundary layer that separates

<sup>1</sup>Correspondence: Rosana Moreira, 310 Scoates Hall, Texas A&M University, College Station, TX 77843-2117. Phone: (409)847-8794.

the crumb and crust that is maintained at 103C. Gamble and Rice (1987, 1988) and Rice and Gamble (1989) noted that the free water at the surface of potato chips evaporated rapidly, the surface became dry, and the inner moisture was converted to vapor, creating a pressure gradient. Oil content in the chips increased as water content decreased during the frying process. The distribution and the amount of oil absorbed were affected by the pre-drying treatment, frying time, surface area, and thickness of the potato chip. Guillaumin (1988) reported that there was a linear relationship between the thickness of potato chips and the amount of oil absorbed. McDonough *et al.* (1993) concluded that the oil diffused into tortilla chips through small channels formed as water evaporated from the product. Moreira *et al.* (1991) showed that most of the oil in tortilla chips were not uniformly distributed and it concentrated around the edges and the in chip's puffed areas.

Several models have been developed to describe moisture desorption characteristics of biological products (Moreira and Bakker-Arkema 1989). Askenazi *et al.* (1984) determined that the water diffusion during frying of french fries was proportional to the square root of the frying time. Gamble *et al.* (1987) used the same model to describe the drying rate of potato chips in deep-fat frying. Kozempel *et al.* (1991) used Fick's law of diffusion to model moisture loss and a zero order kinetics to predict oil absorption during deep-fat frying of french fries. Moreira *et al.* (1991) also used the diffusion model to predict moisture loss for tortilla chips during deep-fat frying.

Many attempts have been made to combine heat and mass transfer principles to describe the temperature and moisture content profiles in a product during deep fat frying process. Ashkenazi *et al.* (1984) proposed a semi empirical model to predict temperature and mass loss in potato strips. Keller and Escher (1989) proposed a more fundamental model based on energy balances and phase diagrams to describe the frying process of french fries. Neither model was able to describe temperature and moisture profiles inside the product.

Many studies have been concentrated in the measurement of the convective heat transfer coefficient as a function of frying time. Hallström (1979) studied the temperature profile of meat patties during deep fat frying and found that the convective heat transfer coefficient varied from 250-300 W/m<sup>2</sup>C before water evaporated from the patty. Dagerskop and Sorenfors (1978) fried meat patties at 190C and reported heat transfer coefficients of 300-700 W/m<sup>2</sup>C during the process. Califano and Calvelo (1991) measured the convective heat transfer coefficient as a function of oil temperature using the lumped method (Holmann 1981) by heating a copper cylinder in a bath of oil. The convective heat transfer coefficient ranged between 150 to 165 W/m<sup>2</sup>C for a temperature range between 50 to 100C. Miller and Singh (1992) using the lumped method concluded that the convective heat transfer coefficient of soybean oil at 188C was higher (282 W/m<sup>2</sup>C) for fresh oil than for used oil (261 W/m<sup>2</sup>C). Similar results were

obtained by Moreira *et al.* (1992) for soybean oil at 190C (285 W/m<sup>2</sup>C for fresh and 273 W/m<sup>2</sup>C for used oil).

Although several researchers have described the moisture loss as diffusion mechanism, it is still not clear how and when the oil is absorbed by the product. Gamble *et al.* (1987) indicated that as the product fries, the inner moisture is converted to steam causing a pressure gradient, and as the surface dries out, the oil adheres to the product's surface and enters the surface at damaged areas. They suggested that most of the oil enters the chips from the adhering oil being pulled into the chip when it is removed from the fryer due to condensation of steam. Matz (1993) commented that if potato chips are removed from the fryer while their temperature is still rising, only 15% of the oil will be absorbed, the remainder will be held on the surface. He added that large part of this oil is drawn into the pores as the chip cools, and the rest runs off. Pinthus and Saguy (1993) demonstrated that interfacial tension significantly affected oil uptake in deep-fat frying of potato products, suggesting that the mechanism for oil absorption is due to capillary forces.

The objectives of this paper were to model the simultaneous heat and mass transfer during the deep fat frying of tortilla chips and then to study the effects of oil temperature on the oil adsorption and water evaporation as function of frying time.

## THEORY

During the frying process of tortilla chips, the heat is transferred from the hot oil to the product surface by convection and from the surface to the center of the chip by conduction. The liquid water moves from inside of the chips to the evaporation zone leaving the product through the surface as vapor. Some of this vapor though, may remain trapped within the pores due to restrictive intercellular diffusion. The vapor in this confined space will expand and become superheated, distorting the pore walls and contributing for the chips porosity. Moreira and Barrufet (1994) proposed that the oil uptake by the chips can be described in terms of capillary forces alone. The large temperature gradient created when the chip is removed from the fryer, causes the pressure of the superheated vapor within the cell to drop until it condenses. This results in a positive capillary pressure. The oil thus imbibes into the chip spontaneously, with a resultant countercurrent flow of the water vapor. Moreira and Barrufet (1994) described the mechanism of oil uptake in tortilla chips using the percolation theory.

## Mathematical Model

Since the chip thickness is one order of magnitude smaller than its length or width, an infinite slab was considered in this study to derive the one-dimensional heat and moisture transfer equations for a tortilla chip during frying. All symbols are defined at the end of the paper. The following assumptions were made:

- (1) the initial moisture and temperature distributions in the tortilla chip are uniform,
- (2) shrinkage is negligible,
- (3) thermal and moisture diffusivities are constants,
- (4) the oil spontaneously imbibes the chip during the cooling down period.

## Heat and Mass Balances During Frying

**1. Mass Balance for Moisture Content of the Product.** The moisture content change of a chip can be described by a diffusion model:

$$\frac{\partial M_w}{\partial t} = D \left[ \frac{\partial^2 M_w}{\partial x^2} \right] \quad (1)$$

**2. Energy Balance for the Product.** The temperature change of a chip can be described by a diffusion equation:

$$\frac{\partial \theta}{\partial t} = \alpha \left[ \frac{\partial^2 \theta}{\partial x^2} \right]$$

Equations (1) and (2) constitute the simulation model for the deep-fat frying of a tortilla chip. The initial and boundary conditions used to solve Eq. (1) and (2) are:

## Initial Conditions

$$M_w(x,0) = M_{w_0}, \quad \theta(x,0) = \theta_0 \quad \text{for } x < a \quad (3)$$

### Boundary Conditions

$$\frac{\partial M_w}{\partial x} \Big|_{x=0} = 0 \quad \text{and} \quad \frac{\partial \theta}{\partial x} \Big|_{x=0} = 0 \quad (4)$$

$$D \frac{\partial M_w}{\partial x} \Big|_{x=x_0} = h_D [M(\text{surf}) - M(\text{eq})] \quad (5)$$

$$-k \frac{\partial \theta}{\partial x} \Big|_{x=x_0} = h(\theta_s - T_\infty) - h_{fg} D \rho \frac{\partial M_w}{\partial x} \Big|_{x=x_0} \quad (6)$$

The resulting system of partial differential equations in time and space dimensions were solved numerically by applying the explicit finite difference method by dividing the tortilla chip thickness into 10 nodes.

### Oil Absorption

It is assumed that after frying the surface of the tortilla chip is covered with oil. It was observed (Moreira *et al.* 1995a) that oil content in tortilla chips increased as frying time increased as result of moisture loss. Palau (1993) observed that tortilla chips fried for 5 s were flexible (not crisp) and had the surface completely covered with oil. However, tortilla chips fried for 60 s were crispier, had a dry surface, and higher oil content than the one fried for 5 s.

In this study, tortilla chips average oil content/frying time data were correlated using a first order exponential equation:

$$\bar{M}_f(t) = M_{fe} [1 - \exp(-k't)] \quad (7)$$

## MATERIALS AND METHODS

### Samples

Tortilla chips were prepared from commercial nixtamalized corn flour tortilla masa (Valley Grain Products, Muleshoe, TX). About 1000 g of the dry masa flour was mixed with 900 g of distilled water at room temperature in a Hobart

mixer (Model A200, Troy, OH) until the dough was formed. It was then fed through a sheeter (Model CH4-STM, Superior Food Machinery, Pico Rivera, CA) to form the tortilla chips. The thickness (about 2 mm) of the tortilla chip was determined by keeping the weight of 10 tortilla chips at approximately 29 to 30 g. The molded masa was baked in a gas fired oven for about 50 s at 343, 222, and 220C for the top, middle, and bottom tiers, respectively (Model CO400, Superior Food Machinery Inc.). The baked tortilla chips were cooled at room conditions for about 15 min.

## Experiments

An average of 30 raw tortilla chips (100 g/batch) were fried at  $190 \pm 5\text{C}$  in partially hydrogenated winterized soybean oil in a deep fat batch fryer (Frymaster Model MJ-35, BLSSP) containing 3 gallons of oil. The raw tortilla chips were fried for 5, 10, 15, 20, 25, 30, 45 and 60 s to determine the amount of water loss and oil absorption in the chips as a function of frying time. The fried chips were drained on paper towels, cooled at ambient conditions, and stored in plastic bags.

## Measurements of Process Variable

Measurements were repeated three times at each experimental condition.

**Moisture Content.** Fried tortilla chips were ground and mixed using a commercial blender (Braun, KSM2). The moisture content of the sample (5 g) was determined using the oven drying method at 105C for 24 h (AACC 1986).

**Oil Content.** Fried tortilla chips were ground and mixed using a commercial blender (Braun, KSM2). The oil content (wet basis) of the sample was determined using the 8 h-soxhlet extraction method with petroleum ether (AACC 1986).

**Tortilla Chip's Temperature.** A thin thermocouple (Type-E, 34-gauge - 0.01") was inserted in the center of a raw tortilla chip and the temperature change during frying was recorded using a datalogger (Model LI-1000; LI-COR, Inc. Lincoln, NE).

The value of oil uptake rate  $k'$  was determined by fitting the experimental data to Eq. (7) using nonlinear regression analysis (Ploti-It, Scientific Programming Enterprises, Haslett, MI).

The value of moisture diffusion  $D$  and  $h_D$  were determined by minimizing the residual mean square between observed and simulated moisture content data.

The average values of thermal conductivity and thermal diffusivity were measured as discussed in Moreira *et al.* (1995b). The convective heat transfer coefficient was estimated using the lumped model for the heat transfer in an aluminum cylinder with a density of 2707 [kg/m<sup>3</sup>], volume of  $1.16244 \times 10^{-5}$  [m<sup>3</sup>], specific heat of 0.89 [kJ/kgC], and area of  $3.014 \times 10^{-3}$  [m<sup>2</sup>]. A thermocouple was inserted in the cylinder geometrical center to allow for time-temperature data to be recorded using a datalogger (Model LI-1000, LICOR, Inc., Lincoln, NE) as the probe was immersed into the frying oil. The convective heat transfer coefficient was calculated by fitting the temperature-time data to the model:

$$T(t) = (T_o - T_\infty) \exp \left[ \frac{-h A t}{\rho C_p V} \right] \quad (8)$$

## RESULTS AND DISCUSSION

### Simulation

The simulation was run for the case of tortilla chips fried at  $190 \pm 5$ C in fresh oil.

The values of the thermal and physical properties of the oil and a tortilla chip used in the simulation are given in Table 1. At  $\Delta x = 0.0001$  m  $\Delta t = 0.1$  s the program is stable. The value for  $h_D$  was determined by using Eq. (5) with the value of  $D$  found with Eq. (1). Although the estimated value for the convective heat transfer coefficient (280 W/m<sup>2</sup>C) used in the simulation applies to bodies with simple geometry and smooth surfaces, it was assumed that this value is typical for the beginning and final stages of the process for tortilla chips when no water is evaporating from the chip. Although the  $h$  value is important for the formation of the crust, Hallström (1979) indicated that during the evaporation process the main resistance to the heat transfer is inside of the product, the high heat transfer coefficient is of minor importance. The values of  $\rho$ ,  $k$ , and  $C_p$  are the average measured values for tortilla chips fried from 5-60 s at 5 s intervals.

**Moisture Loss.** Figure 1 shows the observed and simulated average moisture content during the frying of tortilla chips. The results are the average of three experiments. The standard deviation varied from 0.5 to 2.6% d.b. The evaporation rate was high during the first 15 s of frying, becoming fairly constant as frying continues. The equilibrium moisture content was reached around 20-30 s of frying.

TABLE 1.  
PARAMETERS USED IN THE SIMULATION OF A TORTILLA CHIP FRIED IN USED  
OIL AT 190C

Parameter	Value
$\rho$	1300 kg/m <sup>3</sup>
a	2 mm
k	0.11 W/mC
Cp	2.56kJ/kgC
$\alpha$	$3.3 \times 10^{-8}$ m <sup>2</sup> /s
$h_{fg}$	2200 kJ/kg
$h_D$	0.00187 m/s
D	$9.348 \times 10^{-8}$ m <sup>2</sup> /s
k'	0.223 1/s
h	280 W/m <sup>2</sup> C
$\theta$	25C
T <sub>∞</sub>	190C
M <sub>w0</sub>	53% d.b.
M <sub>fe</sub>	25%

**Heat Transfer.** A good agreement between the observed and simulated temperature profile at the center during frying are presented in Fig. 2. The simulated value for node 5 (middle point) is also presented. The points shown in the plot are the average of the observed values for three different experiments conducted at the same frying conditions (frying temperature of 185C). Larger standard deviation in the data was observed at the beginning of the frying process during the transient phase of the process. The standard deviation in the data varied from 0.6 to 20.8C. The authors consider that the discrepancy between the data in Fig. (5) is due to the difficulty of measuring the center temperature values of the chip accurately.

The center temperature of the tortilla chip reached 100C in about 10 s of frying. It took about 30-40 s for the center temperature of the chip to approach that of the oil.

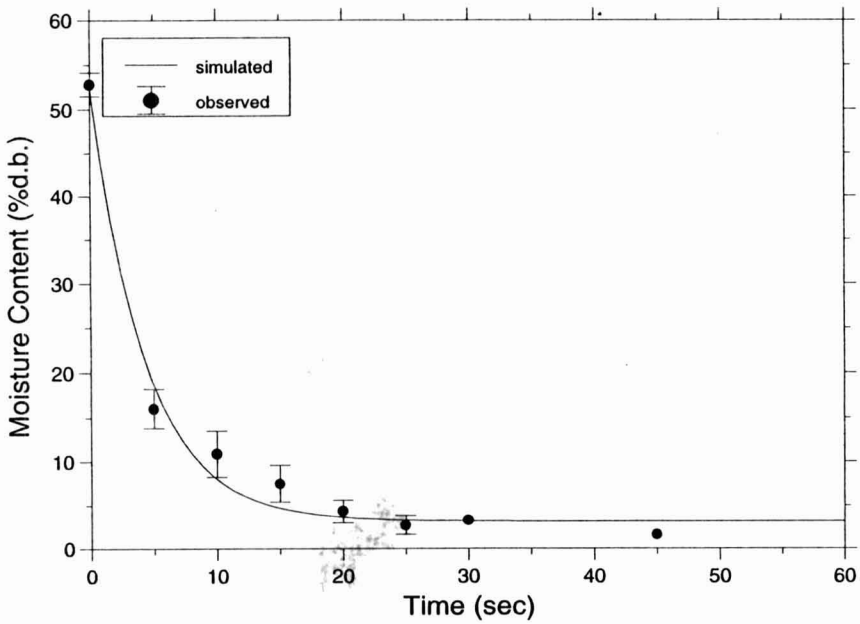


FIG. 1. SIMULATED AND OBSERVED VALUES FOR THE AVERAGE MOISTURE LOSS OF A TORTILLA CHIP DURING FRYING

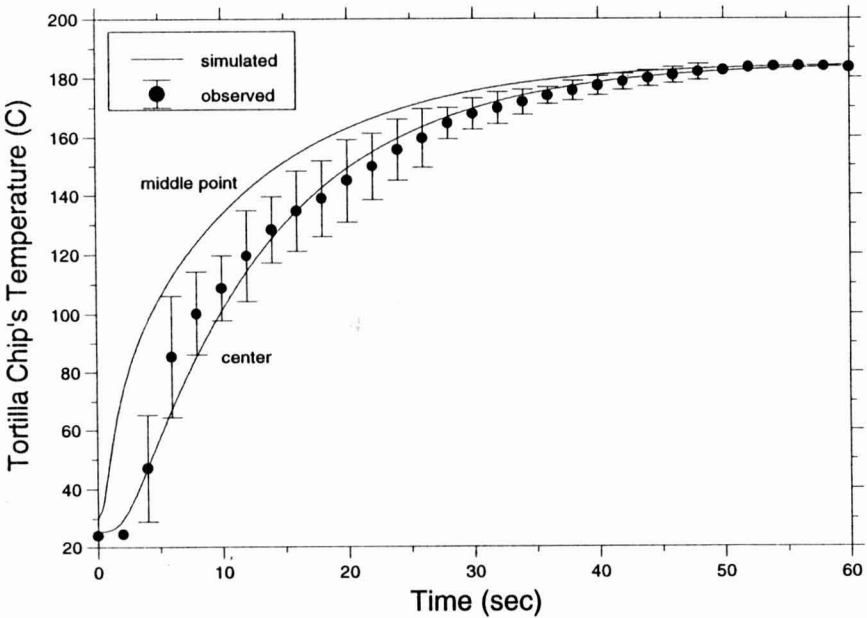


FIG. 2. SIMULATED AND OBSERVED TEMPERATURE PROFILE AT THE CENTER OF A TORTILLA CHIP DURING FRYING

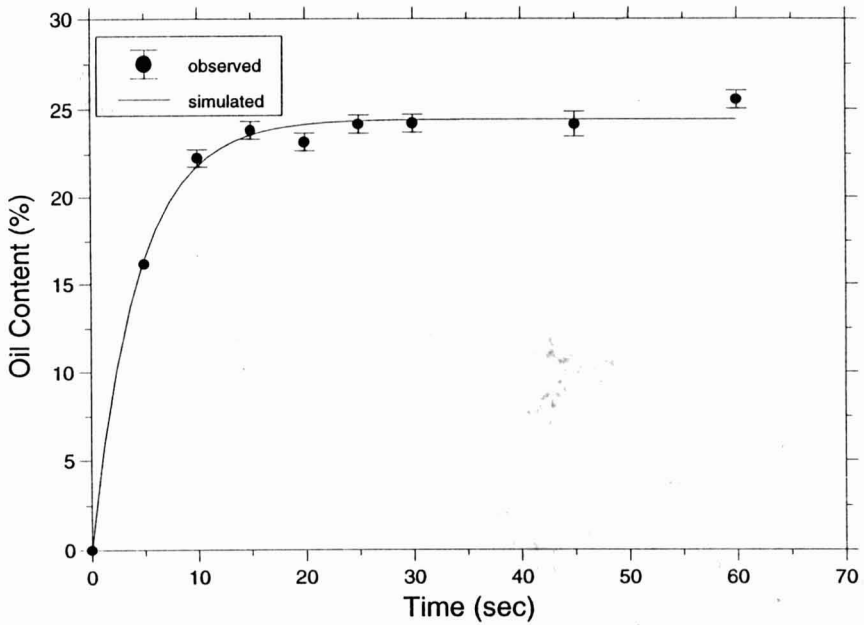


FIG. 3. SIMULATED AND OBSERVED AVERAGE OIL CONTENT OF TORTILLA CHIPS AS A FUNCTION OF FRYING TIME

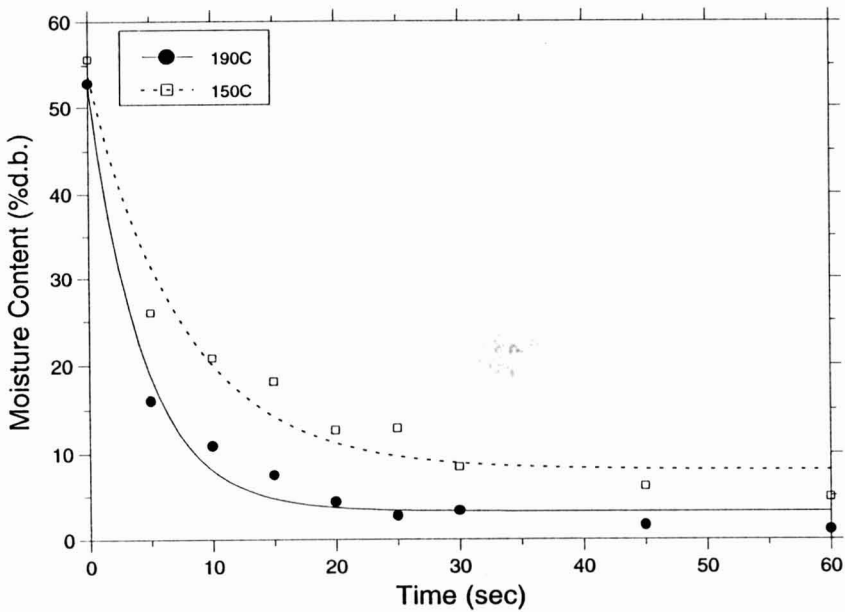


FIG. 4. COMPARISON OF WATER LOSS OF TORTILLA CHIPS FRIED AT DIFFERENT FRYING TEMPERATURES [dots are observed values and lines are the simulated values]

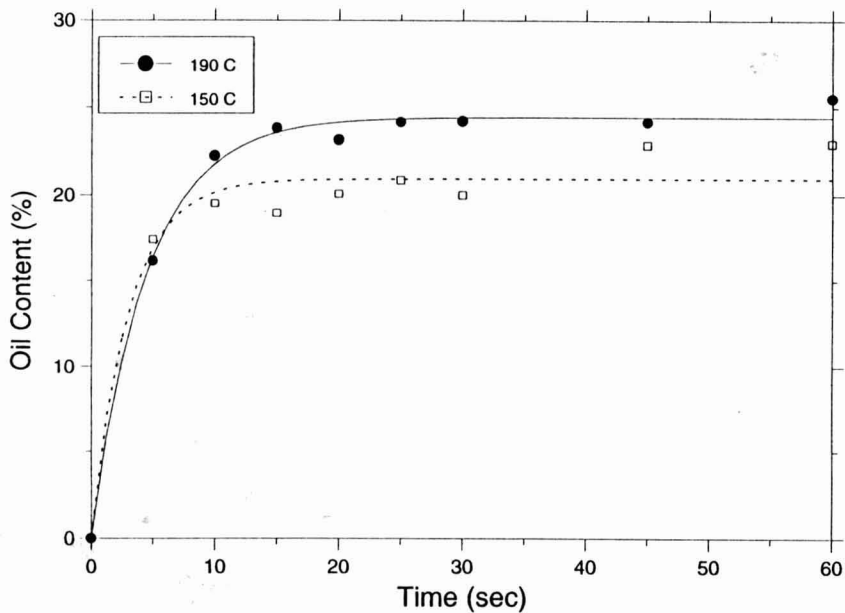


FIG. 5. COMPARISON OF OIL CONTENT OF TORTILLA CHIPS FRIED AT DIFFERENT FRYING TEMPERATURES  
[dots are observed values and lines are the simulated values]

**Oil Absorption.** Figure 3 presents the average observed and simulated values of oil absorption for the tortilla chip fried at 190C. Equation (7) gave a good agreement of oil uptake by the tortilla chips. Most of the oil was absorbed after the first 15 s of frying when most of the water was evaporated from the chip.

### The Effect of Oil Temperature on the Water Loss and Oil Uptake

Figure 4 shows the experimental and simulated results of moisture content as a function of frying time for an average of three tests conducted with tortilla fried at 150 and 190C. Moisture diffusion coefficients were calculated for each frying condition. The values of the diffusion coefficient were larger for the tortilla chip fried at 190C ( $9.348 \times 10^{-8} \text{ m}^2/\text{s}$ ) than at 150C ( $5.408 \times 10^{-8} \text{ m}^2/\text{s}$ ). As expected, water evaporation rate was faster for the tortilla chips fried at 190C than at 150C. The final moisture content was 2-5 (% d.b.) lower for the chips

fried at 190C than for those fried at 150C for the same period of time. It would require more time to fry the chip to the desired final moisture content at 150C.

Figure 5 shows that the oil absorption rate was the same for tortilla chip fried at 150 or 190C in fresh oil; however, the final oil content was about 3%-5% higher for the chip fried at 190C. The values of  $k'$  varied from 0.223 to 0.330  $s^{-1}$  for the tortilla chip fried at 190C and 150C, respectively.

In conclusion, a model describing heat and moisture transfer during deep-fat frying of tortilla chips was proposed and validated. The results showed that the model simulated centerline temperature and average moisture loss during deep fat frying of tortilla chips. Oil content for different frying time was accurately modeled by a first order exponential model.

Moisture loss and oil absorption rates were faster during the first 15 s of frying, and then became fairly constant as frying continued. Moisture loss rate increased as temperature increased. The effects of temperature on oil absorption were not significant during the first 15 s of frying, however, the final oil content was higher for the tortilla chip fried at 190C than at 150C for the same frying time.

## ACKNOWLEDGMENTS

The authors wish to thank the Cereal Quality Lab at the Department of Soil and Crop Sciences at Texas A&M University for allowing the use of the equipment required for data collection.

## NOMENCLATURE

- A = area [ $m^2$ ]
- a = tortilla chips half thickness [m]
- $C_p$  = specific heat [kJ/kgC]
- D = mass diffusivity [ $m^2/s$ ]
- h = convective heat transfer coefficient [ $W/m^2C$ ]
- $h_D$  = convective mass transfer coefficient [m/s]
- $h_{fg}$  = latent heat of vaporization [kJ/kg]
- k = thermal conductivity [ $W/mC$ ]
- $k'$  = constant for Eq. (7) [ $1/s$ ]
- $M_f$  = oil content [%]
- $M_{fc}$  = final oil content [%]
- $M_w$  = moisture content [% db]
- $M_{wo}$  = initial moisture content [% db]
- $M_{we}$  = equilibrium moisture content [% db]

- $T$  = temperature [C]  
 $T_{\infty}$  = temperature of oil [C]  
 $T_0$  = initial temperature [C]  
 $t$  = time [s]  
 $V$  = volume [m<sup>3</sup>]  
 $x$  = variable distance across the thickness of the tortilla chip [m]  
 $x_0$  = surface layer  
 $\alpha$  = thermal diffusivity [m<sup>2</sup>/s]  
 $\theta$  = tortilla chip's temperature [°C]  
 $\rho$  = density [m<sup>3</sup>/kg]

## REFERENCES

- American Association of Cereal Chemists (AACC). 1986. Approved method of the AACC, 8th Ed. Method 30–20. The Association, St Paul, MN.
- ASHKENAZI, N., MIZRAHI, Sh. and BERK, Z. 1984. Heat and mass transfer in frying. In *Engineering in Foods*, Vol. 1, (B.M. McKenna, ed.) Elsevier Publishers, New York.
- CALIFANO, A.N. and CALVELO, A. 1991. Thermal conductivity of potato between 50 and 100°C. *J. Food Sci.* 56, 586–589.
- CRANK, J. 1957. *The Mathematics of Diffusion*. Clarendon Press, Oxford.
- DAGERSKOG, M. and SORENFORS, P. 1978. A comparison between four different methods of frying meat patties: Heat transfer, yield, and crust formation. *Lebensm.-Wiss.u.-Technol.* 11, 306–311.
- GAMBLE, M. H. and RICE, P. 1987. Effect of pre-fry drying of oil uptake and distribution in potato chip manufacture. *Intl. J. Food Sci. Technol.* 22, 535–548.
- GAMBLE, M.H. and RICE, P. 1988. The effect of slice thickness on potato crisp yield and composition. *J. Food Eng.* 8, 31–46.
- GUILLAUMIN, R. 1988. Kinetics of fat penetration in food. In *Frying of Food*, (G. Varela, A.E. Bender and I.D. Morton, eds.) VCH, Chichester, England.
- HALLSTRÖM, B. 1979. Heat and mass transfer in industrial cooking. In *Food Process Engineering*, (P. Linko, Y. Malkki and J. Olkku, eds.), Vol. I, Elsevier Applied Science Publishers, New York.
- HOLMAN, J.P. 1981. *Heat Transfer*, 5th Ed. McGraw-Hill Book Company, New York.
- KELLER, C. and ESCHER, F. 1989. Heat and mass transfer during deep fat frying of potato products. Poster presented at International Congress on Engineering and Food, May, Cologne, Germany.

- KOKEMPEL, M., TOMASULA, P.M and CRAIG, JR., J. 1991. Correlation of moisture and oil concentration in french fries. *Lebensm.-Wiss. u.-Technol.* 24, 445-448.
- MATZ, S.A. 1993. *Snack Food Technology*. Van Nostrand Reinhold/AVI, New York.
- McDONOUGH, C.M., GOMEZ, M.H., LEE, J.K., WANISKA, R.D. and ROONEY, L.W. 1993. Environmental scanning electron microscopy evaluation of tortilla chips microstructure during deep fat frying. *J. Food Sci.* 58(1), 199-203.
- MILLER, K.S. and SINGH, R.P. 1992. Convective heat transfer coefficient for frying oils. Presented at the IFT annual meeting. New Orleans, LA.
- MOREIRA, R.G. and BAKKER-ARKEMA, F.W. 1989. Moisture desorption model for nonpareil almonds. *J. Agric. Eng. Res.* 42, 123-133.
- MOREIRA, R.G. and BARRUFET, M.A. 1994. Spatial distribution of oil after deep-fat frying from a stochastic model. *J. Food Eng.* (In Press).
- MOREIRA, R.G., PALAU, J., CASTELL-PEREZ, M.E. and SWEAT, V.E. 1991. Moisture loss and oil absorption during deep fat frying of tortilla chips. ASAE winter meeting, St. Joseph, MI. Paper No. 916501.
- MOREIRA, R.G., PALAU, J. and SUN, X. 1995a. Deep-fat frying of tortilla chips; an engineering approach. *Food Technol.* 49(4), 146-150.
- MOREIRA, R.G., PALAU, J. and SWEAT, V.E. 1992. Thermal properties of tortilla chips during deep fat frying. ASAE winter meeting, St. Joseph, MI. Paper No. 92-6595.
- MOREIRA, R.G., PALAU, J., SWEAT, V.E. and SUN, X. 1995b. Thermal and physical properties of tortilla chips as a function of frying time. *J. Food Proc. and Preservation* 19, 175-189.
- PALAU, J. 1993. Deep fat frying of tortilla chips: an integrated approach. Master Thesis. Texas A & M University at College Station.
- PINTHUS, E.J. and SAGUY, I.S. 1993. The effect of interfacial tension on oil uptake during deep-fat frying. Abstract from IFT Annual Meeting. Chicago, IL.
- PRAVISAN, M.F. and CALVELO, A. 1986. A minimum cooking time for potato strip frying. *J. Food Sci.* 51, 614-617.
- RICE, P. and GAMBLE, M.H. 1989. Technical Note: Modeling moisture loss during potato slice frying. *Int. J. Food Sci. Technol.* 24, 183-187.

# MATHEMATICAL MODELING OF PARTICULATE TWO-PHASE FLOW IN A HELICAL PIPE

YANSHENG LIU and CARLOS A. ZURITZ<sup>1</sup>

*Department of Agricultural and Biological Engineering  
The Pennsylvania State University  
University Park, PA 16802*

Accepted for Publication September 30, 1994

## ABSTRACT

*The design of helical tubes for continuous sterilization of low-acid foods (pH > 4.6) containing large discrete particles depends on the knowledge of the flow behavior of the suspended particles. The flow behavior of a carrier fluid with suspended solid spherical particles in a helical tube was numerically simulated through an iterative solution of the Navier-Stokes equations and the particle dynamic equations in three dimensions. The Lagrangian approach was used to predict the individual particle velocities and trajectories under solid-liquid two-phase flow situation. The results indicate that the residence time distribution of the particles in helical tube flow was narrower than in a conventional holding tube (consisting of two straight tubes connected with a 180° bend). Also, the average velocity of the particles was closer to the average velocity of the carrier fluid in the helical tubes. The secondary flow induced by the tube curvature greatly reduced the axial dispersion of the particles. There was a substantial particle influence on the fluid flow field. The pressure drop in helical tube was 18% higher for single-phase flow and 51% higher for two-phase flow than in conventional holding tube of equal length.*

## INTRODUCTION

Helical tubes have been used in various fields of industry. In aseptic processing of food products, helical tubes have been used as heating-holding-cooling units with several foods containing particles (Carlson 1991a,b). The major advantages of helical tubes are the simplicity of system

<sup>1</sup>To whom correspondence should be addressed.

design, higher heat transfer rates than other tubular units and higher quality of the processed products, especially for those containing particulates. It has been reported that in helical tubes there is no damage produced to even very fragile products such as whole raspberries, sliced strawberries, sliced bananas, etc. (Carlson 1991a).

The geometric arrangement of the holding tube influences the residence times of the particles suspended in a viscous fluid. The use of helical holding tubes in aseptic processing is an attempt to improve the residence time distribution of the suspended particles. However, the questions that still need answers are: what is the flow characteristic of particulate flow in a helical tube? Is the helical holding tube better than the conventional holding tube (which usually consists of several straight tubes connected with 180° bends) in terms of narrowing particle residence time distribution? The answers to these questions depend on the understanding of flow behavior of the particles in this system. Only limited experimental studies are available in this area (Carlson 1991a,b). Moreover, theoretical investigations of particulate two-phase flow in a helical tube have not been published in the area of aseptic processing.

Whenever a viscous fluid flows through a curved tube or channel, the primary (axial) flow is accompanied by a secondary flow which acts in a plane perpendicular to the tube axis. The centrifugal forces act at right angles to the main direction of flow, so that the radial position of the fluid maximum velocity is shifted from the center of the tube towards the outside wall (Dean 1927, 1928).

Experimental and theoretical studies on convective heat transfer in coiled tubes have shown that secondary flow increases the transfer rates of heat, mass and momentum. (Mori and Nakayama 1965; Patankar *et al.* 1974; Kao 1987; Futagami and Aoyama 1988; Germano 1989). Due to the large resistance to flow associated with flow in curved pipes, the pressure drop is relatively large compared to that in straight tube flow. The early theoretical works by Dean (1927, 1928) were the first to predict secondary flow caused by centrifugal forces. He stated that the dynamic similarity of such flow depends on a nondimensional parameter  $D = [(2r/R)(aW_m/\nu)^2]$  where  $W_m$  is the mean velocity along the tube,  $\nu$  the kinematic viscosity and  $r$  the radius of the tube, which is bent in a circle of radius  $R$ . Koutsky and Alder (1964) indicated that secondary flow stabilized laminar flow, with transition Reynolds numbers of 6000 to 8000 being characteristic of helically coiled tube flow. Mori and Nakayama (1965) obtained theoretical solutions for the rate of heat-transfer in boundary-layer flow for constant wall-temperature and showed that at high Dean numbers, the heat transfer coefficients in the thermally fully developed region were higher in a coiled tube than in a straight tube by a factor which varies as  $D_e^{1/2}$ . A thorough review on flow in curved pipe was given by Berger *et al.* (1983). However, these studies dealt with single phase flow only. The flow behavior of

multi-particles in solid-liquid two-phase flow in helically coiled pipe has received scarce attention, especially in the aseptic processing area.

Therefore, the objectives in the present study were to: investigate the flow behavior of particulate two-phase flow in a helical holding tube, explore the influence of the particles on the flow field of the carrier fluid, and examine the residence time distributions of the particles in a helical holding tube and a conventional holding tube.

### Mathematical Formulation of the Problem

The Lagrangian model was employed to simulate the solid-liquid two-phase flow through a helical holding tube. The assumptions used in the current simulation were the same as those in the conventional tube flow (Liu 1994), which are: laminar flow, carrier medium is an incompressible Newtonian fluid with constant viscosity, inter-particle interactions are neglected, the flow field is under steady state, and the particles fill the whole flow field uniformly (giving a particle concentration of 10%). If particle interactions (collisions) are neglected, the trajectory of the particles will be the same as long as they have the same initial radial position. Therefore, only those particles which have different initial radial positions need to be traced. In this study, nine particles with different radial positions were considered to arrive simultaneously at the inlet cross-section of the tube at every time step, each having a velocity ( $v_p$ ) equal to the stream line velocity ( $v_f$ ) of the fluid passing through the center of the particle. Consequently, The path of these nine particles were traced in this simulation.

The exchange of momentum between the two phases is carried along particle trajectories. This yields additional terms that need to be included in the Navier-Stokes equations. These terms are functions of the slip velocities ( $v_f - v_p$ ) between the two phases. Gain or loss of momentum along the particle path was calculated and included as a sink or source term in the Navier-Stokes equations.

**The Governing Equations of the Two-Phase Flow.** Due to the existence of secondary flow in a helical tube, the three-dimensional form of the Navier-Stokes equations of the fluid phase must be solved with the source term  $S_k$ , which represents the influence of the particle on the fluid flow field. The corresponding governing equation of the fluid phase in vector form is expressed as:

$$\frac{\partial}{\partial t} (\mathbf{v}) + \nabla \cdot (\mathbf{v}\mathbf{v}) = - \frac{1}{\rho} \nabla P + \nu \nabla^2 \mathbf{v} + \mathbf{g} - \frac{\mathbf{S}_k}{\rho} \quad (1)$$

where  $S_k$  is the source term. Mathematically, the source term is calculated by the following expression (Durst 1984):

$$S_k = \dot{N}_k \rho \frac{A_p}{2} \int_{t_i}^{t_o} C_D (\mathbf{v}_f - \mathbf{v}_p) |\mathbf{v}_f - \mathbf{v}_p| dt \quad (2)$$

where  $t_i$  and  $t_o$  are, respectively, the time when the particle enters and leaves the control volume,  $\dot{N}_k$  is the number flow rate of the particles starting at one radial location on the initial tube cross plane,  $\mathbf{v}_f$  is the streamline fluid velocity passing through the particle's center and  $\mathbf{v}_p$  is the particle velocity.

The particles suspended in a three dimensional flow field could be expected to undergo translational and rotational motions in three dimensions. Therefore, both linear and angular particle dynamic equations were considered in the current simulation. These particle dynamic equations were solved simultaneously to describe the motion of the particles. The vector form of the linear particle dynamic equations is given by (Liu 1994):

$$m \frac{d\mathbf{v}_p}{dt} = 6.46 \rho_f a^2 \left( \frac{v}{K} \right)^{\frac{1}{2}} \mathbf{K} \times (\mathbf{v}_p - \mathbf{v}_f) + \pi a^3 \rho_f \boldsymbol{\Omega} \times (\mathbf{v}_p - \mathbf{v}_f) + \frac{1}{2} C_D \rho_f \pi a^2 |\mathbf{v}_f - \mathbf{v}_p| (\mathbf{v}_f - \mathbf{v}_p) + \frac{4}{3} \pi a^3 (\rho_f - \rho_p) \mathbf{g} \quad (3)$$

The terms on the right hand side of the above equation are Saffman lift, Magnus lift, drag and buoyant forces, respectively.

The vector form of the angular particle dynamic equations is given as follow (Liu 1994):

$$\frac{d\boldsymbol{\Omega}}{dt} = \frac{15}{\rho_f r^2} \left[ \frac{\pi \tau}{8} - \boldsymbol{\Omega} \right] \quad (4)$$

The linear and angular particle dynamic equations were coupled with the Navier-Stokes equations through an iterative solution between the phases. A compact fourth-order four-stage Runge-Kutta method was used to solve these equations.

**Physical Domain and Coordinate System.** The physical domain is a helically coiled circular tube; its geometry and coordinate system are shown in Fig. 1. The inside diameter of the tube is 5.08 cm (2.0 in.). The diameter of curvature of the helical coil (2R) is 73.5 cm (28.92 in.) and the angle of inclination of the tube is 2.0°. Therefore, the pitch,  $h$ , is about 8 cm (3.15 in.).

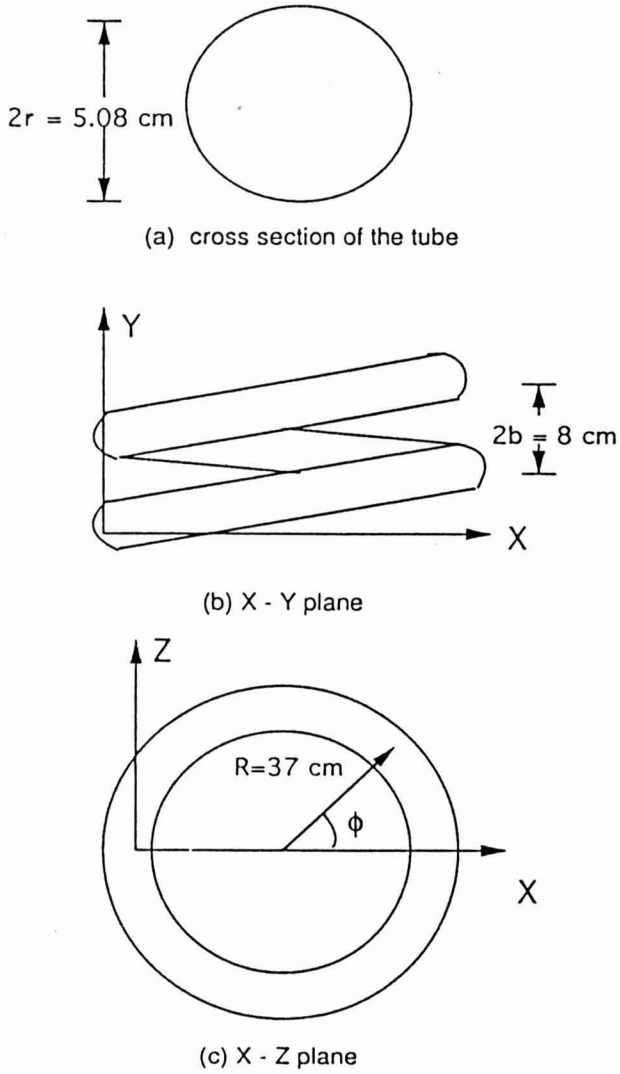


FIG. 1. GEOMETRY AND COORDINATE SYSTEMS USED IN THE HELICAL HOLDING TUBE

These dimensions are within the range of commercially available helical holding tubes. To compare the results from the helical tube flow to those of the conventional tube flow, the length of the helical tube (arc length of the central helix) is the same as that of the conventional tube (628 cm). The total number

of turns is about 2.7. The conventional holding tube (Liu 1994) included two, 3-m long each, straight tubes of inside diameter of 5.08 cm connected with a 180° bend of the same diameter. The diameter of curvature of the 180° bend section was 18.0 cm (centerline measurement) and the whole system had an upward inclination of 1.194° (corresponding to the FDA requirement of 0.25 in. per foot).

The physical velocities are  $u$ ,  $v$ ,  $w$  in  $x$ ,  $y$ ,  $z$  directions, respectively. The axial distance (arc length) from the tube inlet is expressed by  $S = R\theta$ , where  $R$  is the radius of curvature and  $\theta$  the angle between the given plane and entry plane of the helical tube.

In both holding tube arrangements, 351 grid points were considered along the tube axis, and 21 grid points along the horizontal and vertical directions respectively of the tube crosssection.

The model food particles considered are uniform spheres with diameter of 1 cm. Neutrally buoyant conditions were assumed even though the model can handle no neutrally buoyant conditions. The simulations considered a carrier liquid with viscosity of 1 poise (0.1 Pa·s) and density of 1 g/cm<sup>3</sup> flowing with an average velocity of 30 cm/s. The Reynolds number under these conditions is about 150.

**Simulations Procedure.** The equations of motion of the fluid phase (Eq. 1) were solved first without particle influence ( $S_k=0$ ). With the computed fluid flow field, particle velocities and trajectories were determined by solving the particle dynamic equations (Eq. 3 and 4). The source terms were then calculated using Eq. 2 and the computed particle velocities and trajectories. Subsequently, the Navier-Stokes equations were solved again using the new source terms. This iteration process was continued until convergence was attained between the solution of the two phases.

## RESULTS AND DISCUSSION

### Flow Characteristics of the Carrier Fluid and Particle Influence on the Fluid Flow Field

The main characteristic was the development of secondary flow induced by centrifugal forces. The secondary motion was induced by the curvature due to an imbalance between the centrifugal acceleration and the cross stream pressure gradient; the centrifugal forces acting at right angles to the axial direction and the pressure gradients acting toward the center of curvature. The interaction of pressure gradients with centrifugal forces established the secondary flow in the

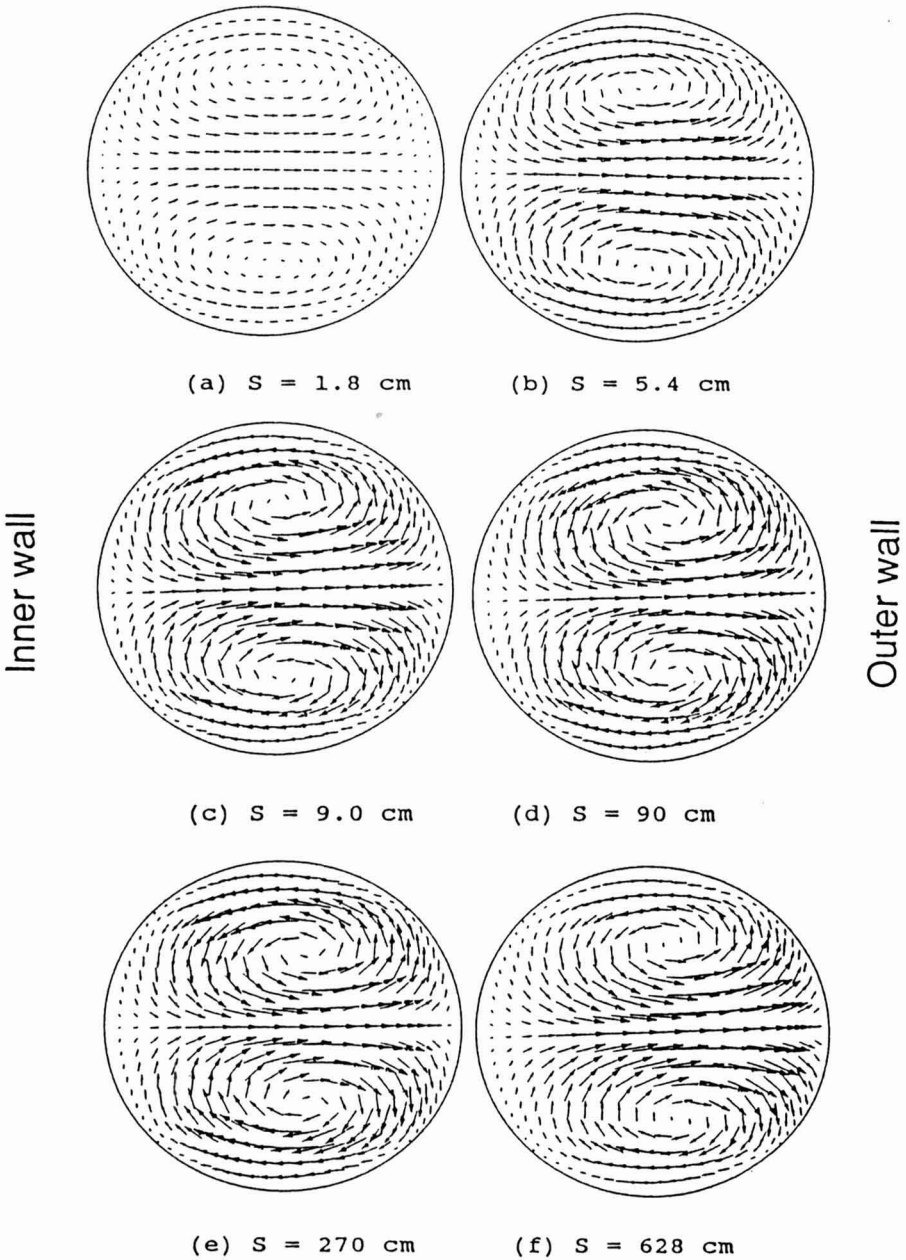


FIG. 2. SECONDARY FLOW ON VARIOUS CROSS SECTIONS OF THE HELICAL HOLDING TUBE

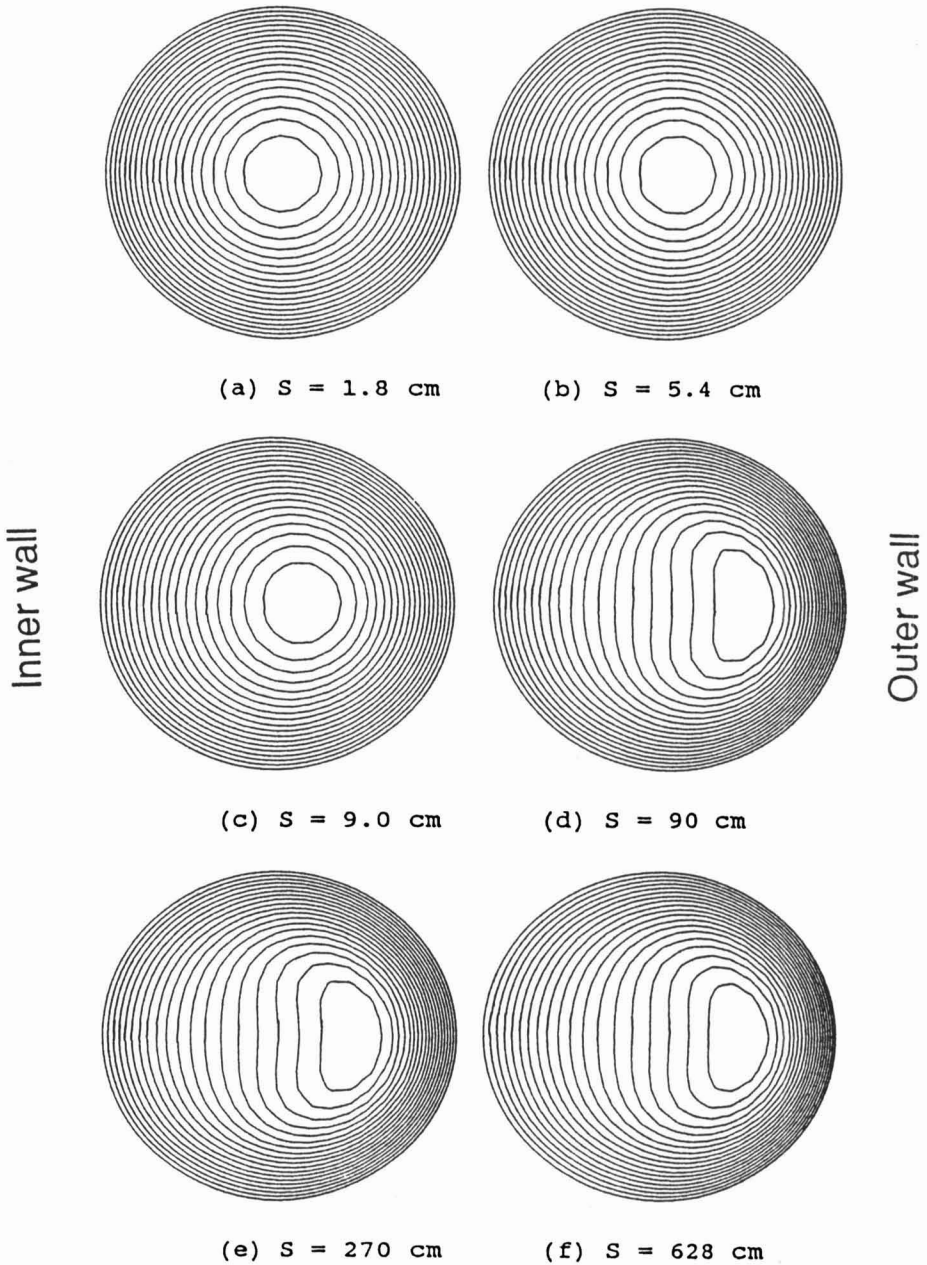


FIG. 3. FLUID AXIAL VELOCITY CONTOURS ON VARIOUS CROSS SECTIONS OF THE HELICAL HOLDING TUBE

cross section of the helical tube. Fluid impinged on the outer wall and then turned to move inward along the top and bottom walls as indicated in Fig. 2. Two vortices perpendicular to the axial flow direction developed in the cross section.

Fluid axial velocity contours at various cross sections of the helical tube (Fig. 3) show that the fluid flow field was distorted from the symmetric profile of Poiseuille flow; the maximum velocity core was gradually shifted towards the outer wall of the tube until a balance was reached between the inwardly directed pressure gradients and outwardly directed centrifugal forces. From the inlet of the tube, the strength of secondary flow increased to a maximum value (about  $S=90$ ), which remained constant through the rest of the tube.

One of the results of the secondary flow was a strong mixing at the tube cross section and a reduction in the spread of residence times in comparison to the flow through the straight tube at the same Reynolds number. Truesdell and Adler (1970) concluded that the secondary flow stabilized laminar flow by increasing the transition Reynolds numbers 2 to 4 times of those in straight tube flow and markedly reduced axial dispersion. For aseptic processing of foods containing particles, the "expanded" laminar region would reduce the occurrence of damage to particles during their flow in the helical tube. This has already been demonstrated experimentally by Carlson (1991a). Furthermore, the reduced axial dispersion would definitely narrow the residence time distribution of both the carrier fluid and suspended particles.

The particle influence on the axial velocity contours of the fluid is displayed in Fig. 4. Comparing Fig. 3(c),(d) and (e) with 4(b), (e) and (f), respectively, it is evident that the particles have a strong effect on the fluid flow. The influence was small at the beginning of the helical tube (up to  $S=30$ ) and became larger downstream. Two factors are involved in this phenomenon: centrifugal forces, which acted at right angles to the axis of the helix (in the horizontal direction) shifting the maximum fluid velocity towards the outer wall, and particle obstruction, which retarded the fluid flow. The velocity profiles on the horizontal plane of symmetry were affected by both effects.

The particle influence on the axial velocity profiles in the horizontal plane of symmetry at selected cross sections of the tube is shown in Fig. 5. The effect was small at the beginning of the tube ( $S=30$ ), but was considerable downstream. The particle influence on the fluid flow field involved a complex mechanism; as the particles kept changing their radial and axial positions, the influence on a given cross plane might come from all of the particles that were near the region under consideration.

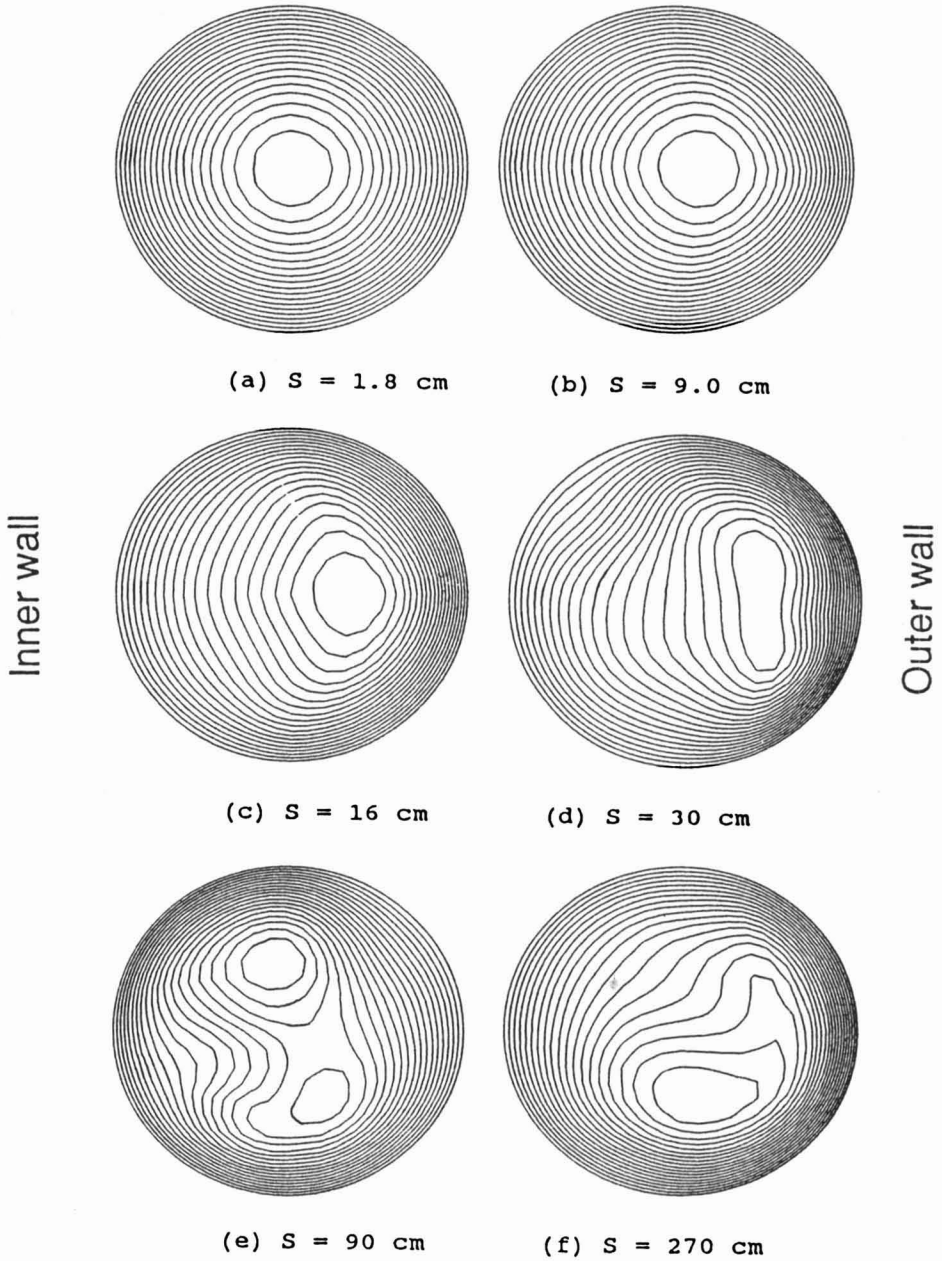


FIG. 4. PARTICLE INFLUENCE ON THE FLUID AXIAL VELOCITY CONTOURS

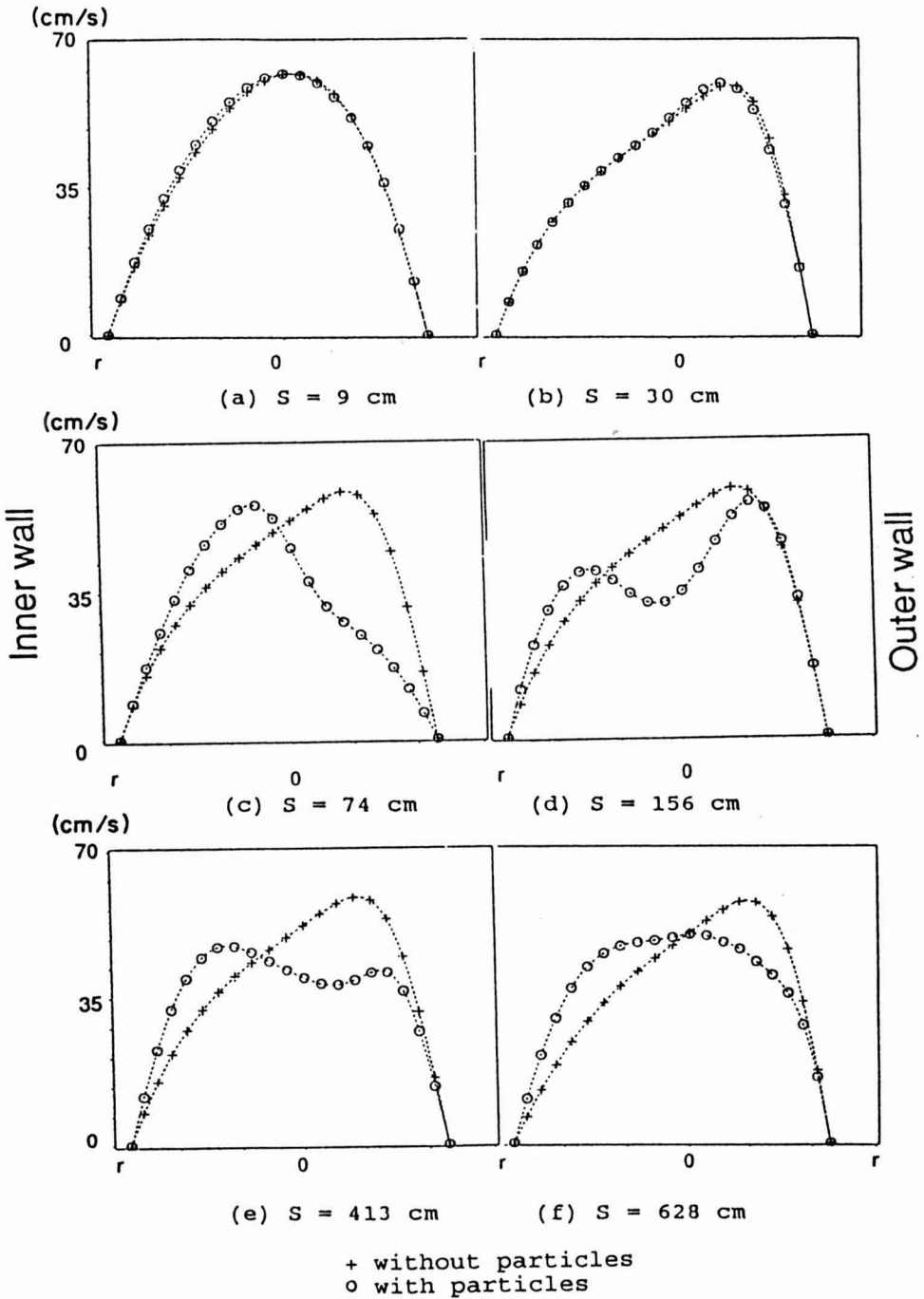


FIG. 5. PARTICLE INFLUENCE ON THE FLUID AXIAL VELOCITY PROFILES (CM/S) ON THE HORIZONTAL PLANE OF SYMMETRY

## Flow Behavior of Suspended Particles

The assumptions underlying the simulation of the helical tube flow were discussed earlier. The initial radial positions of the particles are shown in Fig. 6.

Due to the secondary flow, the radial positions of the particles on the cross section changed continuously as they flowed through the helical tube. This suggests that the particles close to the wall at one instant might move to the center after a short time. Figure 7 shows the radial positions of the particles as they arrived at different cross sections in the first half of the helical tube, whereas the radial positions in the second half of the helical tube are displayed in Fig. 8. As the particles flowed downstream along the tube, the number of radial positions was reduced from the initial nine to two at the tube outlet.

The maximum difference in axial distance between the particles at the tube outlet (between fastest particle leaving the tube and slowest particle upstream) was about 194 cm in the conventional tube flow situation (Liu 1994) and 17 cm in the helical tube flow. This difference can be explained by the fact that, in the helical tube flow, secondary motion caused a strong mixing by continuously sweeping the fluid and the particles between fast-moving and slow-moving regions and as a consequence, all the particles experienced a similar flow field. In the conventional tube, secondary flow was present only in the bend and first part of the second straight tube (up to 147 cm downstream from the bend outlet). Therefore, the sweeping effect was limited and the particles had time to recover a parabolic profile.

It has been suggested in the past that helical tubes be used in order to reduce axial dispersion in pipe flow (Koutsky and Adler 1964). Compared to particulate flow in conventional holding tubes, the smaller axial dispersion found in the present simulation of flow in helical tube suggests that this configuration would improve aseptic processing of foods containing particles, since it would result in a narrower residence time distribution.

## Particle Residence Times in the Helical Tube

The geometric arrangement of the holding tube greatly influences particle flow behavior, i.e. particle velocities and trajectories, residence times and pressure drops. The first two effects have been discussed previously. The following discussion will concentrate on particle residence times and pressure drops in the helical tube. The results are then compared with those from the conventional tube flow.

As a consequence of the continuous secondary flow, the particle residence time distribution was narrowed considerably in comparison with the flow (at the

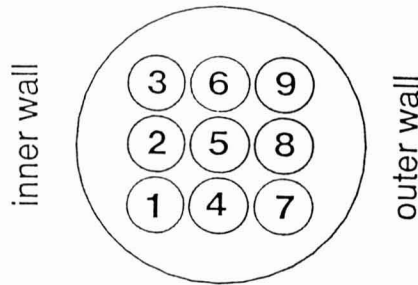


FIG. 6. INITIAL RADIAL POSITIONS OF THE PARTICLES

same Reynolds number) through the conventional tube. The residence times of the particles at various cross sections of both the helical tube and conventional tube are listed in Table 1.

Several conclusions can be drawn from Table 1. First, the differences between maximum ( $RT_{\max}$ ) and minimum ( $RT_{\min}$ ) residence times in the helical tube were always smaller than those in the conventional tube, which suggests that the residence time distribution of the particles in the helical tube was narrower than those in the conventional tube. Furthermore, the values of  $RT_{\max} - RT_{\min}$  did not vary much in the helical tube; they only varied from 1.33 to 1.51 s, whereas in the conventional tube flow, the differences became larger as the particles moved downstream [from 0 to 5.17 s in the first straight tube, from 5.17 to 5.29 s in the bend, and up to 7.9 s at the end of the second straight tube (Liu 1994)].

Second, the particles in the helical tube flow always resided longer than those in the conventional tube flow in terms of average residence time,  $RT_{\text{mean}}$ . In other words, the average velocity of the particles was slower in helical tube flow than in conventional tube flow.

Third, the ratio of mean residence time ( $RT_{\text{mean}}$ ) to the minimum residence time ( $RT_{\min}$ ) decreased from 1.13 to 1.04 in the helical tube and from 1.60 to 1.26 in the conventional tube. As a comparison, this ratio is 2.0 for a laminar straight-tube flow. The reduction in these ratio values in both tubes suggests that if the length of the holding tube were increased, the ratio values would decrease even more. Sandeep and Zuritz (1993), using four straight tubes and three  $180^\circ$  bends, found experimentally that the ratio of mean to minimum particle residence time ranged between 1.06 and 1.16.

Narrower particle residence times distributions (RTD) in aseptic processing of particulate foods would result in more uniform thermal treatment to the particles. From a safety point of view, the sterility of the final product is determined according to the least sterility achieved by the particles. Therefore, particles with narrow residence time distribution would be less over-processed, resulting in more uniform product quality.

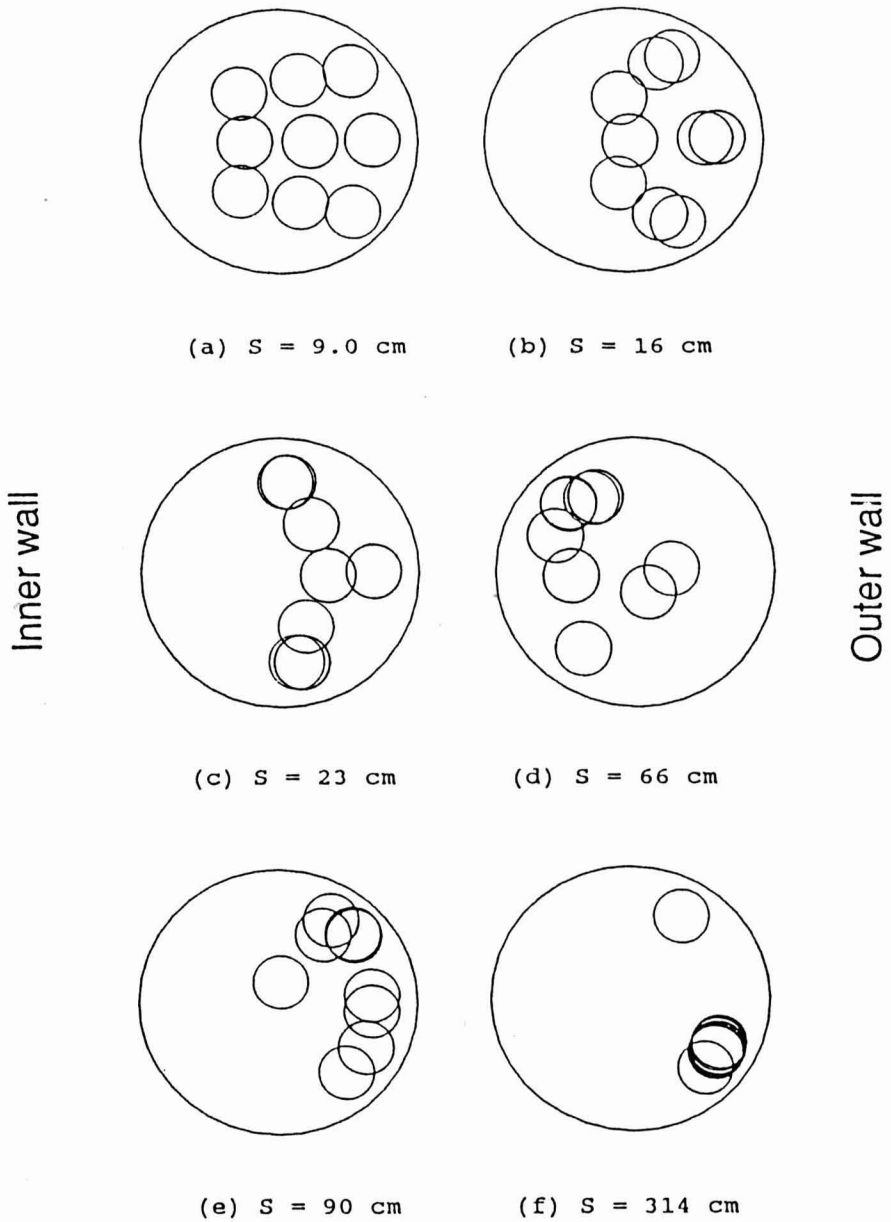


FIG. 7. PARTICLE RADIAL POSITIONS IN THE FIRST HALF OF THE HELICAL HOLDING TUBE

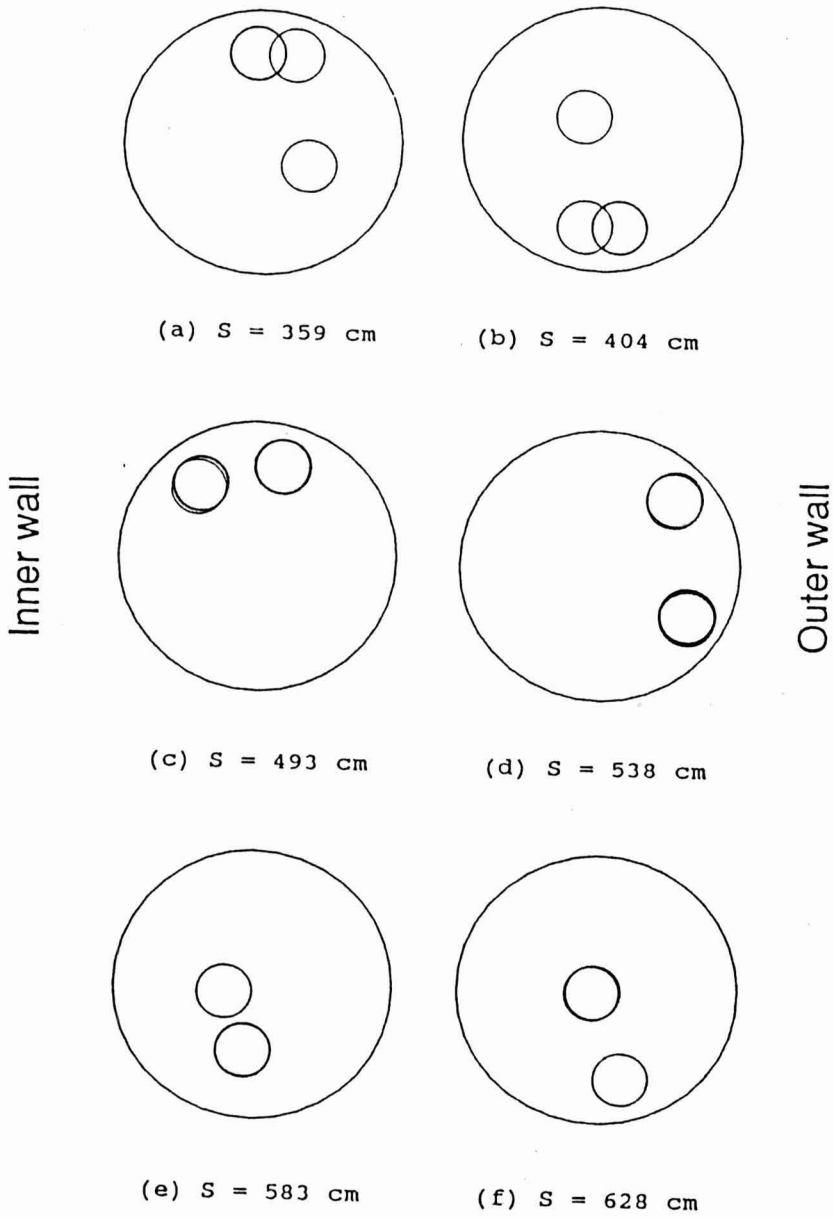


FIG. 8. PARTICLE RADIAL POSITIONS IN THE SECOND HALF OF THE HELICAL HOLDING TUBE

TABLE 1.  
PARTICLE RESIDENCE TIMES IN HELICAL AND CONVENTIONAL HOLDING TUBES

Particle #	L = 200 cm*		L = 428 cm		L = 628 cm	
	H.tube#	C.tube#	H.tube	C.tube	H.tube	C.tube
No. 1	5.97	6.37	14.08	14.38	20.73	18.64
No. 2	5.88	4.78	13.68	10.84	20.64	14.57
No. 3	6.79	5.59	14.63	12.74	21.53	21.67
No. 4	6.83	4.48	14.65	11.44	21.52	19.10
No. 5	6.78	3.16	14.62	9.20	21.53	18.15
No. 6	6.59	4.46	14.70	10.44	21.34	13.77
No. 7	6.65	6.12	13.69	14.00	20.40	19.84
No. 8	7.00	4.85	14.85	11.14	21.76	14.38
No. 9	7.21	5.61	15.01	12.30	21.91	15.52
RT <sub>mean</sub>	6.63	5.05	14.43	11.83	21.26	17.29
RT <sub>mean</sub> /RT <sub>min</sub>	1.13	1.60	1.05	1.29	1.04	1.26
RT <sub>max</sub> -RT <sub>min</sub>	1.33	3.21	1.33	5.18	1.51	7.90

\* L is axial distance from the inlet of the tube

# H.tube is the helical tube; C.tube the conventional tube.

The average velocity of the particles was close to the fluid average velocity in the helical tube flow, whereas the average velocity of the particles was always higher than that of the fluid in the conventional tube flow. The average velocities of the fluid and the particles in both tubes are listed in Table 2.

The flow resistance caused by the curvature resulted in a higher pressure drop compared with that in an equivalent length of straight tube. The existence of particles further increased the pressure drop. The pressure drop in both holding tubes with and without particles are listed in Table 3. It is shown that pressure drop in the helical tube flow was about 18% higher than the pressure drop in the conventional tube for the single-phase flow, whereas for the two-phase flow, this value increased to about 52%. On the other hand, the presence of particles increased the pressure drop by about 36% in the helical tube, and only about 5% in the conventional tube. The length of the curvature in the conventional tube was short (28 cm) and most of its flow field was in straight tubes (600 cm) which in general have less resistance. Therefore, the pressure drop under this situation was smaller than in the helical tube.

TABLE 2.  
AVERAGE VELOCITIES (cm/s) OF THE PARTICLES  
AND FLUID IN THE TWO HOLDING TUBES

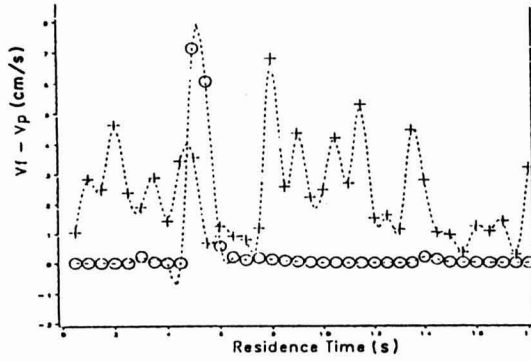
Distance from the Inlet of the Tube	Average Fluid Velocity	Average Particle Velocity	
		Helical Tube	Conventional Tube
L = 200 cm	30.00	30.17	39.53
L = 428 cm	30.00	29.68	36.20
L = 628 cm	30.00	29.64	36.32

TABLE 3.  
PRESSURE DROPS ( $\text{g}/(\text{cm}^2\text{s}^2)$ ) BETWEEN THE INLET AND OUTLET OF  
THE TWO ARRANGEMENTS OF THE HOLDING TUBE  
(WITH AND WITHOUT PARTICLES)

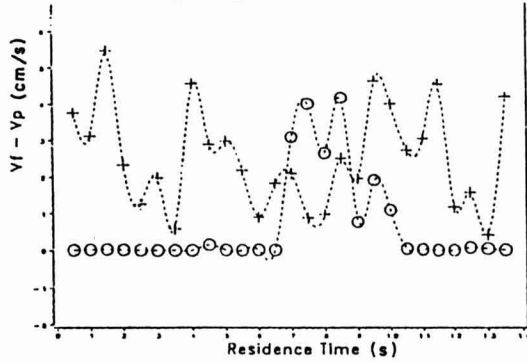
	Helical Tube	Conventional Tube	Change (%)
Without particles	30291	25737	17.7
With particles	40982	27026	51.6
Change (%)	35.5	5.0	

The momentum exchange between the two phases is represented by the drag forces exerted by the fluid on the particles. These drag forces are functions of the slip velocities (streamline fluid velocity passing through the particle's center minus particle velocity,  $v_f - v_p$ ). Figure 9 shows the slip velocities of particles 5, 6 and 7 versus residence times in both tubes. It can be seen from the figure that the slip velocities fluctuated throughout the entire length of the helical tube. As a comparison, the slip velocities in the conventional tube were only significant in the bend and early stage of the second straight tube section where the secondary flow was significant. Furthermore, the slip velocities in the helical tube were always larger than those in the conventional tube except in the bend section.

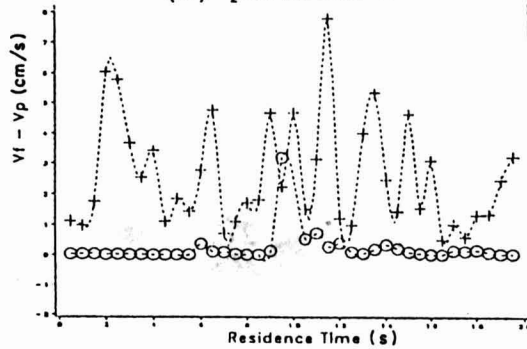
The current model can perform simulations with Newtonian fluids and negligible inter-particle interactions (no collisions). The carrier fluid used in the



(a) particle 5



(b) particle 6



(c) particle 7

O: in the regular holding tube  
 +: in the helical holding tube

FIG. 9. VELOCITY DIFFERENCE ( $v_l - v_p$ ) BETWEEN THE PHASES BASED ON THE PATH OF PARTICLES 5, 6, 7 IN HELICAL AND CONVENTIONAL TUBE FLOW

aseptic processing of foods containing large particles, however, is generally a non-Newtonian fluid and particle interactions are also important, especially when the particle concentration is high. Therefore, the model, in its present form, should be considered as a first attempt to numerically describe the flow behavior of particulate suspensions in holding tubes, and the results interpreted with regard to the comparison between conventional and helical holding tubes, for flow of Newtonian carrier fluids and suspensions of low particle concentration. The computer model is being expanded to account for both non-Newtonian fluid and particle interactions.

## CONCLUSIONS

The flow behavior of particulate two-phase flow in a helical holding tube was simulated through an iterative solution of the fluid Navier-Stokes equations and particle dynamic equations.

Simulation results showed that secondary flow existed in the entire flow field due to the continuous curvature. Secondary flow carried the particles between the various fluid velocity regions iteratively, which significantly reduced the axial dispersion of the particles. As a result, the residence time distribution of the particles in the helical tube was narrower than in the conventional tube flow situation; the ratio of  $RT_{\text{mean}}$  to  $RT_{\text{min}}$  at the tube outlet was 1.04 in the helical tube flow and 1.26 in the conventional tube flow. The average residence time of the particles,  $RT_{\text{mean}}$ , in the helical tube (21.3 s) was longer than the  $RT_{\text{mean}}$  in the conventional tube (17.3 s). The pressure drop in the helical tube was 18% higher than in the conventional holding tube for the single-phase flow, and was 51% higher for the two-phase flow.

## NOMENCLATURE

a, A	Particle radius (cm), projected area (cm <sup>2</sup> )
$C_D$ or $C_d$	Drag coefficient
$D_e$	Dean number ( $= \delta^{1/2}/\text{Re}$ )
F	Force (g*cm/s <sup>2</sup> )
$F_d$	Drag force (g*cm/s <sup>2</sup> )
$F_b$	Buoyancy force (g*cm/s <sup>2</sup> )
$F_l$	Magnus lift force (g*cm/s <sup>2</sup> )
$F_s$	Saffman force (g*cm/s <sup>2</sup> )
$h_f$	Interface heat coefficient (erg/s/cm <sup>2</sup> /K)
K	Curl of velocity

m	Mass of the particle (g)
P	Pressure (g/cm/s <sup>2</sup> )
Pr	Prandtl number
r, R	Radius of tube (cm), radius of curvature (cm)
Re	Reynolds number
RT, RTD	Residence time (s) and its distribution
S <sub>k</sub>	Source term vector in momentum equation (cm/s <sup>2</sup> )
S	Axial distance from tube inlet (cm)
u, v, w	Physical velocities (cm/s)
v	Velocity vector (cm/s)

### Greek Letters

$\delta$	Radius ratio, r/R
$\mu$	Coefficient of viscosity (g/cm*s)
$\nu$	Kinematic viscosity (cm *s)
$\rho$	Density (g/cm <sup>3</sup> )
$\tau$	Shear stress (dynes/cm <sup>2</sup> ) or torsion
$\Omega$	Angular velocity of particle (radian/s)

### Subscripts

d	Drag
f	Fluid
k	Starting location
p	Particle
x, y, z	Derivatives in Cartesian coordinates

### REFERENCES

- BERGER, S.A., TALBOT, L. and YAO, L.S. 1983. Flow in curved pipes. *Ann. Rev. Fluid Mech.* 15, 461-512.
- CARLSON, V.R. 1991(a). HydroCoil Heat Exchangers. Presented at Conference of Food Engineering (CoFE), McCormick Place, Chicago, Illinois, March 11.
- CARLSON, V.R.. 1991(b). Enhancement of Heat Transfer in Heat Exchangers For Aseptic Processing. ASAE Paper No. 91-6608. American Society of Agricultural Engineers, St Joseph, MI.

- DEAN, W.R. 1927. Note on the motion of fluid in a curved pipe. *Philosophy Magazine* 4, 208–223.
- DEAN, W.R. 1928. The stream-line motion of fluid in a curved pipe. *Philosophy Magazine* 5, 673–695.
- DURST, F. 1984. Eulerian and Lagrangian predictions of particulate two-phase flows: a numerical study. *Applied Mathematical Modelling*, Vol.8, April.
- FUTAGAMI, K. and AOYAMA, Y. 1988. Laminar heat transfer in a helically coiled tube. *Int. J. Heat Mass Transfer*. 31(2), 387–396.
- GERMANO, M. 1989. The Dean Equations Extended to a Helical Pipe Flow. *J. Fluid Mech.* 23, 289–305.
- KAO, H.C. 1987. Torsion effect on fully developed flow in a helical pipe. *J. Fluid mech.* 184, 335–356.
- KOUTSKY, J.A. and ADLER, R.J. 1964. Minimization of axial dispersion by use of secondary flow in helical tubes. *Can. J. Chem. Eng.* 42, 239–246.
- LIU, Y.S. 1994. Mathematical Modeling of Solid-Liquid Two-Phase Tube Flow. Ph.D. Dissertation, The Pennsylvania State University.
- MORI, Y. and NAKAYAMA, W. 1965. Study on forced convective heat transfer in curved pipes (1st report, laminar region). *Int. J. Heat Mass Transfer* 8, 67–82.
- PATANKAR, S.V., PRATAP, V.S. and SPALDING, D.B. 1974. Prediction of laminar flow and heat transfer in helically coiled pipes. *J. Fluid Mech.* 62, 539–551.
- SANDEEP, K.P. and ZURITZ, C.A. 1994. Residence Time Distribution in Holding Tubes: Dimensionless Correlations and Statistical Analyses. ASAE Paper No. 93-6577. American Society of Agricultural Engineers, St Joseph, MI.
- TRUESDELL, L.C. Jr. and ADLER, R.J. 1970. Numerical treatment of fully developed laminar flow in helically coiled tubes. *AIChE J.* 16(6), 1010–1015.



# **F N P PUBLICATIONS IN FOOD SCIENCE AND NUTRITION**

## **Journals**

JOURNAL OF FOOD LIPIDS, F. Shahidi  
JOURNAL OF RAPID METHODS AND AUTOMATION IN MICROBIOLOGY,  
D.Y.C. Fung and M.C. Goldschmidt  
JOURNAL OF MUSCLE FOODS, N.G. Marriott, G.J. Flick, Jr. and J.R. Claus  
JOURNAL OF SENSORY STUDIES, M.C. Gacula, Jr.  
JOURNAL OF FOODSERVICE SYSTEMS, C.A. Sawyer  
JOURNAL OF FOOD BIOCHEMISTRY, J.R. Whitaker, N.F. Haard and H. Swaisgood  
JOURNAL OF FOOD PROCESS ENGINEERING, D.R. Heldman and R.P. Singh  
JOURNAL OF FOOD PROCESSING AND PRESERVATION, D.B. Lund  
JOURNAL OF FOOD QUALITY, J.J. Powers  
JOURNAL OF FOOD SAFETY, T.J. Montville  
JOURNAL OF TEXTURE STUDIES, M.C. Bourne and M.A. Rao

## **Books**

OF MICROBES AND MOLECULES: FOOD TECHNOLOGY AT M.I.T., S.A. Goldblith  
MEAT PRESERVATION: PREVENTING LOSSES AND ASSURING SAFETY,  
R.G. Cassens  
S.C. PRESCOTT, M.I.T. DEAN AND PIONEER FOOD TECHNOLOGIST,  
S.A. Goldblith  
FOOD CONCEPTS AND PRODUCTS: JUST-IN-TIME DEVELOPMENT, H.R. Moskowitz  
MICROWAVE FOODS: NEW PRODUCT DEVELOPMENT, R.V. Decareau  
DESIGN AND ANALYSIS OF SENSORY OPTIMIZATION, M.C. Gacula, Jr.  
NUTRIENT ADDITIONS TO FOOD, J.C. Bauernfeind and P.A. Lachance  
NITRITE-CURED MEAT, R.G. Cassens  
POTENTIAL FOR NUTRITIONAL MODULATION OF AGING, D.K. Ingram *et al.*  
CONTROLLED/MODIFIED ATMOSPHERE/VACUUM PACKAGING OF  
FOODS, A.L. Brody  
NUTRITIONAL STATUS ASSESSMENT OF THE INDIVIDUAL, G.E. Livingston  
QUALITY ASSURANCE OF FOODS, J.E. Stauffer  
THE SCIENCE OF MEAT AND MEAT PRODUCTS, 3RD ED., J.F. Price and  
B.S. Schweigert  
HANDBOOK OF FOOD COLORANT PATENTS, F.J. Francis  
ROLE OF CHEMISTRY IN PROCESSED FOODS, O.R. Fennema, *et al.*  
NEW DIRECTIONS FOR PRODUCT TESTING OF FOODS, H.R. Moskowitz  
PRODUCT TESTING AND SENSORY EVALUATION OF FOODS, H.R. Moskowitz  
ENVIRONMENTAL ASPECTS OF CANCER: ROLE OF FOODS, E.L. Wynder *et al.*  
FOOD PRODUCT DEVELOPMENT AND DIETARY GUIDELINES, G.E. Livingston, R.J.  
Moshy, and C.M. Chang  
SHELF-LIFE DATING OF FOODS, T.P. Labuza  
ANTINUTRIENTS AND NATURAL TOXICANTS IN FOOD, R.L. Ory  
UTILIZATION OF PROTEIN RESOURCES, D.W. Stanley *et al.*  
VITAMIN B<sub>6</sub>: METABOLISM AND ROLE IN GROWTH, G.P. Tryfiates  
POSTHARVEST BIOLOGY AND BIOTECHNOLOGY, H.O. Hultin and M. Milner

## **Newsletters**

MICROWAVES AND FOOD, R.V. Decareau  
FOOD INDUSTRY REPORT, G.C. Melson  
FOOD, NUTRITION AND HEALTH, P.A. Lachance and M.C. Fisher  
FOOD PACKAGING AND LABELING, S. Sacharow

# GUIDE FOR AUTHORS

Typewritten manuscripts in triplicate should be submitted to the editorial office. The typing should be double-spaced throughout with one-inch margins on all sides.

Page one should contain: the title, which should be concise and informative; the complete name(s) of the author(s); affiliation of the author(s); a running title of 40 characters or less; and the name and mail address to whom correspondence should be sent.

Page two should contain an abstract of not more than 150 words. This abstract should be intelligible by itself.

The main text should begin on page three and will ordinarily have the following arrangement:

**Introduction:** This should be brief and state the reason for the work in relation to the field. It should indicate what new contribution is made by the work described.

**Materials and Methods:** Enough information should be provided to allow other investigators to repeat the work. Avoid repeating the details of procedures that have already been published elsewhere.

**Results:** The results should be presented as concisely as possible. Do not use tables *and* figures for presentation of the same data.

**Discussion:** The discussion section should be used for the interpretation of results. The results should not be repeated.

In some cases it might be desirable to combine results and discussion sections.

**References:** References should be given in the text by the surname of the authors and the year. *Et al.* should be used in the text when there are more than two authors. All authors should be given in the Reference section. In the Reference section the references should be listed alphabetically. See below for style to be used.

RIZVI, S.S.H. 1986. Thermodynamic properties of foods in dehydration. In *Engineering Properties of Foods*, (M.A. Rao and S.S.H. Rizvi, eds.) pp. 133-214, Marcel Dekker, New York.

MICHAELS, S.L. 1989. Crossflow microfilters ins and outs. *Chem. Eng.* 96, 84-91.

LABUZA, T.P. 1982. *Shelf-Life Dating of Foods*, pp. 66-120, Food & Nutrition Press, Trumbull, CT.

Journal abbreviations should follow those used in *Chemical Abstracts*. Responsibility for the accuracy of citations rests entirely with the author(s). References to papers in press should indicate the name of the journal and should only be used for papers that have been accepted for publication. Submitted papers should be referred to by such terms as "unpublished observations" or "private communication." However, these last should be used only when absolutely necessary.

Tables should be numbered consecutively with Arabic numerals. The title of the table should appear as below:

## TABLE 1.

### ACTIVITY OF POTATO ACYL-HYDROLASES ON NEUTRAL LIPIDS, GALACTOLIPIDS AND PHOSPHOLIPIDS

Description of experimental work or explanation of symbols should go below the table proper. Type tables neatly and correctly as tables are considered art and are not typeset. Single-space tables.

Figures should be listed in order in the text using Arabic numbers. Figure legends should be typed on a separate page. Figures and tables should be intelligible without reference to the text. Authors should indicate where the tables and figures should be placed in the text. Photographs must be supplied as glossy black and white prints. Line diagrams should be drawn with black waterproof ink on white paper or board. The lettering should be of such a size that it is easily legible after reduction. Each diagram and photograph should be clearly labeled on the reverse side with the name(s) of author(s), and title of paper. When not obvious, each photograph and diagram should be labeled on the back to show the top of the photograph or diagram.

**Acknowledgments:** Acknowledgments should be listed on a separate page.

Short notes will be published where the information is deemed sufficiently important to warrant rapid publication. The format for short papers may be similar to that for regular papers but more concisely written. Short notes may be of a less general nature and written principally for specialists in the particular area with which the manuscript is dealing. Manuscripts that do not meet the requirement of importance and necessity for rapid publication will, after notification of the author(s), be treated as regular papers. Regular papers may be very short.

Standard nomenclature as used in the engineering literature should be followed. Avoid laboratory jargon. If abbreviations or trade names are used, define the material or compound the first time that it is mentioned.

**EDITORIAL OFFICE:** DR. D.R. HELDMAN, COEDITOR, *Journal of Food Process Engineering*, Food Science/Engineering Unit, University of Missouri-Columbia, 235 Agricultural/Engineering Bldg., Columbia, MO 65211 USA; or DR. R.P. SINGH, COEDITOR, *Journal of Food Process Engineering*, University of California, Davis, Department of Agricultural Engineering, Davis, CA 95616 USA.

**CONTENTS**

Moisture Sorption and Volumetric Changes of Canola During Hydrothermal Processing N.J. THAKOR, S. SOKHANSANJ, R.T. PATIL and S.D. DESHPANDE . . . . .	233
Adsorption of Bile Acids on Cereal Type Food Fibers C.-M. HUANG and N.H. DURAL . . . . .	243
Mechanisms Involved in the Infusion of Starch Based Porous Food Materials by Oil Based Liquid Foods Z. HIÇSASMAZ and J.T. CLAYTON . . . . .	267
Evaluation of Die Swell and Volumetric Expansion in Corn Meal Extrudates J.F. FALLER, H.E. HUFF and F. HSIEH . . . . .	287
Simultaneous Heat and Mass Transfer During the Deep Fat Frying of Tortilla Chips R. MOREIRA, J. PALAU and X. SUN . . . . .	307
Mathematical Modeling of Particulate Two-Phase Flow in a Helical Pipe Y. LIU and C.A. ZURITZ . . . . .	321